

TECHNISCHE UNIVERSITÄT MÜNCHEN

Lehrstuhl für Siedlungswasserwirtschaft

**CHARACTERISATION OF A BORON-DOPED
DIAMOND ELECTRODE AND APPLICATIONS
FOR THE OXIDATION OF PHARMACEUTICAL
SUBSTANCES AND DISINFECTION IN WATER**

Mateo Joaquín Ureña de Vivanco

Vollständiger Abdruck der von der Fakultät für Bauingenieur- und Vermessungswesen der Technischen Universität München zur Erlangung des akademischen Grades eines

Doktors der Naturwissenschaften (Dr.rer.nat.)

genehmigten Dissertation.

Vorsitzender: Univ.-Prof. Dr.rer.nat. Florian Einsiedl

Prüfer der Dissertation: 1. Univ.-Prof. Dr.rer.nat.habil. Brigitte Helmreich
2. Univ.-Prof. Dr.phil.nat. Michael Schuster
3. Univ.-Prof. Dr.-Ing. Martin Jekel,
Technische Universität Berlin

Die Dissertation wurde am 29.11.2012 bei der Technischen Universität München eingereicht und durch die Fakultät für Bauingenieur- und Vermessungswesen am 04.02.2013 angenommen.

Abstract

In many natural waters around the world, residues from pharmaceutical substances and personal care products can be found. Since some of these substances are bioactive, they can unfold striking effects in the environment. Meanwhile, such residues have been detected even in drinking water, as neither sewage nor water treatment plants are capable of completely eliminating these compounds. On the verge of a new and more stringent European Water Framework Directive, it urges to find and evaluate processes for the removal of undesired substances from water. They should stand two tests: the successful elimination of pollutants and economic operation.

In the present work, a boron-doped diamond (BDD) electrode (BDDE) was investigated. BDDEs belong to the so-called advanced oxidation processes (AOPs), which are technologies aimed at producing hydroxyl radicals, in this specific case, electrochemically and directly from water. Due to their high reactivity, these radicals can degrade all kinds of organic molecules including persistent pollutants. A laboratory scale BDDE was first characterised concerning the identity and amount of oxidising agents (hydroxyl radicals, ozone) it generates. In a subsequent step, the BDDE was evaluated for its capacity to eliminate two model pharmaceuticals, namely carbamazepine (CBZ, antiepileptic) and sulfamethoxazole (SMX, antibiotic) in various water matrices and under different operation conditions. To examine the application of BDD for disinfection purposes, the inactivation of three bacteria strains (*Escherichia coli*, *Enterococcus faecium* and *Pseudomonas aeruginosa*) was studied as well. With the purpose of comparison, hydrogen peroxide photolysis, the photo-Fenton reaction and a micro-scale BDDE directly coupled to mass spectrometry were employed.

The most important finding was that, unlike other AOP technologies, oxidant formation on BDD is governed by current density (j). At low j ($\leq 20 \text{ mA/cm}^2$), theoretically only hydroxyl radicals emerge; at mid j ($20\text{--}100 \text{ mA/cm}^2$), a mixture of radicals and ozone forms whereas at $j \geq 100 \text{ mA/cm}^2$ predominantly ozone arises. Two experimental approaches confirmed this phenomenon: a direct cumulative measurement of the oxidants and a novel approach developed based on the comparison of the transformation products of organic compounds to known products from the ozone and hydroxyl radical pathways in literature.

The consequences of the characterisation could be observed in every further experiment. The abatement of pollutants was more efficient when ozone formed, as it can act in the bulk of the solution (radicals are confined to the electrode surface). The same was true for bacteria inactivation. When working with the effluent of a sewage treatment plant, the pollutant removal efficiency decreased due to competitive reactions. However, the higher chloride levels in this water compensated for the matrix effect during disinfection. Presumably chlorine resulting from the oxidation of chloride played a role. The operation at low current densities (radicals) enhanced the halogenation of organic matter and thus exacerbated by-product formation.

Finally, the energy consumption of the systems was assessed. It was found that the elimination of CBZ and SMX required half of the energy needed to additionally degrade their oxidation products. The energetic demand of the BDDE was comparable to those of conventional technologies.

Zusammenfassung

In vielen natürlichen Gewässern lassen sich einige Arzneimittelrückstände sowie Stoffe aus Körperpflegeprodukten nachweisen. Aufgrund ihrer Bioaktivität können sie schädlich auf die Umwelt wirken. Da weder Klär- noch Wasserwerke dazu in der Lage sind, diese persistenten Stoffe vollständig zu entfernen, wurden sie inzwischen teilweise sogar im Trinkwasser detektiert. Vor dem Hintergrund der bald in Kraft tretenden, europäischen Water Framework Directive drängt es, Prozesse zur Eliminierung persistenter Schmutzstoffe aus dem Wasser zu finden. Diese müssten sowohl den effektiven Abbau von organischen Stoffen bewirken als auch kostengünstig sein.

In der vorliegenden Arbeit werden Untersuchungen mit einer bordotierten Diamantelektrode (BDDE) vorgestellt. BDDE gehören den so genannten Verfahren zur weitergehenden Oxidation (AOPs) an, die zum Ziel haben, Hydroxylradikale zu erzeugen. BDDE produzieren Hydroxylradikale direkt aus Wasser. Diese extrem reaktiven Spezies sind imstande, organische Stoffe anzugreifen. Eine BDDE im Labormaßstab wurde zunächst in Hinblick auf die Oxidantien (Hydroxylradikale, Ozon), die sie erzeugt, charakterisiert. Im nächsten Schritt wurde der Abbau zweier persistenter Stoffe, Carbamazepin (CBZ, Antiepileptikum) und Sulfamethoxazol (SMX, Antibiotikum) mit Hilfe der BDDE in diversen Wassermatrizes und unter verschiedenen Betriebsbedingungen untersucht. Um die Desinfektionswirkung der BDDE zu testen, wurde die Inaktivierung von drei Bakterienstämmen (*Escherichia coli*, *Enterococcus faecium* and *Pseudomonas aeruginosa*) studiert. Darüber hinaus wurde ein Vergleich der BDDE mit anderen AOP-Verfahren wie der Wasserstoffperoxid-Photolyse, der Photo-Fenton-Reaktion und einer miniaturisierten BDDE, die direkt an ein Massenspektrometer gekoppelt war, durchgeführt.

Es wurde herausgefunden, dass die BDDE je nach angelegter Stromstärke unterschiedliche Oxidantien erzeugt. Im Gegensatz zu den anderen AOP-Verfahren, die hauptsächlich Hydroxylradikale produzieren, werden an der BDDE bei geringen Stromdichten ($\leq 20 \text{ mA/cm}^2$) primär nur Radikale erzeugt. Im mittleren Bereich ($20\text{--}100 \text{ mA/cm}^2$) werden sowohl Radikale als auch Ozon gemessen, während im Stromdichtebereich $\geq 100 \text{ mA/cm}^2$ vorzugsweise Ozon entsteht. Zwei unterschiedliche Ansätze konnten dies bestätigen: die direkte Messung der Oxidantien sowie ein neuartig entwickeltes Verfahren, das die oxidativen Spezies indirekt bestimmt. Dabei wurden die organischen Abbauprodukte, die Reaktionen von persistenten organischen Stoffen mit den erzeugten Oxidantien entstammen, mit Literaturdaten verglichen.

Die Folgen der Erzeugung verschiedener Oxidantien machten sich in den weiteren Versuchen bemerkbar. Der Abbau von SMX and CBZ war unter Ozonbedingungen begünstigt, weil Ozon in die wässrige Phase übergeht und nicht wie Hydroxylradikale nur an der Elektrodenoberfläche oxidieren kann. Gleiches wurde bei der Desinfektion beobachtet. Beim Arbeiten mit einem Kläranlagenablauf kam es zu Konkurrenzreaktionen durch die weiteren Matrixkomponenten, so dass der gezielte Abbau von CBZ und SMX sich verlangsamte. Dennoch war die Inaktivierung von Bakterien in dieser komplexen Wassermatrix genauso wirksam wie in saubereren Wässern. Vermutlich spielte die Oxidation von Chlorid zu freiem Chlor, einem starken Desinfektionsmittel, eine Rolle. Der Betrieb bei kleinen Stromstärken (Radikale) führte

zu einer vermehrten Halogenierung der organischen Stoffe, so dass mehr organische Nebenprodukte entstanden.

Schließlich wurde eine energetische Betrachtung durchgeführt. Die Eliminierung von CBZ und SMX benötigte die Hälfte der Energie, die für die Oxidation derer Hauptabbauprodukte zusätzlich notwendig war. Der Stromverbrauch der BDDE war dabei vergleichbar mit dem herkömmlicher AOP-Verfahren.

Eidesstattliche Erklärung

Hiermit versichere ich, dass ich die vorliegende Dissertation selbstständig verfasst habe. Die Ausführungen und Gedanken, die anderen Schriften wörtlich oder sinngemäß entnommen wurden, sowie weitere Quellen und Hilfsmittel sind kenntlich gemacht. Diese Arbeit wurde bisher weder in gleicher noch in ähnlicher Form einer anderen Prüfungsbehörde vorgelegt und auch noch nicht veröffentlicht.

München, den 17. Februar 2014

Acknowledgements

I am deeply thankful to my supervisors for their constant support. To Prof. Brigitte Helmreich, who provided me with a wonderful research topic and was always willing to help me with my questions, formalities and anything thinkable. If we had a friendly atmosphere at work, it was definitely because of her openness and naturalness. To Dr. Thomas Letzel, whom I costed so many hours of conversation. This time was absolutely inspiring and most of my ideas for research arose during those discussions. Also to Prof. Harald Horn, who originally accepted me as a doctoral candidate at the institute and worked very hard for my formal admission at university. All of them offered me optimum research conditions and challenges that definitely made me grow as a person.

Special thanks to the Deutscher Akademischer Austauschdienst (DAAD), who funded me for four years to achieve the PhD degree, and to the Bundesministerium für Bildung und Forschung for the project grant NADINE (ID: 03X0087G). CONDIAS, Antec and the Institute of Microbial Ecology (TUM) are acknowledged for the provision of the BDDE, the ROXYTM-system and the bacteria cultures, respectively.

I could not have accomplished this dissertation if it had not been for the cooperative work with others. Mohamad Rajab, my great companion and biggest motivator, and Carolin Heim, the *think tank* behind experiments and new ideas. Both of them made every single hour of result evaluation meaningful through their supporting comments and discussion. Sebastian Häck, I supervised his Bachelor thesis and he *supervised* my PhD thesis (Lass uns planschen!). With Karin Schübel I was successful in the lab, on the Christmas market and the basketball court. Working with Wolfgang Bittner (high five), Oliver Pagel (Fritz Cola), Franziska Baumer (ratz fatz), Anette Hühn (Wasserflasche), Cornelia Schröpf, Thomas Buscham, Katrin Heermann und Lajos Harsanyi was very productive and also fun. Forgive me for making you fetch ice in the rambling Faculty of Chemistry.

Uncountable hours of chemical analyses were done for me. I really appreciate the help and support of Sylvia Große, Wolfgang Schröder, Ursula Wallentits, Hubert Moosrainer, Miriam Reif, Susanne Thiemann and Stephanie West. Their explanations, measurements and reactors taught me more than books. I am also grateful for the work with the project partners, especially with Dr. Matthias Fryda for the many fruitful discussions, but also with the *Dresdner*, the *Braunschweiger* and the *Itzehoer*. The original instructions were provided by Mr. Becker E&H.

As important as the academic support was the emotional support I got. David Martínez, Christina Klarmann, Christine Kaufmann, Yang Li, Evelyn Walters (who also corrected my papers), Chunyan Li, Danial Taher-Zadeh, Konrad Koch, Tobias Rocktäschel, Romy Scheerle, Susanne Lackner, Riccardo Matruglio, Gökçe Iyicil, Valentin Zerbes, Korbinian Kätzl and all those whose names unfortunately do not fit in this one page. Without you, I would have given up many a time before finishing.

Last but not least, for very few persons there are no proper words to convey my acknowledgements. Marcus Pilz, who swallowed most of my fears and frustrations over three years, and my closer family in Peru, who supported my PhD venture not only with constant advice, but also by accepting my four-year absence from home.

Contents

Abstract	3
Zusammenfassung	5
Eidesstattliche Erklärung	7
Acknowledgements	9
Contents	11
List of Tables	15
List of Figures	17
List of Abbreviations and Symbols	19
Preface	23
1 Introduction	27
1.1 Xenobiotics and Their Impact on the Environment	27
1.2 Advanced Oxidation Processes	29
1.3 Boron-Doped Diamond Electrodes	32
1.3.1 Properties of Boron-Doped Diamond	32
1.3.2 Fabrication of Conductive Diamond Electrodes	32
1.3.3 Oxidant Generation on Boron-Doped Diamond	33
1.4 Fate of the Oxidants in Aqueous Solutions	34
1.4.1 Ozone and Hydroxyl Radical Reactions	34
1.4.2 Ozone Decay	35
1.5 By-Product Formation	36
1.6 State of Knowledge and Objectives of this Work	38
2 Materials and Methods	41
2.1 Chemicals	41

2.2	Reactors	42
2.2.1	Diamond Electrode System (BDD)	42
2.2.2	Miniaturised Diamond Electrode Coupled to Mass Spectrometry (DD*)	42
2.2.3	Hydrogen Peroxide Photolysis (UV/H ₂ O ₂)	46
2.2.4	Photo-Fenton Process	46
2.3	Methods	46
2.3.1	Cumulative Measurements of Reactive Oxygen Species	46
2.3.2	Residual Ozone Measurements in Water	47
2.3.3	By-Products	47
2.3.4	Pharmaceutical Investigations	49
2.3.5	Mass Spectrometry (MS)	49
2.3.6	Disinfection Experiments	50
2.3.7	Further Measurements	51
2.3.8	Charge Input per Volume (Q/V)	51
2.3.9	Calculation of Energy Consumption	53
3	Energetic Comparison of Advanced Oxidation Reactors	55
3.1	Reactor Comparison	55
3.2	Degradation of Indigo Carmine	56
3.3	Energetic Consumption of Individual Components	56
3.4	Summary	60
4	Effect of the Current Density on the Generation of Reactive Oxygen Species	61
4.1	Cumulative Measurements	61
4.2	Ozone Concentration in Deionised Water	64
4.3	Energetic Considerations	66
4.4	Summary	67
5	Effect of the Water Matrix on Ozone Formation and Degradation Efficiency	71
5.1	Ozone Concentration in Different Water Matrices	71
5.1.1	Inorganic Water Components	72
5.1.2	Organic Water Components	75
5.1.3	Ozone Concentrations in Real Wastewater	76
5.1.4	Summarising Remarks - Matrix and Current Effect	77

5.2	Fate of the Organic Matter	77
5.2.1	Transformation of the Bulk Organic Matter	77
5.2.2	Degradation of a Target Compound	77
5.3	Energy Consumption	79
5.4	Summary	80
6	Formation of Organic By-Products	83
6.1	Inorganic Water Components	83
6.2	Organic Water Components	84
6.2.1	Adsorbable Organically Bound Halogens	84
6.2.2	Trihalomethanes	86
6.2.3	Comparison to literature data	87
6.3	Summary	89
7	Inactivation of waterborne bacteria	91
7.1	Current Effect on Bacteria Inactivation	91
7.2	Energy Consumption	93
7.3	Different Bacteria Strains	95
7.4	Matrix Effect on Disinfection	97
7.5	Fate of Organic Matter	98
7.6	By-Product Formation	99
7.7	Summary	99
8	Degradation Pathways of Organic Compounds as a Tool for the Characterisation of Advanced Oxidation Processes	101
8.1	Oxidation Pathways	102
8.2	Characterisation of Hydrogen Peroxide Photolysis (UV/H ₂ O ₂)	103
8.3	Characterisation of the Micro Diamond Electrode Coupled to Mass Spectrometry (DD*)	105
8.4	Characterisation of the Boron-Doped Diamond Electrode (DD)	106
8.5	Conclusive Remarks on AOP Characterisation	107
8.6	Time Courses of the Transformation Products	107
8.7	Energetic Considerations	108
8.8	Summary	111
9	Conclusions	115
9.1	Characterisation of the Diamond Electrode	115

9.2	Consequences of Different Oxidising Agents on Water Treatment . . .	116
9.3	Pragmatic Recommendation	117
9.4	New Approaches for Water Treatment	117
10	Outlook	121
10.1	Research Topics for the Future	121
10.2	Practical Approaches to Follow	122
	References	123
	Appendix A (Mass Spectrometric Databases)	135
	Appendix B (Time Courses and Energetic Requirements of CBZ)	141
	About the Author - Curriculum Vitae	145
	Index	147

List of Tables

1.1	Standard and calculated redox potentials of selected oxidants at pH = 7	30
1.2	Half-lives of dissolved ozone in water at different temperatures	35
2.1	Chemical composition of the employed water matrices	43
2.2	Experimental parameters for the employed AOPs during the indigo carmine decolouration experiments	48
2.3	Summary of cultivation and analysis methods for <i>E. coli</i> , <i>P. aeruginosa</i> and <i>E. faecium</i>	52
2.4	Commercial chemical substances and the conversion of their price to energy values	52
2.5	$E_{EO,rx}$ and $E_{EO,tot}$ calculation chart for the photo-Fenton reaction . .	54
3.1	Energetic requirements of electrolysis, photolysis and the photo-Fenton reaction	57
4.1	Initial ozone concentrations in deionised water	63
4.2	Comparative power data of selected laboratory-scale ozone generators and BDD	68
5.1	Initial accumulation rate of ozone in water at different current densities in dependence of the water matrix	72
5.2	Energy consumption (E_{PC_0} , electrolysis only) for single-step oxidation of CBZ in different water matrices	79
6.1	Average AOX formation rate in dependence of the charge input in <i>HORG</i> and <i>STPE</i> at different current densities	86
6.2	Comparison of AOX measurements in this study and literature in dependency of the applied current density	88
7.1	Calculated energy consumption for log 5 and log 7.4 (complete) <i>E. coli</i> inactivation in <i>soft-b</i> in dependence of j	94
7.2	DOC, AOX and chloride concentrations in <i>soft-b</i> and <i>STPE-b</i> before and after disinfection at 208 mA/cm ²	99

8.1	Energy consumption for the treatment until total elimination of SMX (t_{PC_0}) and full abatement of its known transformation products (t_{TP_0})	110
8.2	SMX degradation products observed with mass spectrometry	113
8.3	CBZ degradation products observed with mass spectrometry	114
9.1	Calculated energy consumption (electrolysis only), AOX concentration and bacteria inactivation for the complete oxidation of CBZ (t_{PC_0}) or its TPs (t_{TP_0}) in STPE-pb	119
A1	SMX transformation product database	136
A2	CBZ transformation product database	139
B1	Energy consumption for treatment until complete elimination of CBZ (t_{PC_0}) and full abatement of its known transformation products (t_{TP_0})	142

List of Figures

1.1	Working principles of boron-doped diamond (BDD), hydrogen peroxide photolysis (UV/H ₂ O ₂) and the (photo-)Fenton reaction	31
2.1	Schemes of the employed BDD and DD* reactors	44
2.1	(<i>continued</i>) Schemes of the employed UV/H ₂ O ₂ and photo-Fenton reactors	45
3.1	Decolouration dependent on the process energy input ($E_{E,pro}$) for BDD, UV/H ₂ O ₂ and the photo-Fenton reaction	58
3.2	Effective electrical energy per order of magnitude ($E_{EO,rx}$) for the decolouration of indigo carmine with BDD, UV/H ₂ O ₂ and the photo-Fenton reaction	59
4.1	Measured formation rate of ozone and hydroxyl radicals in dependence of the current density	62
4.2	Geometries of the employed electrolytic chamber and the suggested electrolytic cell with enhanced exposure to hydroxyl radicals	64
4.3	Ozone concentrations in deionised water in dependence of the time or the charge input	65
4.4	Measured power of the BDD electrode (electrode only, $E_{E,pro}$) during the cumulative experiments at various current densities	67
5.1	Residual ozone concentrations measured in deionised water, model water matrices and STPE during the electrolyses with BDD	73
5.2	Influence of the electrical conductivity of a medium on the ozone yield	74
5.3	Ozone concentrations against the charge input measured in STPE over 120 min of treatment with BDD at different current densities	76
5.4	Carbamazepine degradation with BDD in different water matrices	78
5.5	Measured power of BDD (electrode only) during the electrolysis at 208 mA/cm ² in different water matrices	80
6.1	Influence of the current density and the water matrix on chloride consumption and AOX formation in STPE and <i>HORG</i>	85

6.2	THM formation in <i>HORG</i> upon BDD treatment	87
7.1	<i>E. coli</i> inactivation and ozone concentrations in <i>soft-b</i> in dependency of the charge input per volume and the <i>ct</i> (O_3 only) at various current densities	92
7.2	Inactivation of <i>E. coli</i> , <i>P. aeruginosa</i> and <i>E. faecium</i> and corresponding ozone concentrations during electrolysis in <i>soft-b</i> at 208 mA/cm ² .	96
7.3	<i>E. coli</i> inactivation and simultaneous CBZ degradation in <i>soft-pb</i> and STPE-pb at 208 mA/cm ²	97
8.1	Degradation pathways and detected degradation products of SMX upon HO [•] attack and ozonation according to literature	104
8.2	Degradation pathways and detected degradation products of CBZ upon HO [•] attack and ozonation according to literature	105
8.3	Course of SMX and selected degradation products during the DD', DD'' and UV/H ₂ O ₂ experiments	109
9.1	Graphical representation of the current effect and the matrix effect .	120
B1	Course of CBZ and its identified degradation products during the DD' and the UV/H ₂ O ₂ experiments	143

List of Abbreviations and Symbols

ρ	density (g/mL)
Δ	deviation from real mass (ppm)
ACR	acridine
ACR-CHO	acridine-9-carboxaldehyde
ACR-OH	1-hydroxyacridine or 2-hydroxyacridine
ads	adsorbed
AOP(s)	advanced oxidation process(es)
AOX	adsorbable organically bound halogens
aq	aqueous
BDD	boron-doped diamond
BDDE(s)	boron-doped diamond electrode(s)
BP(s)	by-product(s)
BQD	1-(2-benzaldehyde)-(1 <i>H</i> ,3 <i>H</i>)-quinazoline-2,4-dione
BQM	1-(2-benzaldehyde)-4-hydro-(1 <i>H</i> ,3 <i>H</i>)-quinazoline-2-one
BSA	bovine serum albumin
CBZ	carbamazepine: 5 <i>H</i> -dibenz[<i>b,f</i>]azepine-5-carboxamide (antiepileptic drug)
CFU	colony forming unit
COD	chemical oxygen demand (mg/L)
<i>ct</i>	ozone exposure (mg·min/L) as the product of ozone concentration and <i>time</i>
DBP(s)	disinfection by-product(s)
DD'	treatment with boron-doped diamond at 42 mA/cm ²
DD''	treatment with boron-doped diamond at 208 mA/cm ²
DD*	miniaturised boron-doped diamond electrode directly coupled to mass spectrometry
deionised	pure water
deionised-p	pharmaceutical-spiked pure water
DOC	dissolved organic carbon (mg/L)
$E_{E,chem}$	electrical energy contained in chemicals (Wh/L)
$E_{E,mix}$	electrical energy for mixing (stirring, pumping) devices (Wh/(L·min))
$E_{E,log5}$	energy consumption until a log 5 bacteria reduction
$E_{E,log7.4}$	energy consumption until a log 7.4 (here: complete) bacteria reduction
$E_{E,pro}$	process-intrinsic electrical energy (Wh/(L·min))

$E_{E,tot}$	total electrical energy ($E_{E,pro} + E_{E,mix} + E_{E,chem}$) (Wh/L)
E_{EO}	electrical energy per order of magnitude (Wh/(L·order))
$E_{EO,rx}$	effective electrical energy per order of magnitude (Wh/(L·order))
$E_{EO,tot}$	total electrical energy per order of magnitude (Wh/(L·order))
E_{ox}°	standard oxidation potential (V)
E_{PC_0}	energy consumption for single-step oxidation of a parent compound
$E_{pH=7}$	reduction potential (V) at a pH of 7 ($[H^+] = 10^{-7}$ M instead of 1 M)
E_{red}°	standard reduction potential (V)
E_{TP_0}	energy consumption until the full degradation of transformation products
EAOP	electrochemical advanced oxidation process
EE2	17 α -ethinylestradiol (estrogenic compound found in anti-fertility pills)
ESI	electrospray ionisation
[Fe ²⁺]	ferrous concentration (μ M)
<i>hard</i>	model hard potable water matrix
<i>hard-p</i>	pharmaceutical-spiked model hard potable water matrix
HO \cdot	hydroxyl radical
[H ₂ O ₂]	hydrogen peroxide concentration (μ M)
<i>HORG</i>	artificial hard water matrix with organic material
<i>HORG-p</i>	pharmaceutical-spiked hard water matrix with organic material
HP	hydrogen peroxide photolysis (only in Chapter 8)
IC	indigo carmine (5,5'-indigodisulfonic acid sodium salt)
[IC] _i	initial IC concentration (μ M)
[IC] _t	IC concentration at time <i>t</i> (μ M)
<i>j</i>	current density (mA/cm ²)
LOD	limit of detection
MPN	most probable number
MS	mass spectrometry
N ₀	initial bacterial counts (CFU/mL)
N	bacterial counts (CFU/mL)
NOM	natural organic matter
NOM _{ox}	oxidised natural organic matter
OM	orders of magnitude
p.a.	<i>pro analysi</i> in Chapter 2; <i>person·annum</i> elsewhere
preBQM	hydrated precursor of BQM
Q/V	charge input per volume (mAh/L)
R ²	correlation coefficient
RM	reference mass
RNO	N,N-dimethyl-4-nitrosoaniline
ROS	reactive oxygen species
rpm	revolutions per minute
s _x	sample x
SMX	sulfamethoxazole: 4-amino-N-(5-methylisoxazol-3-yl)-benzenesulfonamide (antibiotic)
<i>soft</i>	model soft potable water matrix
<i>soft-b</i>	bacteria-spiked model soft potable water matrix

<i>soft-p</i>	pharmaceutical-spiked model soft potable water matrix
<i>soft-pb</i>	pharmaceutical and bacteria-spiked model soft potable water matrix
sol	solution
<i>SORG</i>	artificial soft water matrix with organic material
SPE	solid polymer electrolyte
STP(s)	sewage treatment plant(s)
STPE	sewage treatment plant effluent
STPE-b	bacteria-spiked sewage treatment plant effluent
STPE-p	pharmaceutical-spiked sewage treatment plant effluent
STPE-pb	pharmaceutical and bacteria-sewage treatment plant effluent
$t_{\log 5}$	time required to achieve a log 5 bacteria reduction
$t_{\log 7.4}$	time required to achieve a log 7.4 bacteria reduction (complete in-activation)
t_{PC_0}	time required for total oxidation of the parent compound (min)
t_{TP_0}	time required for total oxidation of known transformation products of the parent compound (min)
THM(s)	trihalomethane(s)
TOC	total organic carbon (mg/L)
ToF	time-of-flight (mass spectrometer)
TP(s)	transformation product(s)
UV	ultraviolet
UV/H ₂ O ₂	hydrogen peroxide photolysis
vis	visible light
Wh	watt hour; 1 Wh = 3600 J

Preface

The present work has been partially published and/or publicly presented in the following forms.

1. Publications

- (a) Heim, C., Ureña de Vivanco, M., Rajab, M., Glas, K., Horn, H., Helmreich, B., Letzel, T., 2011. Ozone II: Characterization of In Situ Ozone Generation Using Diamond Electrodes. *Brewing Science*, 64, 83–88.
- (b) Ureña de Vivanco, M., Rajab, M., Heim, C., Letzel, T., Helmreich, B. 2013. Setup and Energetic Considerations for Three Advanced Oxidation Reactors Treating Organic Compounds. *Chemical Engineering and Technology*, 36, No. 2, 355–361.

2. Oral Presentations

- (a) Ureña de Vivanco, M., Desinfektion und Abbau von persistenten Arzneimittelwirkstoffen mit Hilfe nanomodifizierter Diamantelektroden, CHEM-LAB Workshop II, Weihenstephan, 14.04.2011.
- (b) Ureña de Vivanco, M., Abbau von Arzneimittelwirkstoffen und Mikroorganismen durch in-situ erzeugtes Ozon, 5. Wasserseminar für die Getränke- und Lebensmittelindustrie, Waidring, 15.-16.09.2011.
- (c) Ureña de Vivanco, M., Heim, C., Application of a Diamond Electrode for Water and Wastewater Disinfection, GDCh Wissenschaftsforum Chemie, Bremen, 04.-07.09.2011, short presentation on Poster 3c, elected among the *top 10*.
- (d) Ureña de Vivanco, M., Carbamazepine Electrochemical Degradation by a Boron-Doped Diamond Electrode in Various Waters, 6th IWA Specialist Conference: Oxidation Technologies for Water and Wastewater Treatment, based on poster 3l, Goslar, 7.-9.05.2012.

3. Scientific Poster Presentations

- (a) Ureña de Vivanco, M., Letzel, T., Helmreich, B., Die Diamantelektrode: Wie ein Isolator zur erfolgsversprechenden elektrochemischen Methode für die Abwasserreinigung werden kann, ANAKON-Tagung, Zürich 22.-25.03.2011.

-
- (b) Helmreich, B., Ureña de Vivanco, M., Letzel, T., Heim, C., Glas, K., Horn, H., Abbau von Arzneimittelwirkstoffen mit einer Diamantelektrode. 1. Clustertreffen der NanoCare- und NanoNature-Projekte, DECHEMA, Frankfurt/Main, 10.-11.05.2011.
 - (c) Heim, C., Ureña de Vivanco, M., Rajab, M., Helmreich, B., Glas, K., Letzel, T., Horn, H., Einsatz einer Diamantelektrode zur Wasser- und Abwasserdesinfektion, GDCh Wissenschaftsforum Chemie, Bremen, 04.-07.09.2011.
 - (d) Ureña de Vivanco, M., Heim, C., Schübel, K., Letzel, T., Helmreich, B., Horn, H., Oxidation of Pharmaceutical Substances with Nano-Modified Diamond Electrodes, GDCh Wissenschaftsforum Chemie, Bremen, 04.-07.09.2011.
 - (e) Letzel, T., Ureña de Vivanco, M., Helmreich, B., Horn, H., Pos/Neg-Switching LC-MS Detection of Pharmaceutical Degradation Products from Diamond Electrode Treatment of Water and Wastewater, ITP-Tagung, Tbilisi 28.-31.08.2011.
 - (f) Letzel, T., Ureña de Vivanco, M., Helmreich, B., Horn, H., Pos/Neg-Switching LC-MS Detection of Pharmaceutical Degradation Products from Diamond Electrode Treatment of Water and Wastewater, 5. Wasserseminar für die Getränke- und Lebensmittelindustrie, Waidring, 15.-16.09.2011.
 - (g) Heim, C., Ureña de Vivanco, M., Rajab, M., Helmreich, B., Glas, K., Letzel, T., Horn, H., Parlar, H., Desinfektion von Wasser und Abwasser unter Einsatz einer Diamantelektrode, 5. Wasserseminar für die Getränke- und Lebensmittelindustrie, Waidring, 15.-16.09.2011.
 - (h) Heim, C., Ureña de Vivanco, M., Rajab, M., Buscham, T., Glas, K., Horn, H., Parlar, H., Einsatz von ozonhaltigem Wasser zur Desinfektion von Brauereianlagen, 5. Wasserseminar für die Getränke- und Lebensmittelindustrie, Waidring, 15.-16.09.2011.
 - (i) Letzel, T., Ureña de Vivanco, M., Helmreich, B., Horn, H., Pos/Neg-Switching LC-MS Detection of Pharmaceutical Degradation Products from Diamond Electrode Treatment of Water and Wastewater, 8. Längener Wasserforum, Langenau, 7.-8.11.2011.
 - (j) Helmreich, B., Ureña de Vivanco, M., Rajab, M., Glas, K., Heim, C., Letzel, T., Abbau von Carbamazepin bei gleichzeitiger Inaktivierung von *Escherichia coli* mit einer bordotierten Diamantelektrode, DECHEMA, Frankfurt, 12.-14.03.2012.
 - (k) Letzel, T., Ureña de Vivanco, M., Scheerle, R., Studying Oxidative and Reductive Reactions Using a Potentiostat Coupled To MS: Applications in Water Research and Enzymology, Gemeinschaftliche Tagung der Polnischen Gesellschaft für Massenspektrometrie mit der 45. DGMS-Jahrestagung, Poznan, 04.-07.03.2012.
 - (l) Ureña de Vivanco, M., Letzel, T., Helmreich, B., Carbamazepine Electrochemical Degradation by a Boron-Doped Diamond Electrode in Various

Waters, 6th IWA Specialist Conference: Oxidation Technologies for Water and Wastewater Treatment, Goslar, 7.-9.05.2012.

- (m) Rajab, M., Ureña de Vivanco, M., Heim, C., Letzel, T., Helmreich, B., The Applicability of a Boron-Doped Diamond Electrode for Water Disinfection, 6th IWA Specialist Conference: Oxidation Technologies for Water and Wastewater Treatment, Goslar, 7.-9.05.2012.
- (n) Ureña de Vivanco, M., Rajab, M., Helmreich, B., Letzel, T., Oxidation von Carbamazepin mit Hilfe einer bordotierten Diamantelektrode, Elektrochemie-Massenspektrometrie, UV/H₂O₂ oder der Photo-Fenton-Reaktion: Massenspektrometrische Studien der Abbauprodukte, Kolloquium LC-MS in der Umweltanalytik 2012, Leipzig, 11.-13.06.2012.
- (o) Ureña de Vivanco, M., Rajab, M., Helmreich, B., Letzel, T., Oxidation von Carbamazepin mit Hilfe einer bordotierten Diamantelektrode, Elektrochemie-Massenspektrometrie, UV/H₂O₂ oder der Photo-Fenton-Reaktion: Massenspektrometrische Studien der Abbauprodukte, 9. Langenauer Wasserforum, Langenau, 12.-13.11.2012.
- (p) Ureña de Vivanco, M., Rajab, M., Helmreich, B., Letzel, T., Massenspektrometrischer Vergleich der Abbauwege des Sulfamethoxazol bei verschiedenen AOPs, 9. Langenauer Wasserforum, Langenau, 12.-13.11.2012.
- (q) Ureña de Vivanco, M., Rajab, M., Heim, C., Helmreich, B., Letzel, T., Degradation Pathways of Organic Compounds as a Tool for the Characterisation of Advanced Oxidation Processes, ANAKON-Tagung, Essen 4.-7.03.2013.

In addition, the following publications are planned.

1. Publications

- (a) Heim, C., Ureña de Vivanco, M., Rajab, M., Müller, E., Letzel, T., Helmreich, B., Rapid Inactivation of Waterborne Bacteria Using Boron-Doped Diamond Electrodes, based on Chapter 7.
- (b) Ureña de Vivanco, M., Heim, C., Rajab, M., Häck, S., Letzel, T., Helmreich, B., Generation of Reactive Oxygen Species on a Boron-Doped Diamond Electrode in Pure Water, based on Chapter 4.
- (c) Ureña de Vivanco, M., Heim, C., Rajab, M., Letzel, T., Helmreich, B., Influence of the Water Matrix on Ozone Formation and Treatment Efficiency with a Boron-Doped Diamond Electrode, based on Chapter 5.
- (d) Ureña de Vivanco, M., Heim, C., Rajab, M., Letzel, T., Helmreich, B., Formation of Organic By-Products in Real Waters upon Electrolysis with a Boron-Doped Diamond Electrode, based on Chapter 6.
- (e) Ureña de Vivanco, M., Rajab, M., Heim, C., Helmreich, B., Letzel, T., Degradation Pathways of Organic Compounds as a Tool for the Characterisation of Advanced Oxidation Processes, based on Chapter 8.
- (f) Wasser in der Getränkeindustrie (book), contribution for *Kapitel 4 - Inhaltsstoffe und Belastungen in Wasser*, estimated release: 2014, Vogel Verlag.

Chapter 1

Introduction

1.1 Xenobiotics and Their Impact on the Environment

Since the development of sensitive analytical techniques for water monitoring in the last century, it has become apparent that many natural waters contain trace concentrations of xenobiotics. These are substances that neither originate in organisms, nor are they naturally found in the ecosystem. There are several sources of xenobiotics in natural waters. Industrial products such as flame retardants, lubricants, and dyes partly remain in the industrial wastewaters. Also heavy metals are usually present in industrial wastewaters or enter groundwater through landfill leaching (Bradl, 2005). Pesticides and veterinary medicines reach the hydrological cycle through their application in the field and farms (Kümmerer, 2010). Another group of pollutants enter the environment through municipal wastewater, as the biological treatment in sewage treatment plants (STP) is not able to completely eliminate these persistent compounds. This group comprises personal care products, surfactants and human pharmaceuticals both in unaltered form and as stable metabolites. Additionally, halogenated disinfection by-products form during wastewater treatment and remain as persistent pollutants in the effluent (Schwarzenbach et al., 2006).

Due to their chemical stability, these man-made substances are often marked by low degradation rates in the environment. Other chemicals may be more readily degradable, however, if they are continuously released into surface waters, their enrichment therein can ensue. Such accumulation may endanger the ecosystem by exposing organisms to low, but chronic concentrations. For example, Ternes (1998) reported concentrations of many pharmaceutical classes such as antiphlogistics, lipid regulators, psychiatric drugs, antiepileptic drugs and beta blockers in the lower $\mu\text{g}/\text{L}$ -range in rivers and streams. Moreover, xenobiotics can percolate through the soil and attain a passage into ground water, which together with rivers is an important source of drinking water. As a result, pharmaceutical residues have already been detected even in tap water at concentrations in the ng/L -range (Jones et al., 2005). Carbamazepine (CBZ), for instance, is a widely-used antiepileptic drug that is also a persistent micropollutant present at all levels of the hydrological cycle: from STP

influent and effluent, rivers and other fresh waters through to drinking water. Carbamazepine was measured in German rivers at a median concentration of 0.25 µg/L (Ternes, 1998). In the United States, CBZ has been reported in drinking water at concentrations up to 0.26 µg/L (Stackelberg et al., 2004).

It is still unknown whether the chronic exposure to trace concentrations of xenobiotics has effects on humans or not. However, because pharmaceutical substances are designed to have a targeted pharmacological effect in the organism, metabolic processes in humans and non-humans could be unfolded by these substance families even in very low concentrations. Three cases exemplified the environmental toxicity of such residues in the last ten years.

Oaks et al. (2004) identified the usage of the anti-inflammatory drug diclofenac in husbandry as the cause for the observed massive vulture die off in Pakistan. Most retailers and veterinarians in the region sold diclofenac daily for treating hoofed livestock. Whenever a cow died, it was left out for scavengers to feed on its flesh. Vultures which fed on this diclofenac contaminated flesh would die from kidney failure caused by this drug. A vulture population decline > 95 % in ten years was noted.

Sanchez et al. (2011) studied the impact of a pharmaceutical factory discharging wastewater into a river on the ecology of the receiving waters. The discharge contained a mixture of different pharmaceutical substances including anti-inflammatory and diuretic drugs (Gilbert, 2011). They reported that the ratio of intersex fish in downstream waters dramatically rose. The 5 % intersex fish found upstream multiplied to an average of 60 % downstream. The blood levels of vitellogenin, a protein found in eggs, were higher in male fish downstream. This *feminisation* of fish prevented them from breeding and decimated their population. Indeed, several years before, Kidd et al. (2007) performed a whole-lake experiment from which they concluded that the long term exposure to 17 α -ethinylestradiol (EE2) nearly produced the extinction of fathead minnow. The concentration of EE2 employed for the experiment (5–6 ng/L) was lower than those reported for many other pharmaceutical substances in natural waters.

Antibiotic residues have been proved to cause resistance in different classes of microorganisms in the environment. Although resistant strains occur naturally, rivers receiving effluents from slaughterhouses and coastal areas polluted with fish farm waters contained organisms resistant to more than one anti-infective compound class (Halling-Sørensen et al., 1998; Kümmerer, 2010). Some of these had developed plasmids encoding resistance genes (Ash et al., 2002). This is an indirect way in which pharmaceutical residues can negatively affect human health. Besides interrupted antibiotic treatments, environmental pollution even at nanomolar concentrations of antibiotics expose bacteria to non-lethal doses of these compounds. Resistant microorganisms pose a severe threat to the efficiency of anti-infective therapies. Anti-infectives were highly ranked by Cooper et al. (2008) in their risk assessment. Cooper et al. processed five different combinations of physical-chemical and toxicological parameters from literature in their calculations and classified between 16 and 33 anti-infectives as high-risk (top 100) environmental pollutants (especially for marine and estuarine life).

Since there are 7428 medicines approved for use in Germany (Rote Liste Service GmbH, 2012), it can be expected that natural waters contain mixtures of persistent active compounds. Combination effects may be more hazardous to ecology than individual substances are (Cleuvers, 2003).

1.2 Advanced Oxidation Processes

To prevent pollutants from entering the water cycle at point sources, the implementation of an additional, quaternary treatment step at sewage (or industrial) treatment plants is being intensively discussed (Schwarzenbach et al., 2006; Gälli et al., 2009; Gilbert, 2011; Owen and Jobling, 2012). After physical cleaning (elimination of bulk solids), biological treatment (elimination of around 90 % of the total organic carbon (TOC) in water, Gujer, 2007) and nutrient removal (to prevent eutrophication through elevated N and P concentrations), the quaternary treatment would be aimed at the abatement of micropollutants. Although these refractory substances occur in wastewaters at very low concentrations, and the last treatment step would eliminate only a very small amount of the organic load, this small fraction carries bioactive compounds and thus is of concern (see Section 1.1). Furthermore, quaternary treatment should eliminate pathogens from the effluent.

One of the current technologies that efficiently removes micropollutants from water is the adsorption onto granular activated carbon (Owen and Jobling, 2012). Yet this process is related to high material costs and also involves burning the carbon with the refractory substances. In addition, adsorption has no effect on bacteria removal, so this method poses no disinfection potential. Alternatives are offered by chemical treatment. Conventional chlorination is capable of transforming many problematic substances such as endocrine-disrupting compounds into innocuous derivatives and is used for disinfection world-wide. However, the application of chlorine to waters containing organic matter leads to chlorination of the organic molecules, from which toxic chlorine disinfection by-products (DBPs) result. Also the application of chloramine is bound to the formation of carcinogenic DBPs, such as N-nitrosodimethylamine and bromate (Sedlak and von Gunten, 2011). Hence, neither the application of chlorine nor chloramine represents a suitable treatment.

The advanced treatment would have to be based on oxidation reactions involving no halogens, but using species that are also very reactive. One possibility is not far to seek. Oxidation could be carried out with *reactive oxygen species*, ROS, especially with ozone and the highly reactive hydroxyl radicals (HO^\bullet), as both are able to induce the degradation of pollutants (Ikehata et al., 2006). Furthermore, ozone is a powerful disinfectant. Nevertheless, these oxidising agents are not equally efficient in the diverse tasks of water treatment. For some applications, *e.g.* disinfection, ozone is more effective because it can penetrate the cell wall and directly attack DNA (Cho et al., 2010). For other applications, like the elimination of persistent pollutants, HO^\bullet are preferred as they are able to attack even very refractory substances non-selectively (Andreozzi et al., 1999).

Table 1.1 contrasts the standard reduction potentials (E_{red}^\ominus) of various commonly used oxidants. It is notorious that hydroxyl radicals are the strongest oxidising

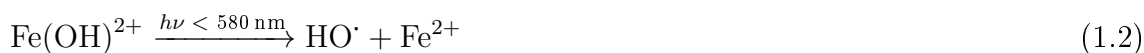
Table 1.1 – Standard (E_{red}^{\ominus}) and calculated ($E_{\text{pH}=7}$) redox potentials of selected oxidants at pH = 7.

oxidising agent	half reaction	E_{red}^{\ominus} (V)	$E_{\text{pH}=7}$ (V) ^d
hydroxyl radical ^a	$\text{HO}\cdot + \text{H}^+ + \text{e}^- \rightleftharpoons \text{H}_2\text{O}$	2.80 ^c	-
atomic oxygen ^b	$\text{O}\cdot + 2\text{H}^+ + 2\text{e}^- \rightleftharpoons \text{H}_2\text{O}$	2.42	-
ozone ^b	$\text{O}_3 + 2\text{H}^+ + 2\text{e}^- \rightleftharpoons \text{O}_2 + \text{H}_2\text{O}$	2.08	1.66
hydrogen peroxide ^b	$\text{H}_2\text{O}_2 + 2\text{H}^+ + 2\text{e}^- \rightleftharpoons 2\text{H}_2\text{O}$	1.76	1.35
hypochlorite ^b	$\text{HOCl} + \text{H}^+ + 2\text{e}^- \rightleftharpoons \text{Cl}^- + \text{H}_2\text{O}$	1.49	1.28
monochloramine ^b	$\text{NH}_2\text{Cl} + 2\text{H}^+ + 2\text{e}^- \rightleftharpoons \text{Cl}^- + \text{NH}_4^+$	1.48	1.13
chlorine ^a	$\text{Cl}_2(\text{aq}) + 2\text{e}^- \rightleftharpoons 2\text{Cl}^-$	1.40	1.40
molecular oxygen ^b	$\text{O}_2 + 4\text{H}^+ + 4\text{e}^- \rightleftharpoons 2\text{H}_2\text{O}$	1.23	0.82
bromine ^a	$\text{Br}_2(\text{aq}) + 2\text{e}^- \rightleftharpoons 2\text{Br}^-$	1.10	1.10

^a Harris (2007); ^b Holleman et al. (2007); ^c Kraft (2007); ^d calculated

agents. Only fluorine has an even higher E_{red}^{\ominus} (3.05 V) (Holleman et al., 2007). Theoretically, $\text{HO}\cdot$ could mineralise the organic content of water (Matilainen and Sillanpää, 2010), *i.e.* transform organic compounds such as humic substances, aminoacids or carbohydrates completely to inorganic compounds (CO_2 and H_2O among others). In practise, such a complete oxidation is not realistic from an economic standpoint, though. The matrix components scavenge the radicals and thus compete with the target compound for the oxidative species. Therefore, the process is more inefficient. Although the attachment of an oxygen atom to a molecule is less problematic than its chlorination, the toxicity and persistence of oxygenated products can not be neglected.

The generation of ROS can be carried out by the so-called *advanced oxidation processes* (AOPs). These technologies are aimed at generating hydroxyl radicals. There are many types of AOPs. A first group is purely chemical, *e.g.* the *Fenton reaction*, which is based on the heterolytic splitting of hydrogen peroxide upon reaction with a ferrous salt. The reaction produces a hydroxyl radical and a hydroxide ion (eq. 1.1). Some AOPs (for example $\text{O}_3/\text{H}_2\text{O}_2$) use and even destroy ozone in the process of hydroxyl radical generation. In this way, they achieve enhanced oxidation potentials.



Other processes use an energy source in combination with chemicals, *e.g.* *hydrogen peroxide photolysis* ($\text{UV}/\text{H}_2\text{O}_2$). In contrast to the Fenton reaction, $\text{UV}/\text{H}_2\text{O}_2$ makes use of the homolytic cleavage of H_2O_2 into two $\text{HO}\cdot$ through ultraviolet light (Figure 1.1b). It is also possible to combine the Fenton reaction with a source of visible light to recycle iron. In that case, the process is called *photo-assisted Fenton reaction* or just *photo-Fenton reaction* (eq. 1.2 and Figure 1.1c). Both the Fenton reaction and $\text{UV}/\text{H}_2\text{O}_2$ are *homogeneous AOPs*. In these, hydroxyl radicals emerge in the bulk of the solution, with no concentration gradients throughout the volume.

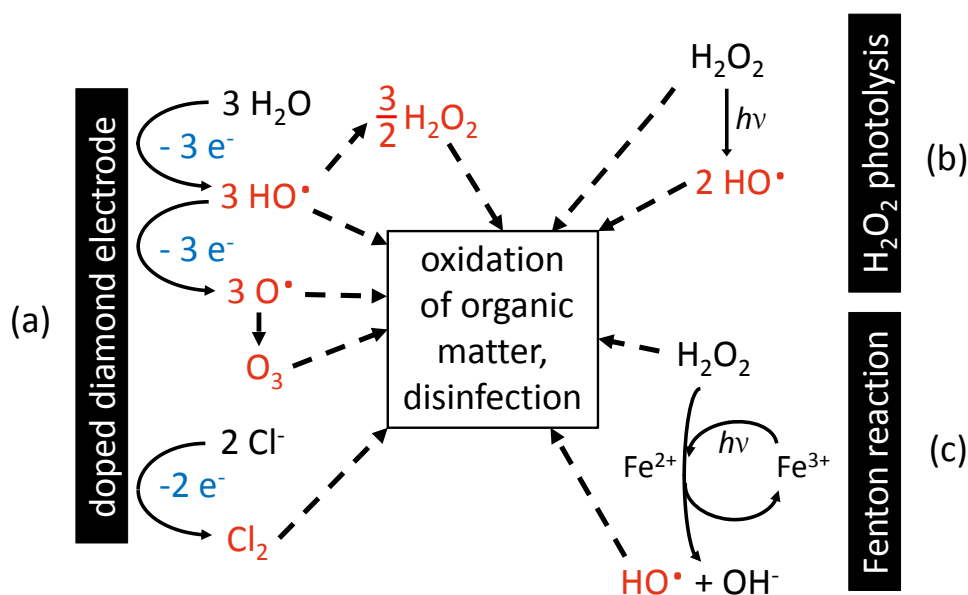


Figure 1.1 – Working principles of (a) boron-doped diamond (BDD), (b) hydrogen peroxide photolysis (UV/H₂O₂) and (c) the (photo-)Fenton reaction.

A final group of AOPs uses no chemicals, but only an energy input. This group includes sonolysis, which produces HO[•] directly from water through the cavitation produced by ultrasound waves (Méndez-Arriaga et al., 2009). Furthermore, electrochemical methods are included in this category. These are also called *electrochemical advanced oxidation processes* (EAOPs), and they work by generating the oxidative species directly from (waste)water. EAOPs belong to the *heterogeneous AOPs*, which are characterised by comparatively higher radical concentrations that are localised on an interface (*e.g.* electrode-solution, catalyst-solution). Commonly used electrodes are made of glassy carbon, lead dioxide (PbO₂) and boron-doped diamond (BDD, Section 1.3). Their utilisation is based on the special adsorptive characteristics of these materials. If water was plainly electrolysed to oxygen and hydrogen, the materials could not be used, at least not for water cleaning but rather for energy production. A requirement is that the electrode materials suppress the formation of oxygen and enforce the generation of stronger oxidising agents. The usual problem with conventional electrode materials is that the strong ROS produced attack the electrode itself, so that after some hours of operation, C is oxidised to CO₂ and "evaporates", whereas PbO₂ is solubilised as Pb²⁺ when the polarity is inverted (necessary to remove calcareous deposits from the electrode, Kraft et al., 2003), increasing the toxicity of the treated water (Switzer et al., 2006).

1.3 Boron-Doped Diamond Electrodes

Boron-doped diamond electrodes (BDDE) have gained attention as an easy-to-use and energy-efficient process for the generation of hydroxyl radicals directly from water (Pleskov, 2002; Michaud et al., 2003; Marselli et al., 2003; Kraft, 2007). This popularity lies on the unique properties of diamond.

1.3.1 Properties of Boron-Doped Diamond

First of all, diamond has a poor adsorption capacity. The diamond surface creates a high electrochemical overpotential for oxygen evolution. As a result, oxygen evolution is suppressed at low potentials and sets in only at potentials higher than required for the evolution of hydroxyl radicals. Thus, doped diamond is the material with the broadest potential window known in water (~ 3.55 V, Fujishima et al., 2005). Other oxidative reactions can take place within this potential window before oxygen evolves. This also opens the possibility of application in sensor technology.

A second important property of diamond is its inertness to most chemical reagents. Owing to the very strong sp^3 bonds in its lattice structure, this carbon allotrope is not only one of the hardest materials known, but it also possesses extremely high chemical stability. Practically, this means that the electrode does not corrode with the oxidants it generates (Pleskov, 2002).

Diamond itself is a non-conductor (isolator) because it has no free electrons. In order to use it as an electrode material, it is necessary to dope it (Pleskov, 2002; Comninellis and Chen, 2009). What doping does is to replace other elements for carbon at certain positions of the diamond lattice. Such impurities must have a different number of valence electrons than carbon. A fewer electron, as in the case of boron, introduces a movable charge into the lattice by creating bond gaps. In terms of the molecular bands in the material, doping with boron reduces the total amount of electrons in the lattice and partially empties the valence band. Consequently, the positive charges can move along the material (*i.e.* the electrons flow to fill the holes) and electricity is conducted. The dopant (boron) concentration needs not be higher than 8000 ppm (Fryda et al., 2003). Doping with boron to produce a p-type semiconductor is more efficient than using for example nitrogen to create an n-type semiconductor (May, 2008).

1.3.2 Fabrication of Conductive Diamond Electrodes

Diamond electrodes are produced by chemical vapour deposition. This process consists in the deposition of carbon and boron atoms onto a carrier material (the substrate). An appropriate substrate material is for instance niobium, because the junction overvoltage is low and Nb is thermostable, so that it does not expand or contract much upon heating. A flow of hydrogen gas (96–99 %) containing 10–200 ppm diborane and the rest of methane (0.5–2.5 %) is decomposed on a hot filament at 2200–2600 °C into its elements. Next, the hot atom flow encounters the substrate, which is considerably colder than the gas (700–925 °C). As a result, the

atoms deposit on the surface of the carrier. If a C atom adopts a false allotropic form such as amorphous carbon, it is quickly reduced by the passing gas to methane and "evaporates". If the next C atom adopts the correct diamond form, its bonds to the neighbouring atoms are so strong that it does not detach.

The process is carried out at low pressure (10–50 mbar) to avoid the recombination of the atoms in the hot gas flow before they reach the substrate. Diamond film growth rates of 0.2–1.0 $\mu\text{m}/\text{h}$ with a B concentration of 500–50 000 ppm in the film are attained (Honda et al., 2013; Kapałka et al., 2009; Michaud et al., 2003). The resulting resistivities of the so-produced diamond are between 5–100 $\text{m}\Omega\text{cm}$ (Fryda et al., 2003).

1.3.3 Oxidant Generation on Boron-Doped Diamond

Diamond electrodes have the ability to generate very strong oxidants directly from water (Fujishima et al., 2005). It is described in literature that the primary reaction taking place on BDD is the formation of hydroxyl radicals either from water (eq. 1.3, Michaud et al., 2003) or hydroxide (eq. 1.4, Bergmann, 2010).



Radical species are in general extremely reactive and undergo diverse chain reactions. Two $\text{HO}\cdot$ may combine with each other to form hydrogen peroxide (eq. 1.5, Michaud et al., 2003).



The combination can retrieve water, too, and generate an oxygen radical as reported by Babak et al. (1994) in eq. 1.6. An alternative mechanism of oxygen generation is shown in eq. 1.7, where atomic oxygen arises from the oxidation of hydroxyl radicals.



These reactions start a pathway leading to molecular oxygen (eq. 1.8) and finally ozone (eq. 1.9). The oxygen species in these equations do not adsorb on BDD as effectively as on *e.g.* PbO_2 (Panizza and Cerisola, 2005), which would actually hamper eqs. 1.7-1.9. However, ozone formation is observed even in electrolyte-free media when a solid polymer membrane at zero-gap (direct contact) to the electrode is employed (Kraft et al., 2006b). The role of the membrane is to confine the activated oxygen to the diamond surface, increasing its density and thus the ozone formation rate.



In addition, the membrane enhances the proton transport to the cathode, where protons are reduced to hydrogen gas (eq. 1.10).



Although it is not possible to establish a fixed mass balance of radical reactions, it is likely that the formation of ozone according to eqs. 1.6 to 1.9 involves the reaction of six hydroxyl radicals (eq. 1.11). The residual hydrogen atoms would reduce at the cathode.



A mix of oxidants (O_3 , H_2O_2 , $\text{HO}\cdot$, $\text{O}\cdot$ and further radicals), together termed ROS, is then available for oxidation. In real waters, some additional oxidative species may form through reactions with the inorganic components, such as free chlorine from chloride. BDDs can generate a mix of all of these oxidants ($\text{HO}\cdot$, $\text{O}\cdot$, $\text{Cl}\cdot$ and further radicals; H_2O_2 , O_3 , O_2 and Cl_2) during the electrolysis of water and represent a very promising alternative for water treatment (Figure 1.1a).

1.4 Fate of the Oxidants in Aqueous Solutions

1.4.1 Ozone and Hydroxyl Radical Reactions

Ozone is an electrophile and reacts with electron-rich organic compounds, preferentially with moieties like double bonds, activated aromatic rings and deprotonated amines (Heim and Glas, 2011). When these compound classes are present in water, ozone loses stability as it reacts with rate constants in the order of $10^6 \text{ M}^{-1}\text{s}^{-1}$ (von Gunten, 2003a). With electron-poor compound classes, the rate constants of O_3 can be low ($10^{-1} \text{ M}^{-1}\text{s}^{-1}$) to not measurable. Ozone can be used to exert oxidation away from the electrode surface, for instance in reactor or bottle cleaning in the food and drink industry (Heim et al., 2011) and in the disinfection of medical equipment.

Opposite to ozone, $\text{HO}\cdot$ are more powerful oxidants (Table 1.1) and thus extremely highly reactive with an estimated half-life of 1 ns (Sies, 1993). The extremely low steady-state concentration of $\text{HO}\cdot$ during ozonation processes ($\leq 10^{-12} \text{ M}$) reflects this fact (Elovitz and von Gunten, 1999). Kapałka et al. (2009) derived an equation to simulate the concentration of $\text{HO}\cdot$ in dependence of the distance to the electrode surface. Their range of action is limited to 1 μm above the surface, so that $\text{HO}\cdot$ can not diffuse away from the electrode. Consequently, $\text{HO}\cdot$ can be used for oxidation as long as the pollutants to be destroyed are brought into contact with the electrode. Hydroxyl radicals react with both inorganic and organic compounds with kinetic rate constants in the order of $10^7 - 10^9 \text{ M}^{-1}\text{s}^{-1}$, which means that its reactions are diffusion controlled. Hydroxyl radicals form not only from water electrolysis at BDD, but also from ozone decay.

Table 1.2 – Half-lives of dissolved ozone in water (pH= 7) at different temperatures (Lenntech, May 2012).

T (°C)	half-life (min)
15	30
20	20
25	15
30	12
35	8

1.4.2 Ozone Decay

Ozone is an unstable gas in water that has to be produced at the point of use (Gottschalk et al., 2010). It is ten times more soluble in water than oxygen (around 500 mg/L at 1 atm and 20 °C, von Sonntag and von Gunten, 2012, chap. 2). Its solubility depends on the Henry's Law (eq. 1.12 where p_{O_3} is the partial O_3 pressure, b_{O_3} the molality of ozone in solution and K_{O_3} the Henry's constant for O_3 in water (= 0.0126 mol/(kg·bar) at 20 °C, National Institute of Standards and Technology), which in turn is strongly dependent on temperature.

$$p_{O_3} = b_{O_3} K_{O_3} \quad (1.12)$$

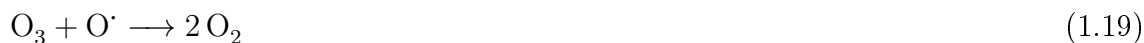
However, high ozone concentrations are hardly achievable in real waters. There are several factors by which ozone decay is favoured in practise, so that the observed steady-state concentration does not represent the solubility concentration (Roth and Sullivan, 1981). First, temperature plays a very important role in ozone stability. Sotelo et al. (1989) reported that an increase from 10 °C to 50 °C reduced the steady-state ozone concentration from 11 mg/L to 1 mg/L in sodium phosphate. In the same way, the efficiency of electrochemical ozone production increased from 13 % to 32 % when reducing the temperature from 10–15 °C to –15 °C during the electrolysis with PbO_2 anodes in phosphoric and perchloric acids (da Silva et al., 2003). In pure water, the ozone half-life is around 20 min at 20 °C and it reduces to 12 min at 30 °C (Table 1.2).

Second, the pH value of water affects ozone stability. Von Gunten (2003a) stated that the decay of ozone is initiated by hydroxide according to eq. 1.13. Hydroperoxide results from the initiation and it can decompose ozone to hydroxyl and superoxide radicals (eq. 1.14). Superoxide radicals contribute to further ozone decomposition, which results in more hydroxyl radicals. The first step of the long reaction sequence is shown in eq. 1.15; for more details, refer to von Gunten (2003a).



Third, as seen in Figure 1.1a, BDD produces an "oxidant cocktail" at the anode. It means that ozone will meet several oxidants both at the electrode surface, with high

local concentration of ROS and oxygen ions, and in solution. These species can act as ozone scavengers as seen in equation 1.16. The so formed hydrogen superoxide radical is present at pH 4.8 in both dissociated and non-dissociated form (eq. 1.17), so that the superoxide radical ion could proceed with ozone scavenging according to eq. 1.15 and 1.18. Other ROS may as well take part in the decomposition of ozone. Reaction with atomic oxygen (eq. 1.19) or hydrogen superoxide radical (eq. 1.20) in the vicinity of the electrode could convert ozone to oxygen (Holleman et al., 2007; Sotelo et al., 1987). Furthermore, as described in Section 1.2, the combination O_3/H_2O_2 is used to produce hydroxyl radicals from ozone (by decomposing it).



Ozone can react with species generated at the cathode as well, if the set-up of the electrolytic cell allows for contact, or if the reactor is operated in recirculation (as is the case in this work). When the dissolved ozone completes one cycle in the reactor, it comes into contact with nascent hydrogen, which can reduce passing ozone according to eq. 1.21 and 1.22 (Sehested et al., 1983). Equation 1.23 shows a termination mechanism for the hydrogen superoxide (Sotelo et al., 1987).



Reactor set-up also influences the effective partial pressure exerted on the water, on which ozone dissolution depends.

Last but not least, ozone can be consumed by the water components (Chapter 5). When ozone reacts with inorganic compounds, by-products can form (Chapter 6).

1.5 By-Product Formation

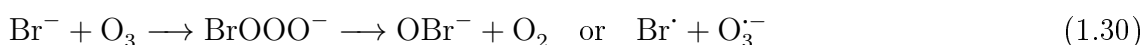
Only in rare cases does one have a solution of a pure pollutant to treat. More commonly, the pollutant to eliminate is just one component of a more complex wastewater. Thus, the further compounds present in water compete with the target pollutant for the oxidant species. By-products of two types form from these competence reactions. The first class consists of halogenated organic compounds, while the second class comprises inorganic halogen ions in high oxidation states.

Von Gunten (2003b) described the oxidation of chloride (eq. 1.24) by hydroxyl radicals ($E_{\text{red}}^\ominus = 2.80 \text{ V}$, eq. 1.25 and 1.26). Ozone ($E_{\text{red}}^\ominus = 2.08 \text{ V}$) is not strong enough

to bring about this oxidation.



Similar equations have been demonstrated for bromine (eq. 1.27 to 1.29), except that bromide can additionally be oxidised by ozone (eq. 1.30).



The so formed halogen atoms (from eq. 1.26 and 1.29) or hypohalogenous acids can react with organic substances and halogenate them. As a result, halogenated by-products, which can be measured as *adsorbable organically bound halogens* (AOX), are created (eq. 1.31 and 1.32 exemplary for the reaction of natural organic matter (NOM) with Br, von Gunten, 2003b; Anglada et al., 2011; Kraft et al., 2003).



Because the presence of both organic matter and halides is required for by-product formation, they are called *AOX precursors*. Halogenated compounds are, generally speaking, more resistant to further oxidation than their non-halogenated counterparts (Boudreau et al., 2010). Eventually, at advanced treatment stages, the formed AOX can be mineralised at BDD (Kraft et al., 2003), but this is usually bound to treatment costs above those thinkable for water treatment applications.

Trihalomethanes (THMs) are a subgroup of AOX and are believed to be human carcinogenic compounds (Reemtsma and Jekel, 2007, chap. 10). For instance, the United States Environmental Protection Agency (EPA) has regulations for THMs. Total THMs must not exceed an annual average of 80 $\mu\text{g/L}$ in drinking water.

A further by-product class comprises inorganic ions. In chloride-rich waters, chloride becomes chlorite, chlorate and perchlorate upon prolonged treatment times (Polcaro et al., 2008, 2009). Bromide is oxidised in a similar fashion. The carcinogenic bromate forms in bromide-containing waters (Bergmann et al., 2011).

It is not always disadvantageous to have chloride oxidised upon treatment though. Free chlorine plays an important role in disinfection (Cho et al., 2010), so that chloride-rich waters could provide a significant antimicrobial effect during electrolysis. Generally speaking, there is a trade-off between efficient disinfection and by-product formation (Reemtsma and Jekel, 2007, chap. 10). The longer the treatment time, the higher the disinfection grade, but the more by-products form.

By-products ought not to be confused with transformation products. *Transformation products* are those organic compounds that result from the oxidation of a target pollutant, "daughter compounds". They are indicative for an effective treatment and thus desired. *By-products* stem from competitive reactions of the accompanying water matrix components and diminish the energy efficiency of treatment. They do not necessarily lead to a degradation of the target pollutants. When they do, they halogenate the transformation products, which renders them more refractory. By-products are hence unwanted.

1.6 State of Knowledge and Objectives of this Work

Previous studies on BDD have focused on three aspects: the mechanisms of oxidant production, the treatment of diverse target compounds or wastewaters and further applications of BDDEs such as chemical analysis or synthesis. The first two aspects are directly relevant to wastewater treatment.

Doped diamond has been shown to produce hydroxyl radicals and ozone directly from water (Pleskov, 2002, and references therein). Several studies have focused on the working principle of BDD (Pleskov, 2002; Michaud et al., 2003; Kapałka et al., 2009) and on the role of current density (Kraft et al., 2006b; Frontistis et al., 2011) and flow rate (Kraft et al., 2006b) in oxidant formation. However, the relationship between the current density and the formation of different oxidants has not been extensively studied yet, let alone the consequences that different oxidising agents have on the removal efficiency of persistent compounds and by-product formation. Understanding that relationship would be very valuable, as the relative importance of individual oxidants can vary depending on the treatment goal (Section 1.2).

Therefore, Chapter 4 studies the influence of the current density on the formation of hydroxyl radicals and ozone. The yields of radical and ozone formation are further assessed in Chapter 4 and compared to conventional ozonators. This comparison is based on the methodology introduced in Chapter 3, which allows for the evaluation and comparison of the energetic requirements of unlike reactor technologies.

An overall reduction of the *chemical oxygen demand* (COD) in complex water matrices such as model phenolic waters (Tröster et al., 2004) and hardening plant wastes (Schmalz et al., 2008) has been reported. In order to extend knowledge in this area, CBZ was treated in various synthetic and natural water matrices containing increasing concentrations of background ions and organic matter. Chapter 5 deals first with ozone formation in the different water matrices and evaluates ozone availability in them. Furthermore, the fate of CBZ in these waters is investigated. Energetic costs for the elimination of CBZ in the various waters are calculated. The reactions between the inorganic ions and the organic compounds contained in the water upon electrolysis produces halogenated by-products. This topic is addressed in Chapter 6. The action of the different oxidant species on the oxidation of CBZ and by-product formation is emphasised.

Researchers reported that BDDEs were suitable also for disinfection purposes (Schmalz et al., 2009; Haaken et al., 2010; Frontistis et al., 2011), as well as

simultaneous disinfection and target pollutant removal (Frontistis et al., 2011). Nevertheless, no differentiation of the oxidant species was performed in literature. Chapter 7 evaluates the disinfection of three bacterial strains, namely *Escherichia coli*, *Enterococcus faecium* and *Pseudomonas aeruginosa* with BDD in dependence on the current density applied and thus on the oxidant species involved. The influence of the water matrix on disinfection is evaluated as well and information on by-product formation and the simultaneous oxidation of CBZ and disinfection is provided.

Other studies with BDD investigated the degradation of various different pollutant classes, ranging from phenols, chlorophenols and surfactants (Panizza and Cerisola, 2005) to lubricants, dyes, soluble polymers, drugs (Kraft, 2007) and estrogen hormones (Frontistis et al., 2011), to name a few. The effect of pollutant concentration (Panizza and Cerisola, 2005; Frontistis et al., 2011), temperature (Cañizares et al., 2004), pH value (Cañizares et al., 2004; Rodrigo et al., 2010) and treatment time (Tröster et al., 2004; Frontistis et al., 2011) have also been studied. However, very few studies dealt with specific degradation products, nor did they work on reaction pathways. Understanding these, not only from a theoretical but also from an experimental point of view, should be an important step toward a thorough characterisation of every new technology.

Chapter 8 thus examines the degradation of two model compounds, sulfamethoxazole and CBZ with BDD and compares their transformation products with those reported in literature for the ozone and hydroxyl radical pathways. Moreover, Chapter 8 keeps track of the degradation products until they are themselves oxidised and offers an energetic evaluation of the diamond electrode, not only regarding the treatment of these model compounds but also in comparison to a further AOP. This investigation provides an additional and novel proof that the oxidising agents generated by BDD are truly hydroxyl radicals and ozone. By using different current densities, insights are gained into the mechanisms of oxidant production and their effects on pollutant removal.

In short, this PhD thesis is aimed at characterising a BDDE regarding the oxidant species it produces at different current densities. It evaluates the consequences that the formation of these oxidants has on the treatment of persistent pollutants in various waters, bacteria inactivation and by-product formation. Furthermore, it offers an energetic comparison for treatment in different waters as well as with different AOP reactors. The ultimate goal is to study the suitability of BDDEs for quaternary treatment in STPs.

Chapter 2

Materials and Methods

2.1 Chemicals

The following chemicals (p.a., Merck, Germany) were utilised: 5,5'-indigodisulphonic acid sodium salt (indigo carmine, IC), phosphoric acid (85 %), sodium hydroxide, sodium sulphite, hydrogen peroxide (30 %) and nitric acid (65 %). Additionally, N,N-dimethyl-4-nitrosoaniline (RNO, p.a.) and ferrous sulphate heptahydrate (reagent grade) were purchased from Sigma-Aldrich (USA). Sulphuric acid (for analysis) was purchased Carl Roth (Karlsruhe, Germany). For the preparation of the different water matrices, the following salts (p.a.) from the company Merck were used: calcium chloride, potassium bromide, potassium iodide, magnesium sulphate heptahydrate, sodium hydrogen carbonate and sodium nitrate. Additionally, bovine serum albumin (BSA, for biology, Merck, Germany) and native humic acid (30–40 %, soil extract, Carl Roth, Germany) were utilised as a source of organic matter for the artificial waters. The water matrices were prepared by dissolving the corresponding salts and organic compounds in deionised water (conductivity: 0.055 $\mu\text{S}/\text{cm}$ at 25 °C, produced with a deioniser "Milli-Q Plus 185").

Six water matrices, of which five had fixed compositions, were employed (Table 2.1). Besides deionised water, two model waters (resembling soft and hard potable water) and two artificial water matrices with organic matter were investigated. As a sixth water matrix, the real effluent of the sewage treatment plant (STPE) in Garching (urban area of Munich, Germany) was studied (variable composition). This sewage treatment plant is connected to 31 000 population equivalents and uses mechanical as well as biological treatment. STPE samples were collected on weekdays at 08:45 am after secondary sedimentation (and before the last step of UV disinfection applied in the bathing season). Some chemical analyses of STPE can be found in Table 2.1. For clarity, these six water matrices get the suffix "-p" when they are pharmaceutical-spiked (Chapters 5, 6 and 8) and the suffix "-b" when they are bacteria-spiked (Chapter 7). The suffix "-pb" is used when they were spiked with both, a pharmaceutical substance and bacteria (Chapter 7).

Carbamazepine and sulfamethoxazole were purchased from Sigma-Aldrich (USA). Stock solutions of both pharmaceutical substances in deionised water ($[\text{CBZ}] = 44 \mu\text{M}$, $[\text{SMX}] = 100 \mu\text{M}$) were diluted for individual experiments. The amount of

pure water in the water matrices containing CBZ was adapted so that all final concentrations remained equal. Only for STPE did the addition of CBZ (normally 437 mL) to an STPE volume of 3062 mL imply a dilution of 0.875:1.

2.2 Reactors

Figure 2.1 schematically shows the reactors built for the oxidation experiments.

2.2.1 Diamond Electrode System (BDD)

The conductive diamond system (BDD, termed DD in Chapter 8, Figure 2.1a) consisted of a controlling unit (CONDIAPURE[®], CONDIAS, Germany) with a pump (PY-2071, Speck Pumpen, Germany) linked to an electrolytic glass chamber with a volume of 0.092 L (numbers 5, 7, 8 and 9 in Figure 2.1a, Esau&Hueber, Germany) and an ozone mixing chamber (9 in Figure 2.1a). The electrode stack (DIACHEM[®]) comprised one cathode and one anode (active surface area of $24 \times 50 \text{ mm}^2$ each) of boron-doped diamond (1–5 μm thickness) on a niobium substrate. The electrodes were placed in direct contact (zero gap) to a Nafion cation exchange membrane, which locally increases the current density in the vicinity of the contact points, hence promoting ozone formation and enabling operation at very low conductivities (Kraft et al., 2006b). Through two hoses, the system was connected at its input and output (recirculation, flow rate: 4.0 L/min) with a cooled ($20 \pm 1^\circ\text{C}$) vessel containing the solution to be treated. The applied current was adjustable between 0.0 and 10.0 A.

2.2.2 Miniaturised Diamond Electrode Coupled to Mass Spectrometry (DD*)

A flow-through electrochemical cell from the company Antec (The Netherlands) was employed (DD*, refer to the amperometric thin-layer cell described by Baumann and Karst (2010) and see Figure 2.1b). It consisted of a ROXYTM-potentiostat equipped with a μ -PrepCellTM electrolysis cell bearing a boron-doped diamond electrode ("Magic Diamond") with $30 \times 12 \text{ mm}^2$ active surface area and 11 μL reaction volume. With a syringe pump, a 10 μM CBZ or SMX solution in Milli-Q water was pumped at 50 $\mu\text{L}/\text{min}$ into the tempered electrochemical cell. The electrochemical potential of the working electrode was increased at 10 mV/s from 0 to 2.4 V. The cell was kept at a temperature of $35 \pm 2^\circ\text{C}$ during the experiment. From the cell, the flow was nebulised in a jet stream electro-spray ionisation (ESI) source and the resulting ions were detected with a high-accuracy mass spectrometer. The DD*-measurements were carried out in duplicate.

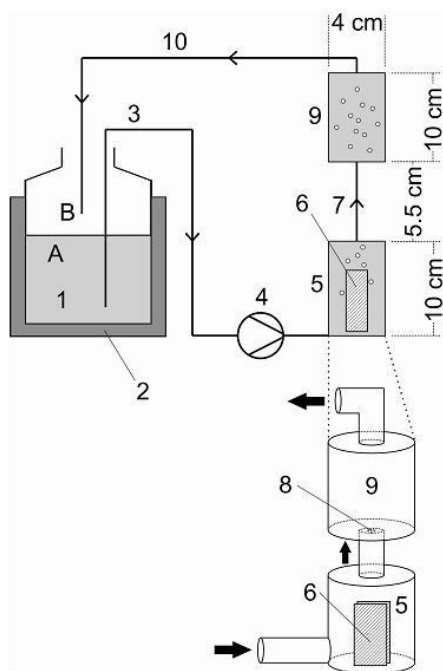
Table 2.1 – Chemical composition of the employed water matrices.

chemical	units	deionised(-p)	<i>soft</i> (-p)	<i>SORG</i> (-p)	<i>hard</i> (-p)	<i>HORG</i> (-p)	STPE(-p)
calcium	mg/L	n.d.	11.3	11.3	141.3	141.3	78.5
magnesium	mg/L	n.d.	15.2	15.2	50.6	50.6	21.1
hydrogen carbonate	mg/L	n.d.	122	122	122	122	284
bromide	mg/L	n.d.	0.1	0.1	1.0	1.0	0.116
nitrate	mg/L	n.d.	10.0	10.0	50.0	50.0	48.5
chloride	mg/L	n.d.	20.0	20.0	250	250	150–215
sulphate	mg/L	n.d.	60.0	60.0	200	200	45.4
iodide	mg/L	n.d.	n.a.	n.a.	0.1	0.1	<LOD
DOC	mg/L	n.d.	n.a.	n.a.	n.a.	n.a.	6–13
TOC (BSA and humic acids)	mg/L	n.d.	n.a.	2	n.a.	5	n.d.
pH	-	7.0	8.9	9.0	8.7	8.9	8.0
conductivity	µS/cm	0.055	382	351	1230	1202	1150

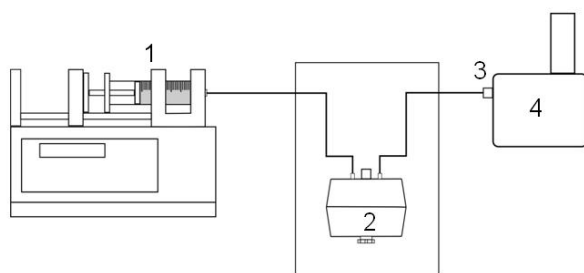
soft: soft drinking water; *SORG*: soft drinking water with added organic matter; *hard*: hard drinking water; *HORG*: hard drinking water with added organic matter; STPE: sewage treatment plant effluent; DOC: dissolved organic carbon; TOC: total organic carbon; n.a.: not added; n.d.: not determined; <LOD: under the limit of detection.

(-p): pharmaceutical-spiked (carbamazepine, sulfamethoxazole), details in Section 2.3.4

(-b): bacteria-spiked, details in Section 2.3.6



(a) BDD

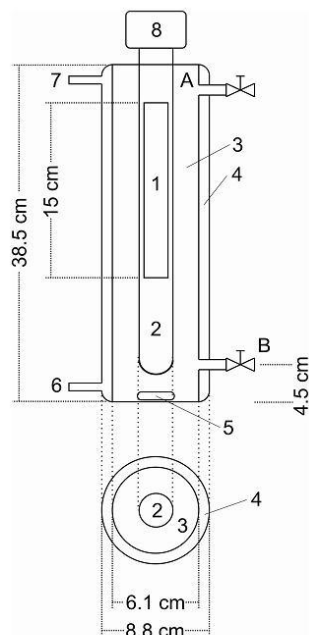


(b) DD*

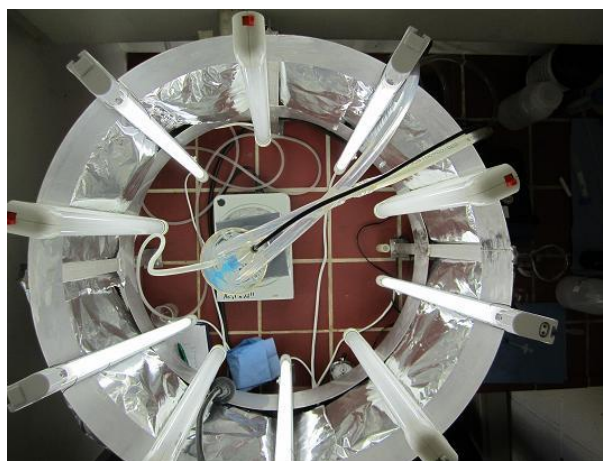
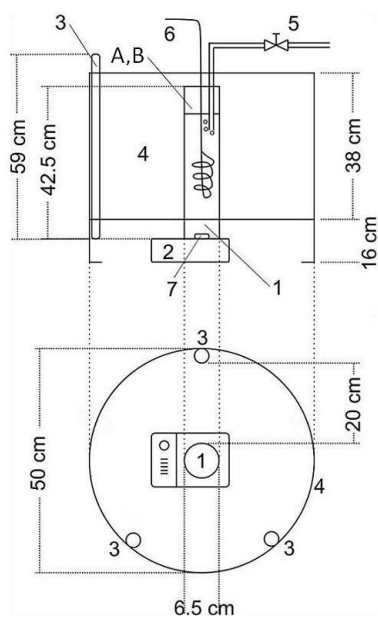
Figure 2.1 – Schemes and photographs of the employed (a) boron-doped diamond (BDD) electrode reactor and (b) miniaturised BDD coupled to mass spectrometry system (DD*).

(a) **Boron-doped diamond electrode** – 1: reaction solution; 2: ice bath; 3: inlet hose; 4: recirculation pump; 5: electrode chamber; 6: diamond electrode; 7: connecting piece; 8: 6 mm-nozzle; 9: ozone mixing chamber; 10: outlet hose; A: sensor point; B: sampling point.

(b) **Miniaturised BDDE coupled to mass spectrometry** – 1: syringe pump; 2: tempered electrochemical cell; 3: jet stream ESI source; 4: high-accuracy mass spectrometer.



(c) UV/H₂O₂



(d) photo-Fenton

Figure 2.1 – (continued) Schemes and photographs of the employed (c) hydrogen peroxide photolysis (UV/H₂O₂) and (d) photo-Fenton reactors.

(c) **Hydrogen peroxide photolysis.** – 1: UV-lamp; 2: submerging unit; 3: reaction solution; 4: cooling jacket; 5: magnetic stirrer; 6: cool water inlet; 7: cool water outlet; 8: lamp socket; A: sensor point; B: sampling point.

(d) **Photo-Fenton reactor** – 1: quartz reactor with reaction solution; 2: stirrer; 3: fluorescent lamps; 4: irradiation scaffold; 5: air bubbling; 6: cooling hose; 7: magnetic stirrer; A: sensor point; B: sampling point.

2.2.3 Hydrogen Peroxide Photolysis (UV/H₂O₂)

The hydrogen peroxide photolytic reactor (UV/H₂O₂, termed HP in Chapter 8, Figure 2.1c) consisted of a 0.9 L cylindrical glass reactor with a cooling jacket made of brown glass for visual protection. A low-pressure, mercury-vapour UV lamp (Heraeus GPH 212 T5L/4, ozone-free, 10 W, UV-Consulting Peschl, Germany) in a submerging quartz unit (Tauchrohr System 25/354-10L, Deconta, Germany) was placed in the middle of the reactor. A stopcock on the bottom of the cylinder served for sample extraction. The solution was magnetically stirred at 700 rpm and the temperature was kept at 20 ± 1 °C.

2.2.4 Photo-Fenton Process

The photo-Fenton reactor (Figure 2.1d) comprised a quartz glass cylinder (1.0 L) surrounded by an irradiation scaffold bearing three fluorescent lamps of the type "Osram Luminix De Luxe Daylight L 13W/954". The solution was magnetically stirred. Air was bubbled through the upper part of the solution to improve mixing at the top (Soriano, 2010). Cooling to 20 ± 1 °C was carried out with a coiled hose connected to a cooling water system and submerged in the reaction solution.

2.3 Methods

2.3.1 Cumulative Measurements of Reactive Oxygen Species

Based on the ozone determination by Bader and Hoigné (1981) and the hydroxyl radical determination by Kraljić and Trumbore (1965), an experimental set-up was worked out. Solutions of indigo carmine (26.7 µM, pH around 5.3, uncontrolled, total volume 3.0 L) and RNO (40 µM, pH = 9, controlled, total volume 2.0 L) in pure water were circulated and treated in the BDDE reactor. The reactor was run at the following current densities: 42, 83, 125, 167, 208, 250, 292 and 333 mA/cm². The resulting potentials were between 5-10 V for IC solutions and 8-18 V for RNO solutions. The results are shown in Chapter 4.

Additionally, comparative runs with IC were carried out in the BDDE, UV and photo-Fenton reactors (Chapter 3) with fixed conditions (22.5 µM (= 10.5 mg/L), experimental parameters are shown in Table 2.2). The IC concentration was chosen in order to be able to observe one full order of magnitude (OM) in the absorbance values (until decolouration). The amounts of chemicals were chosen based on a series of experiments aimed at achieving a reaction time around 15 minutes. This would allow for comparability with the other AOPs, while minimizing the use of chemicals to keep costs down. The pH value (around 5.2) was left unadjusted, as it is favourable for the generation of oxidants (Anglada et al., 2011) and ions such as phosphate and sulphate are oxidised by HO[•] and interfere with measurements (Costa et al., 2009). Furthermore, by not having to regulate the pH, chemical costs were reduced and corrosion was prevented. Only for the photo-Fenton reaction was a pH range of 2.0–7.0 evaluated and the value of 4.0 was determined to be most favourable (data

not shown). A minimum reaction volume of 1.0 L was required so that sampling did not affect the reaction. Depending on the reactor set-up, it was not always possible to adhere to 1.0 L (submerging UV lamps, internal volume of the diamond electrode equipment). However, all measured energy values were normalised to the reactor volume. The photolytic systems were stirred at 700 rpm to ensure proper mixing of the entire volume, despite the presence of hydraulic obstacles (lamps, cooling hose). An optimum recirculation rate of 4 L/min for the BDDE was determined in preliminary experiments. At this flow rate, ozone transport into the solution was maximised. Finally, all systems were cooled to 20 ± 1 °C for the sake of comparability.

The reactors were sampled at different time intervals (between 10 s for reactions whose duration was under 3 min and 300 s for longer reactions), until the reaction was completed. The overall decolouration times are presented in Table 3.1, column t). For this purpose, 7.0 mL of the solution were pipetted from the corresponding point B (in Figure 2.1) and poured into two polymethyl-2-methylpropenoate (PMMA) cuvettes. Their absorbances were measured with a UV/Vis-spectrophotometer (UV-1601, Shimadzu, USA) at 610 nm (IC) or 440 nm (RNO). The average absorbance was used for further calculation. A solution was considered decoloured when its absorbance sank to approximately 0.050. The electricity consumption during operation was monitored. Besides the technology-specific devices like irradiation units and electrodes, mixing apparatuses (pumps and stirrers) were included, but neither sensors (thermometer, pH-meter) nor analytical devices were.

2.3.2 Residual Ozone Measurements in Water

In contrast to the method in Section 2.3.1, three litres of a water matrix were treated at 42, (83,) 208 and 333 mA/cm² for 30 min (for STPE 120 min) after which the current was turned off. The dye IC reacted with ozonated water samples after their extraction from the system, so that only ozone (and not radicals) were captured. The ozone concentrations at 0, 1, 2, 3, 5, 7.5, 10, 12.5, 15, 20 and 30 min were determined following the method by Bader and Hoigné (1981) and Yates and Stenstrom (2000) using phosphoric acid in place of phosphate buffer. The ozone decay was monitored with further measurements after 30 min. For *SORG*, *HORG*, STPE and bacteria-spiked solutions, the partially bleached indigo carmine solution was filtered through 0.45 µm-polyvinylidene difluoride (PVDF) filters in order to eliminate photometric diffraction by undissolved particles. All experiments were carried out at 20 ± 1 °C in duplicate or triplicate.

2.3.3 By-Products

The artificial water matrices with organic matter (*SORG* and *HORG*) were subjected to chemical analysis of THMs (chloroform, dichlorobromomethane, chlorodibromomethane, bromoform) and AOX after 0, 15 and 30 min of reaction at 208 and 333 mA/cm². Additionally, AOX were measured for STPE at the beginning and end of treatment. AOX samples (500 mL) were given 5 mL of a 1 M sulphite solution as ozone scavenger and 1 mL of concentrated HNO₃ to adjust the pH. THM samples (250 mL) were given 2.5 mL of the sulphite solution. All samples were vortexed for

Table 2.2 – Experimental parameters for the employed AOPs during the indigo carmine decolouration experiments.

	units	boron-doped diamond	H ₂ O ₂ photolysis	photo-Fenton
[IC]	µM	22.5	22.5	22.5
[H ₂ O ₂]	µM		294	1125
[Fe ²⁺]	µM			6.0
volume	L	3.0	0.9	1.0
pH	-	5.3	5.1	4.0 (adjusted)
temperature	K	293 ± 1	293 ± 1	293 ± 1
initiator	-	current power-on	UV lamp power-on	addition of H ₂ O ₂
stirring		4 L/min recirculation	700 rpm	700 rpm
repetitions	n	duplicate	duplicate	duplicate

30 s and then cooled to $4 \pm 2^\circ\text{C}$ in brown flasks. The AOX content was measured with an ABIMED TOX-10 organic halogen analyzer according to the standard method EN ISO 9562, DEV H14. The limit of detection (LOD) was $10\ \mu\text{g/L}$. THMs were measured on the basis of DIN EN ISO 10301, with an LOD of $0.1\ \mu\text{g/L}$, except for bromoform ($0.5\ \mu\text{g/L}$). Chloride and bromide were measured by ion chromatography with a DIONEX ICS-1000 device according to DIN EN ISO 10304-1, DEV E19 and a LOD of $0.05\ \text{mg/L}$ for bromide and chloride. All parameters are reported as the average of two single measurements and every experiment was carried out in duplicate.

2.3.4 Pharmaceutical Investigations

Carbamazepine Degradation in Different Water Matrices

CBZ solutions ($5.5\ \mu\text{M} \approx 1.3\ \text{mg/L}$) in the different water matrices were treated between 15 and 30 min (for STPE 60 min) with the diamond electrode. Samples were taken in time intervals ranging between 1 and 10 min, filtered through $0.2\ \mu\text{m}$ cellulose filters, vortexed and measured with a time-of-flight mass spectrometer (see Section 2.3.5). Experiments were carried out at $20 \pm 1^\circ\text{C}$ in duplicate.

Characterisation of AOPs

SMX and CBZ solutions in deionised water were treated with HP (UV/ H_2O_2 , 25 min), DD* and DD (30 min). For DD, the working j was $42\ \text{mA/cm}^2$ (DD') for CBZ and SMX. Additionally, $208\ \text{mA/cm}^2$ (DD'') were applied for SMX. The reactors were sampled over the duration of treatment. For CBZ, different concentrations were tested ($10\ \mu\text{M}$ for DD*, $5.5\ \mu\text{M}$ for UV/ H_2O_2 and $1.0\ \mu\text{M}$ for DD'). An SMX concentration of $10\ \mu\text{M}$ was used for all technologies (HP, DD*, DD' and DD''). For HP, the applied hydrogen peroxide concentrations were: $[\text{H}_2\text{O}_2]_{\text{CBZ}} = 2.39\ \text{mM}$, $[\text{H}_2\text{O}_2]_{\text{SMX}} = 1.00\ \text{mM}$. The pH of all solutions was approximately 6.0. Pharmaceutical samples were filtered through a cellulose membrane ($0.45\ \mu\text{m}$) and stored at $4 \pm 2^\circ\text{C}$ until measurement. Experiments were carried out at $20 \pm 1^\circ\text{C}$ in duplicate.

2.3.5 Mass Spectrometry (MS)

A time-of-flight (ToF) mass spectrometer (Agilent 6230 Accurate-Mass ToF LC/MS, USA) was used for the analysis of pharmaceutical substances. Filtered pharmaceutical samples were directly injected into the mass spectrometer with a syringe pump (flow rate: $5\ \mu\text{L/min}$). A multimode ion source (MMI) in ESI mode produced the ions for measurement. A capillary voltage of 2500 V and a charging voltage of 2000 V were applied for the degradation experiments in different water matrices (Section 5.2.2). Jet Stream Electrospray Ionisation (JS-ESI) with a capillary voltage of 4000 V and a nozzle voltage of 1000 V was applied for the characterisation of AOPs (Chapter 8). A nitrogen stream of $5\ \text{L/min}$ at 250°C (325°C for DD* experiments) was used as the drying gas. The nebuliser pressure was set to 20 psig.

Measurements in positive and negative ionisation mode were carried out in the m/z -range from 70 to 1000. The signals were recorded for one minute and the average spectrum was used for evaluation.

Mass correction was executed with the Agilent API-TOF Reference Mass Solution Kit (part no. G1969-85001). For the HP and DD* treatment of SMX in positive mode, the m/z 922.0098 ($C_{18}H_{19}O_6N_3P_3F_{24}^+$) was used in addition to the reference masses (RMs) shown in Table 8.2. In negative mode, the m/z 252.0444, (SMX-H)⁻ and 955.9719 ($C_{18}H_{18}O_6N_3P_3F_{24}+Cl$)⁻ were employed. For CBZ, the RM used were m/z 121.0509, ($C_5H_4N_4+H$)⁺ and 922.0098, $C_{18}H_{19}O_6N_3P_3F_{24}^+$ for DD', the latter in addition for DD*, besides (CBZ+H)⁺ (Table 8.3).

2.3.6 Disinfection Experiments

Preparation of Bacteria Solutions

Bacterial strains of *Escherichia coli* (ATCC 11775) and *Pseudomonas aeruginosa* (ATCC 10145) were received from the Institute of Microbial Ecology at Technische Universität München. *Enterococcus faecium* (ATCC 19434) was cultivated from the bacteria collection at the Institute of Water Quality Control at Technische Universität München.

E. coli were cultured in 250 mL tryptophane bouillon (Merck Inc., Germany), *E. faecium* in 250 mL Luria Bertani (LB) bouillon containing 10.0 g/L tryptophane, 5.0 g/L yeast extract and 5.0 g/L NaCl at pH 7.0 and incubated at 37 ± 1 °C for 18 h with continuous shaking. Then, cells were collected by centrifugation at 6000 rpm for 6 min. Pellets were resuspended in 2 mL phosphate buffer saline (PBS) medium containing 8.0 g/L NaCl, 0.2 g/L KCl, 1.44 g/L Na_2HPO_4 , 0.2 g/L NaH_2PO_4 at pH 7.0 to form a stock solution of the microorganisms with an approximate bacterial density up to 10^9 – 10^{10} colony forming units (CFU)/mL. *P. aeruginosa* were cultured in the same way in PC bouillon containing 5.0 g/L caseine peptone, 2.5 g/L yeast extract and 1 g/L glucose at pH 7.0 with resuspension of the cell pellets using 16 mL of 1/4 concentrated Ringer's solution (Merck Inc., Germany), respectively. Aqueous bacteria solutions were prepared from 3 L of the particular water matrix that was spiked with the bacteria suspension to produce initial bacteria concentrations of approximately 10^7 – 10^8 CFU/mL. The temperature of the solution was kept at 20 ± 1 °C during electrode operation. Cultivation and analysis methods of the three bacteria strains are summarised in Table 2.3

Sampling

Samples were taken from point B (Figure 2.1a) at 0, 1, 5, 10, 15, 20 and 30 min of disinfection for determination of the number of CFU/mL, residual ozone concentration as well as chloride, dissolved organic carbon (DOC) and AOX. Samples from CBZ and bacteria-spiked water were taken after 2, 5, 10 and 15 min, filtered through 0.45 µm cellulose filters, vortexed and measured with mass spectrometry.

Microbial Analysis

The analytical methods used to determine the bacterial number for each sample were based on the German and International Standard Methods (DIN). According to the German Drinking Water Ordinance 2012, no bacteria should be detectable in a 100 mL water sample. Based on those methods, 100 mL of bacteria solutions were filtered through 0.45 μm cellulose nitrate filters (Sartorius, Germany), which were then either placed directly into the medium tubes or onto the agar plates. Briefly, *E. coli* solutions were cultivated in 4-methylumbelliferyl- β -D-glucuronide (MUG) lauryl sulfate bouillon after filtration. Dilution series were established in PBS solution and incubated for 24 h at $37 \pm 1^\circ\text{C}$. Bacteria were counted according to the most probable number (MPN) method. *E. faecium* was cultivated according to ISO 7899-2 and incubated for 48 h at $37 \pm 1^\circ\text{C}$. *P. aeruginosa* solutions were diluted with 1/4 concentrated Ringer's solution. After filtration according to ISO 7899-2 membrane filters were placed on selective agar (ISO 12780:2002 CP67.1) and incubated for 48 h at $37 \pm 1^\circ\text{C}$. Based on the change in the bacterial count of the sample after a certain disinfection period, the inactivation rate was calculated as the logarithmic reduction of bacteria ($\log(N/N_0)$), with N_0 and N representing the initial and the sample bacterial counts, respectively.

2.3.7 Further Measurements

The total organic (TOC) and dissolved organic (DOC) carbon were measured with an Elementar high TOC II-analyzer according to EN 1484, DEV H3 prior to and after filtration through a 0.45 μm polypropylene membrane filter, respectively (LOD: 0.5 mg/L). The pH was measured according to DIN EN ISO 10523, DEV C5 with a WTW pH-electrode SenTix 41 and the pH-meter was of the type WTW pH 197-S (Germany). The dissolved oxygen concentration of the water matrices was measured with a WTW CelloX 325 electrode and a WTW multi 340i meter (Germany). The electricity consumption of all systems was monitored during operation with a Voltcraft energy monitor 3000.

2.3.8 Charge Input per Volume (Q/V)

Generally speaking, a depiction of all measurements not against time but against the charge input per volume is more accurate, as it normalises the measurements to the energy (introducing an association to efficiency) and the volume, even considering the volume reduction upon sampling (association to experimental set-up). The Q/V was calculated for every BDD experiment by subtracting the sampling volume from the total volume at every sampling time to get the actual volume. The sampling time was multiplied with the current applied and the result was then divided by the actual volume in the system. The calculus was carried out automatically with the aid of a spreadsheet chart.

Table 2.3 – Summary of cultivation and analysis methods for *E. coli*, *P. aeruginosa* and *E. faecium*.

microorganism	cultivation	resuspension / dilution series	analysis method
<i>E. coli</i>	tryptophane bouillon	PBS medium	MUG lauryl sulfate bouillon ^a
<i>P. aeruginosa</i>	PC bouillon	1/4 Ringer's solution	filtration: DIN EN ISO 7899-2 cultivation: EN ISO 12780:2002 CP67.1
<i>E. faecium</i>	LB bouillon	PBS medium	DIN EN ISO 7899-2

^a determination of bacteria numbers according to the MPN method.

Table 2.4 – Commercial chemical substances and the conversion of their price to energy values.

chemical	company	art. no.	volume (L)	%	ρ (g/mL)	price (€)	kg	€/kWh	€/kg	Wh/kg
H ₂ O ₂	Carl Roth	CP26	25	30.0	1.11	81.6	8.33	0.2495	9.80	39.29
FeSO ₄ · 7 H ₂ O	Carl Roth	3722	-	99.5	-	155.7	24.88	0.2495	6.26	25.09
H ₂ SO ₄	Carl Roth	971	25	95.0	1.84	88.7	43.70	0.2495	2.03	8.14
H ₂ O ₂ [1]	-	-	-	100	-	-	1.00	-	-	10.00

[1]: Müller and Jekel, 2001.

2.3.9 Calculation of Energy Consumption

Bolton et al. (2001) described figures of merit for different AOPs. With these, it is possible to normalise the efficiency of an AOP to enable comparability. The method by Bolton was extended to consider individual energetic components (see Chapter 3). The electrical energy per order of magnitude (E_{EO}) for the decolouration of IC was calculated according to the extended method as follows. For every sampling time, the number of orders of magnitude for the decolouration of indigo carmine was calculated from the absorbance value. The energy consumed by the operation of the reactor was divided by this number in the case of the diamond electrode. For UV/H₂O₂ and photo-Fenton, in addition to the operational energy, technical-scale commercial prices (Table 2.4) were taken for hydrogen peroxide, ferrous sulfate, and sulfuric acid and converted to energy values (Cañizares et al., 2009) for Germany in 2011 (0.2495 €/kWh, Brachvogel, 2011) as follows:

$$\left(\frac{81.6 \text{ €}}{25 \text{ L H}_2\text{O}_2 \text{ 30 \%}} \right) \left(\frac{1 \text{ L H}_2\text{O}_2 \text{ 30 \%}}{1.11 \text{ kg 30 \%}} \right) \left(\frac{1 \text{ kg 30 \%}}{0.3 \text{ kg H}_2\text{O}_2} \right) \left(\frac{1 \text{ kWh}}{0.2495 \text{ €}} \right) = 39.29 \text{ Wh/g}$$

$$0.115 \text{ mL H}_2\text{O}_2 \text{ 30 \%} \left(\frac{1.11 \text{ g 30 \%}}{\text{mL H}_2\text{O}_2 \text{ 30 \%}} \right) \left(\frac{0.3 \text{ g H}_2\text{O}_2}{\text{g 30 \%}} \right) \left(\frac{39.29 \text{ Wh}}{\text{g H}_2\text{O}_2} \right) = 1.50 \text{ Wh}$$

Additionally, values reported in literature were partially used as a lower threshold (Müller and Jekel, 2001). The total calculation of E_{EO} is shown for the photo-Fenton reaction in Table 2.5. Although the reactors described here are laboratory-scaled, technical prices were regarded as a better approximation of the real cost of a chemical substance. The prices used for calculation are not necessarily the lowest available. Only operational costs and no capital or maintenance costs were considered.

Table 2.5 – $E_{EO,rx}$ and $E_{EO,tot}$ calculation chart for the photo-Fenton reaction. Electricity costs are divided into irradiation ($E_{E,pro}$) and total ($E_{E,pro} + E_{E,mix}$) costs. Chemical costs ($E_{E,chem}$) are added to obtain the effective electrical energy per order of magnitude ($E_{EO,rx}$) or the total electrical energy per order of magnitude ($E_{EO,tot}$). OM: order of magnitude. For more details on the calculation, refer to Chapter 3.

calculation formula	time	average absorption	removal efficiency	OM	electricity		chemicals + electricity		$E_{EO,rx}$	$E_{EO,tot}$
					irradiation	total	irradiation	$E_{E,tot}$	irradiation	total
units	s	%	-	-	Wh/L		Wh/L		Wh/(L·order)	
sample ₀	0	0.458	0	0	0	0	2.25	2.25	-	-
s ₁	60	0.347	27.2	0.12	0.51	0.72	2.77	2.98	22.96	24.69
s ₂	120	0.310	36.3	0.17	1.03	1.44	3.28	3.70	19.35	21.82
...	150	0.279	43.9	0.22	1.28	1.80	3.54	4.06	16.43	18.85
...	210	0.250	51.0	0.26	1.80	2.53	4.05	4.78	15.40	18.18
...	270	0.217	59.1	0.32	2.31	3.25	4.56	5.50	14.06	16.96
...	330	0.184	67.2	0.40	2.82	3.97	5.08	6.22	12.82	15.72
s _x	390	0.149	75.9	0.49	3.33	4.69	5.59	6.95	11.43	14.20
...	450	0.115	84.1	0.60	3.85	5.41	6.10	7.67	10.17	12.78
...	510	0.076	93.6	0.78	4.36	6.14	6.61	8.39	8.48	10.76
...	570	0.070	95.2	0.82	4.87	6.86	7.13	9.11	8.70	11.13
...	630	0.058	98.2	0.90	5.39	7.58	7.64	9.83	8.48	10.91
...	750	0.050	100	0.96	6.41	9.02	8.67	11.28	9.01	11.72

Chapter 3

Energetic Comparison of Advanced Oxidation Reactors¹

This chapter initially presents the set-up of the built AOP reactors. The degradation of indigo carmine as a test compound is then studied using the three technologies (BDD, UV/H₂O₂ and photo-Fenton) as a measure of their oxidising potential. The focus of this chapter is set on the calculation of the energetic costs for process operation. A subdivision of the total energy demand of each system, which allows for a better comparison of various set-ups, is provided.

3.1 Reactor Comparison

The reactors to be compared are shown in Figure 2.1. For the photo-Fenton reaction, three fluorescent lamps (nominal 13 W each) were used to treat a total volume of 1 L. Hence the electric power measured was high (30.78 W/L). The decolouring reaction was performed to evaluate the time and energy consumption required to meet a defined end point in batch modus.

Hydrogen peroxide photolysis required dosage of hydrogen peroxide and turning on the ultraviolet lamp. With one 10 W ultraviolet lamp required for a total volume of 0.9 L, its measured power was 12.12 W/L. The reaction was also carried out in batch modus.

In comparison to the previous two AOPs, the diamond electrode represents a heterogeneous AOP. The radicals are located in a thin layer above the electrode surface, so that the active reaction volume is not as large as the nominal volume. Nevertheless, the electrode additionally generates ozone through radical reactions. Ozone dissolves in water, thus acting throughout the entire volume. Hence, although the diamond electrode is chiefly a heterogeneous technology, it has a component of a homogeneous AOP. As a batch system was desired and it was not possible to cool the reactor directly, a recirculation system with an externally-cooled vessel was used. At a flow rate of 4 L/min, the 3 L of solution would have statistically come into

¹The results presented in this chapter were published in *Chemical Engineering and Technology*, **2013**, *36*, No. 2, 355–361.

contact with the electrode (radicals) every 45 seconds. In contrast, ozone exposure would have been constant throughout. For BDD, three configurations were chosen as the identity of the oxidants formed at the anode (hydroxyl radicals, H_2O_2 , ozone, *etc.*) can be altered with current density (Bergmann, 2010). This can impact the oxidation efficiency and degradation pathways. At current densities of 42, 208 and 333 mA/cm^2 , the measured power outputs were 0.57, 3.80 and 5.66 W/L , respectively.

3.2 Degradation of Indigo Carmine

In order to test the efficiency of the reactors, the test compound indigo carmine (IC) was oxidised. It is known from literature that up to fifteen percent of the dye produced worldwide is lost with the industrial effluent after the dyeing process (Zollinger, 2003). Studies have shown that hydroxyl radicals and other oxidizing agents such as ozone can effectively attack IC (Hammami et al., 2012; Ammar et al., 2006; Bechtold et al., 2006; Aleboyeh et al., 2005; Camarero et al., 1997; Bader and Hoigné, 1981). The rate constants for IC are $9.4 \times 10^7 \text{ M}^{-1}\text{s}^{-1}$ with ozone and $\approx 10^9 \text{ M}^{-1}\text{s}^{-1}$ with $\text{HO}\cdot$. For these reasons and the ease of photometric measurements, IC was selected for assessing the generation of oxidants in each system.

Decolouration was selected as the parameter to monitor, as it is more closely associated with the single-step oxidation of persistent pollutants than other water parameters. For instance, the COD or DOC capture not only IC, but also its transformation products. Therefore, these parameters correspond more to the degree of mineralization, which is beyond the goal of advanced treatment due to elevated costs.

The three AOP reactors were capable of decolouring IC. Table 3.1 presents the energetic requirements of the AOPs used. Boro-doped diamond showed a $E_{EO,tot}$ of 0.86 and 1.03 $\text{Wh}/(\text{L}\cdot\text{order})$ at high current densities (333 and 208 mA/cm^2 , respectively), and an $E_{EO,tot}$ of 23.88 $\text{Wh}/(\text{L}\cdot\text{order})$ when a weaker current density of 42 mA/cm^2 was applied. Both UV/ H_2O_2 and the photo-Fenton reaction had electricity consumptions in between with 7.42 and 11.72 $\text{Wh}/(\text{L}\cdot\text{order})$, respectively, to decolour IC.

3.3 Energetic Consumption of Individual Components

In order to improve the comparability of the systems, it was decided to subtract the energy applied for mixing and displays (stirrers, pumps, screens; $E_{E,mix}$) from the total consumption of each technology required for decolouration. To do this, the electricity consumption of the individual components was determined.

The sum of mixing ($E_{E,mix}$), process ($E_{E,pro}$), and chemical ($E_{E,chem}$) energy results in the total energy ($E_{E,tot}$), where $E_{E,pro}$ is the energy associated with processes intrinsic to a technology. For example, this includes the electrode in the case of the

Table 3.1 – Energetic requirements of electrolysis (BDD, three settings), photolysis (UV/H₂O₂) and the photo-Fenton reaction.

AOP	t	OM	$E_{E,mix}$	$E_{E,pro}$	$E_{E,chem}$	$E_{E,tot}$	$E_{EO,rx}$	$E_{EO,tot}$
	min	-	Wh/L				Wh/(L·order)	
BDD	42 mA/cm ²	0.37	8.64	0.24	0	8.88	0.64	23.88
BDD	208 mA/cm ²	1.06	0.92	0.17	0	1.09	0.16	1.03
BDD	333 mA/cm ²	1.02	0.69	0.19	0	0.88	0.18	0.86
	UV/H ₂ O ₂	1.00	3.55	3.43	0.44	7.42	3.86	7.42
	Photo-Fenton	0.96	2.61	6.41	2.25	11.28	9.01	11.72

t: decolouration time; OM: orders of magnitude = $\log_{10}([\text{IC}]_i/[\text{IC}]_t)$; $E_{E,mix}$: electrical energy for mixing; $E_{E,pro}$: process-intrinsic electrical energy; $E_{E,chem}$: cost of chemicals converted to energy; $E_{E,tot}$: total electrical energy; $E_{EO,rx}$: process-intrinsic electrical energy per order; $E_{EO,tot}$: total electrical energy per order of magnitude.

electrolytic system and the corresponding lamps for conventional AOPs. It is this process energy that when added to the chemical energy for UV/H₂O₂ and photo-Fenton, effectively brings the reaction about (see Table 2.5 for the calculations using the example of the photo-Fenton reaction). Table 3.1 shows the contributions of each type of energy to the total consumption.

It was only necessary to factor $E_{E,chem}$ into the UV/H₂O₂ and photo-Fenton reactions. $E_{E,chem}$ was greater for photo-Fenton due to the higher H₂O₂ concentration and additional chemicals required (Table 2.2).

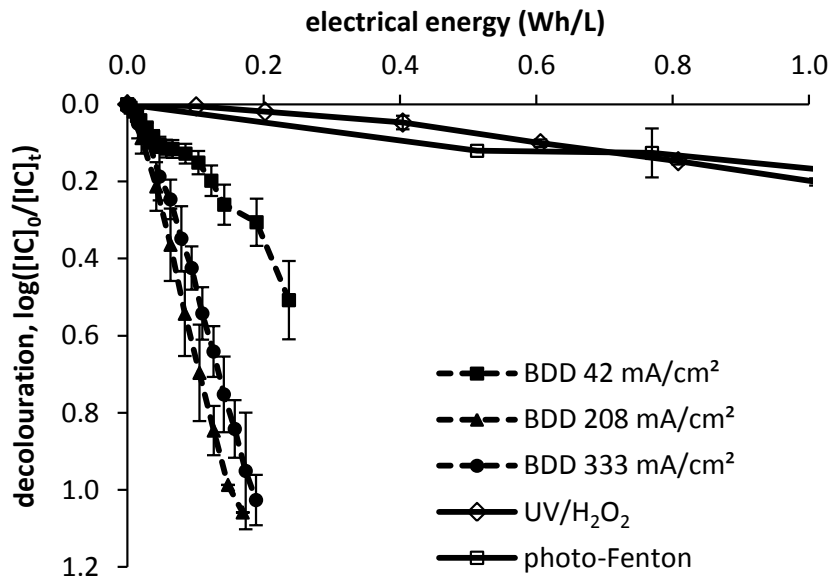


Figure 3.1 – Decolouration dependent on the process energy input ($E_{E,pro}$) for BDD, UV/H₂O₂ and the photo-Fenton reaction.

Figure 3.1 shows the electrical consumption of the systems in terms of $E_{E,pro}$. $E_{E,pro}$ was higher for both radiative systems (3.43 and 6.41 Wh/L) than for electrolysis (0.24 Wh/L). When operated at high j , the electrolytic system was characterised by rapid decolouration rates. At the lower j of 42 mA/cm², BDD was more efficient when considering $E_{E,pro}$ than in terms of $E_{E,tot}$. UV/H₂O₂ and photo-Fenton were characterised by rather small changes in the order of magnitude per electrical energy unit. From 0.75 Wh/L on, UV/H₂O₂ outperformed photo-Fenton. In particular, the three lamps used for photo-Fenton significantly contributed to its overall consumption.

For all technologies except photo-Fenton, $E_{E,mix}$ was the largest contributor to the total electrical consumption (Table 3.1). It was especially high when long treatment times were required. For example, when the BDD electrode was operated at 42 mA/cm² for 25 min, the increase in total energy consumption was mainly due to $E_{E,mix}$ (8.64 Wh/L). Thus, the best energy balance for the BDD technology occurred at high j , when the reaction time was shorter and pumping costs were reduced. This factor also explains why $E_{E,tot}$ was lower for the operation of BDD at 333 mA/cm²

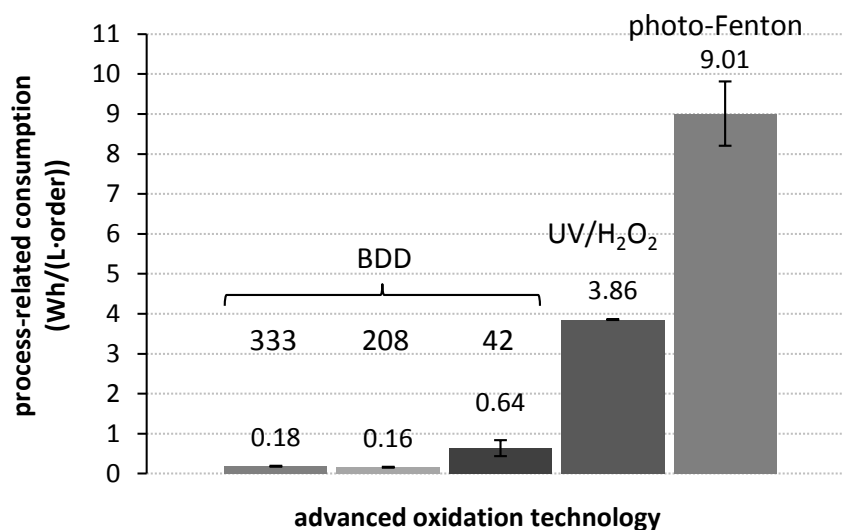


Figure 3.2 – Effective electrical energy per order of magnitude ($E_{EO,rx}$) for the decolouration of indigo carmine with BDD (units: mA/cm²), UV/H₂O₂ and the photo-Fenton reaction.

in comparison to 208 mA/cm² (0.86 vs. 1.03 Wh/(L-order)). The electrolytic process ($E_{E,pro}$) itself consumed 0.19 Wh/L at 333 mA/cm² and 0.17 Wh/L at 208 mA/cm². However, when the reaction time was shorter (at 333 mA/cm²), pumping costs were significantly reduced ($E_{E,mix}$, 0.69 vs. 0.92 Wh/L). In the frame of disinfection experiments with bacteria, it was found that 333 mA/cm² did not reduce the inactivation time in comparison to 208 mA/cm² (Chapter 7). In such a case, the latter j would be preferred, as its gross energy consumption for the same operation time would be lower than for 333 mA/cm².

$E_{E,mix}$ is the factor least related to oxidation of organic compounds and most dependent on the specific reactor settings. If the reactors were scaled-up to technical plants, $E_{E,mix}$ could be minimised. The parameter $E_{EO,rx}$ (effective electrical energy per order of magnitude) is intended to offer the most realistic approximation of the energy required by any AOP to accomplish degradation. It is calculated with only two energetic components (eq. 3.1).

$$E_{EO,rx} = \frac{E_{E,pro} + E_{E,chem}}{OM} \quad (3.1)$$

Figure 3.2 illustrates $E_{EO,rx}$ for the systems tested.

The $E_{EO,rx}$ for BDD ($E_{E,chem} = 0$) at 42 mA/cm² was three to four times greater than that at higher current densities. At low j, it was observed that a higher proportion of hydroxyl radicals formed in comparison to ozone (Chapters 4 and 8). Because radicals are short-lived, they are only effective in the vicinity of the electrode. On the other hand, ozone is more stable and therefore can diffuse into the bulk of the solution, thus accelerating decolouration. In the case of UV/H₂O₂ and photo-Fenton, the additional component $E_{E,chem}$ was required. For UV/H₂O₂, it was also mixing that was costly with respect to energy consumption. As a result, its $E_{EO,rx}$ was about one-half of its $E_{EO,tot}$, with values between 3.53 (lower threshold) and 3.86 Wh/(L-order) (measured). Of the individual contributors to $E_{EO,rx}$

for the photo-Fenton reaction, both $E_{E,chem}$ and $E_{E,pro}$ were higher than for other technologies. This is due to the large amount of chemicals that were used as well as the electric consumption of the lamps. Its $E_{EO,rx}$ was between 7.06 (lower threshold) and 9.01 Wh/(L·order). Mixing did not have a pronounced effect in the end (2.61 Wh/L, around 20% of $E_{EO,tot}$).

3.4 Summary

The three advanced oxidation systems built were able to effectively decolour the dye indigo carmine. An energetic comparison was performed on two levels. When considering total energy requirements, both UV/H₂O₂ and photo-Fenton had a consumption of around 11 Wh/(L·order). The total energy requirements of the BDD electrode, however, varied significantly from 23.88 to 0.86 Wh/(L·order), depending on the applied current density.

In a second approach, mixing costs ($E_{E,mix}$) were neglected as they are subject to reactor size and do not directly cause the reaction to happen. Thus, only process-intrinsic energy was considered for comparison. As a result, photo-Fenton had an $E_{EO,rx}$ of 9.01 Wh/(L·order) and UV/H₂O₂ 3.86 Wh/(L·order) to decolour IC. Values for BDD were one order of magnitude lower and more favourable at a current density of 208 mA/cm² (0.16 Wh/(L·order)) in the systems tested. The lower current density (42 mA/cm²) was less energy-efficient because of its predominant generation of hydroxyl radicals, which are confined to the electrode surface. When operated at a higher j (333 mA/cm²), $E_{E,pro}$ became so high that even the reduction in reaction time could not compensate for it.

Chapter 4

Effect of the Current Density on the Generation of Reactive Oxygen Species

The evaluation of various configurations of the BDD electrode in Chapter 3 showed marked differences in their energetic consumptions. A given amount of energy did not bring about the same level of decolouration (oxidation) at the different currents tested. Hence, there should be a difference in the mechanism of oxidant formation within the j range 42–333 mA/cm².

The purpose of this chapter is to quantify the oxidising agents created by BDD at different current densities. By calculating the yield of oxidants per amount of current, it should be shown how efficient BDD is as an oxidation technique. For this energetic calculation, the process-intrinsic energy presented in Chapter 3 is utilised. Furthermore, the quantification of oxidants at increasing current densities should clarify mechanistic details of the electrochemical process.

The oxidant yield was quantified in deionised water with two methods. First, an experiment for the cumulative quantification of ozone and hydroxyl radicals on the electrode surface was developed and compared to theoretical values. Second, deionised water was electrolysed and the dissolved ozone concentrations in it were measured. The results are compared to the ozone yields of conventional ozone generators with regard to energy consumption.

4.1 Cumulative Measurements

The first attempt to quantify the total amount of hydroxyl radicals and ozone being generated by the electrode was carried out with cumulative measurements (the method is described in Section 2.3.1). Because these two species are very reactive and cannot be measured but at the moment they form, the following experiments focus on them and neglect *e.g.* hydrogen peroxide.

The idea was to bring sensitive dyes directly into the electrolytic system, so that it can react in situ with the oxidants and thus minimise losses related to the extremely

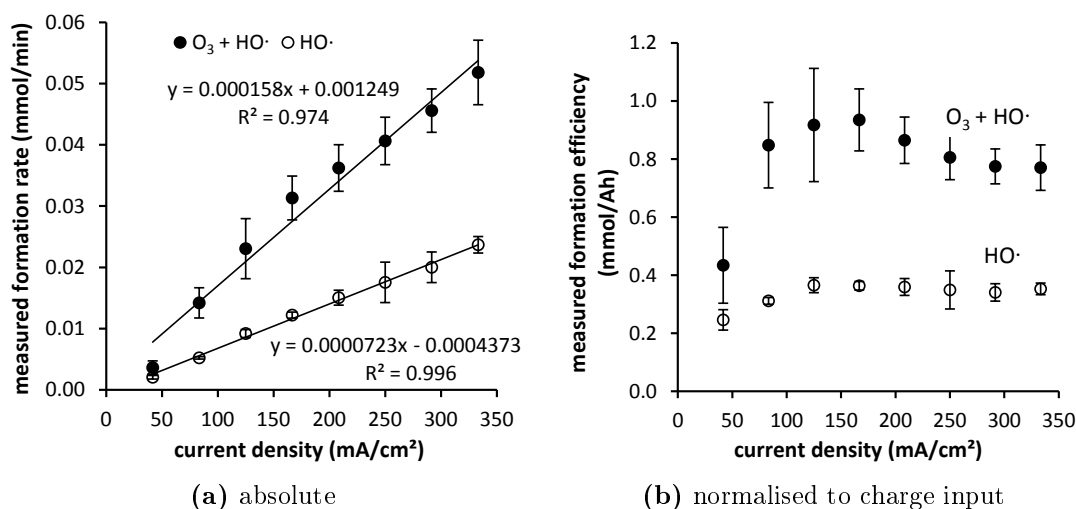


Figure 4.1 – Measured formation rate of ozone and hydroxyl radicals in dependence of the current density.

fast reactions that these species could undergo upon sampling, or due to outgassing. Two experiments were carried out: the first one used IC as a probe compound for ozone. Due to the fact that further ROS such as $HO\cdot$ and atomic oxygen are captured by the IC experiment as well (Muff et al., 2011), a second experiment with an ozone-resistant dye (RNO) was performed. The direct oxidation of the dyes on the anode can be neglected because electrode operation was current-controlled and the potential was always higher than that required for water oxidation to hydroxyl radicals. This means that both water and dye would be oxidised. Considering that water concentration was $5.5 \times 10^{-5} \text{ M}$ at 20°C , whereas dye concentration was less than $5.0 \times 10^{-5} \text{ M}$, the clear advantage is on the side of water with 6 orders of magnitude.

In the first instants of electrolysis, the system comprises only dye molecules, water and ROS. As dye molecules undergo a reaction with ROS, they convert into colourless degradation products and the absorption is approximately linear. If one of these colourless products scavenges an ROS, this ROS would be lost to analysis. As a result, the curve flattens into an exponential function. Thereby, only the initial decolouration rate is relevant to the experiment. Figure 4.1a shows the initial (1 minute) measured formation rates of ozone and $HO\cdot$ in dependence of the current density. There was a positive correlation between the formation rates and the applied current. It can be seen that an increase of j brought about a more marked increase in ozone (slope: 1.58×10^{-4}) than it did in $HO\cdot$ (slope: 7.23×10^{-5}). This implies that eq. 1.11 in Section 1.3.3 was favoured at high current densities, so that the generation of different oxidants could be controlled over the current. The lower the j , the more $HO\cdot$ formation was favoured. At higher current densities, the efficiency of ozone generation over $HO\cdot$ increased. Therefore, if j had been further reduced (for instance, down to 20 mA/cm^2 , the ozone formation threshold for the employed electrode in pure water at 20°C , internal communication with CONDIAS), the full and open dots in Figure 4.1a would have laid upon each other and no ozone would have been produced (not shown).

Since dye concentrations were in the same order of magnitude, the absolute ROS

amounts in Figure 4.1a can be subtracted. The vertical space between the full and open dots corresponds to the amount of pure ozone. So for instance at 83 mA/cm^2 , $0.0090 \text{ mmol O}_3/\text{min}$ were formed, whilst at 42 mA/cm^2 it was only $0.0016 \text{ mmol O}_3/\text{min}$.

Figure 4.1b displays the normalisation to unit charge of the ROS generation rates. At 42 mA/cm^2 , the amount of oxidants formed for a given charge was lower than at all other higher currents tested. In the case of HO^\cdot , the efficiency stabilised after 125 mA/cm^2 at around 0.355 mmol/Ah . In the case of ozone and other ROS, the efficiency increased up to 0.935 mmol/Ah at 167 mA/cm^2 to fall again and apparently stabilise at around 0.771 mmol/Ah from 292 mA/cm^2 onwards. From these data, a j of 167 mA/cm^2 would be the most efficient for both HO^\cdot and O_3 .

When comparing the cumulative measurements with the theoretical yields (as expected from Faraday's Law, assuming an electrolytic efficiency of 100 %, Table 4.1), these accounted for no more than 1 % and 9 % for HO^\cdot and ozone (+ ROS) respectively. Two explanations are reasonable for the low efficiencies. The first one is associated to the rather high current densities applied, which were high enough to support ozone formation. Due to the reactivity of HO^\cdot , the reaction may not stop after decolouration (attack to the chromophore) and a single dye molecule could react with more than one ROS at different points of its molecular structure. Even though the total organic carbon (TOC) of the solution remained unchanged after complete decolouration (not shown), meaning no mineralisation took place, the multiple radical attack may have led to underestimation of the radical formation rate.

The other reason concerns the electrolytic chamber (5 in Figure 2.1a), which contains free-flowing areas for the treated water far away from the electrode surface (Figure 4.2a). It is clear that the electrolytic chamber used does not represent a convenient asset to the electrolytic reactor. A kind of electrolytic chamber which promotes the contact of the electrode with the fluid would be recommended. It could be shaped like a square prism in such a way that it envelopes the electrode on all sides and forces the fluid to stream close by its surface (Figure 4.2b). Due to the higher flow rates and shear forces on the electrode, incipient ozone bubbles could get

Table 4.1 – Initial ozone concentrations (mg/L) in deionised water (percentages of theoretical yield are shown in parentheses).

j	O_3 after 1 min (mg/L)					
	cumulative (%)		measured (%)		theoretical (%)	
42	0.025 ± 0.018	(3.0 ± 2.2)	0.143 ± 0.023	(17.2 ± 2.8)	0.829	(100)
208	0.339 ± 0.112	(8.2 ± 2.7)	1.621 ± 0.309	(39.1 ± 7.5)	4.146	(100)
333	0.450 ± 0.084	(6.8 ± 1.3)	2.128 ± 0.448	(32.1 ± 6.8)	6.633	(100)

cumulative: calculation derived from the cumulative measurements (Section 4.1);
 measured: directly measured during ozonation of deionised water (Section 4.2); the-
 oretical: calculated from Faraday's Law. j in mA/cm^2 .

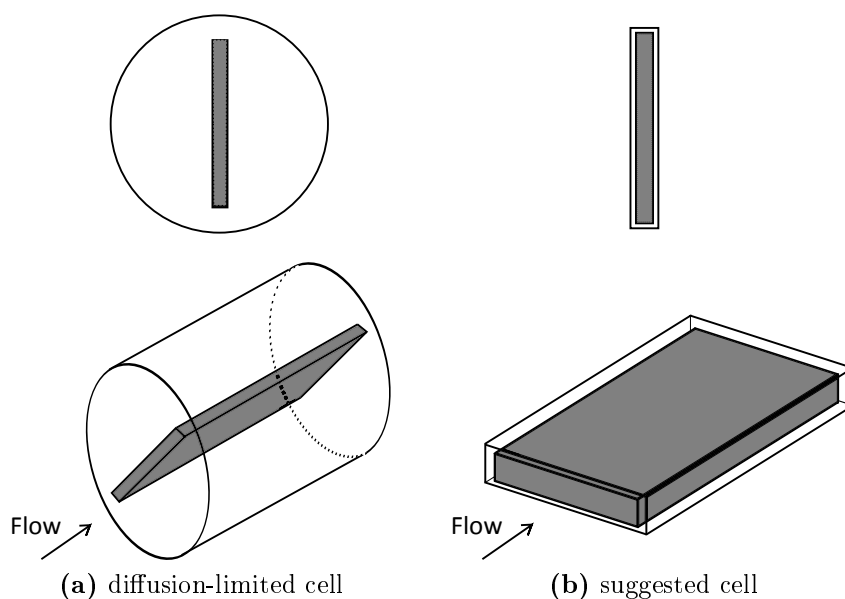


Figure 4.2 – Geometries of (a) the employed electrolytic chamber and (b) the suggested electrolytic cell with enhanced exposure to hydroxyl radicals.

Top: cross sections, bottom: 3D-schemes. Grey blocks represent the electrode.

dragged by the fluid when they are still small enough to dissolve. Hence, it could heighten the concentration of dissolved ozone, making the use of a mixing chamber (9 in Figure 2.1a) superfluous and increasing the oxidising potential (through the enhanced contact with radicals) of the system altogether. Probably a compromise between radical exposure and hydrodynamic hindrance would have to be made.

For different applications of the BDD electrode, distinct oxidants may be of relevance. For instance ozone is a more effective disinfectant than HO^\bullet , whereas the latter are more powerful against refractory chemical compounds. It is a promising characteristic of BDD to allow for regulation of the oxidants produced by means of the applied current. These cumulative measurements are an incentive for further research on reactor geometries and ozone yields.

4.2 Ozone Concentration in Deionised Water

Because the cumulatively measured ROS yield did not go beyond 9% of the theoretical value, another approach for the ozone determination was then followed. The electrode was operated in pure (fully deionised) water and the ozone concentrations were not measured in situ as during the cumulative approach, but by taking samples out of the reactor (the method is described in Section 2.3.2). As deionised water does not contain impurities, it represents an appropriate medium for studying the electrolytic process while minimising side reactions, and thus approaching the yield determination.

Figure 4.3a shows the measured dissolved ozone concentrations in deionised water against time. Ozone was enriched in water to a maximum concentration and then began to fall, so that the ozone curves showed maxima and no plateau concentra-

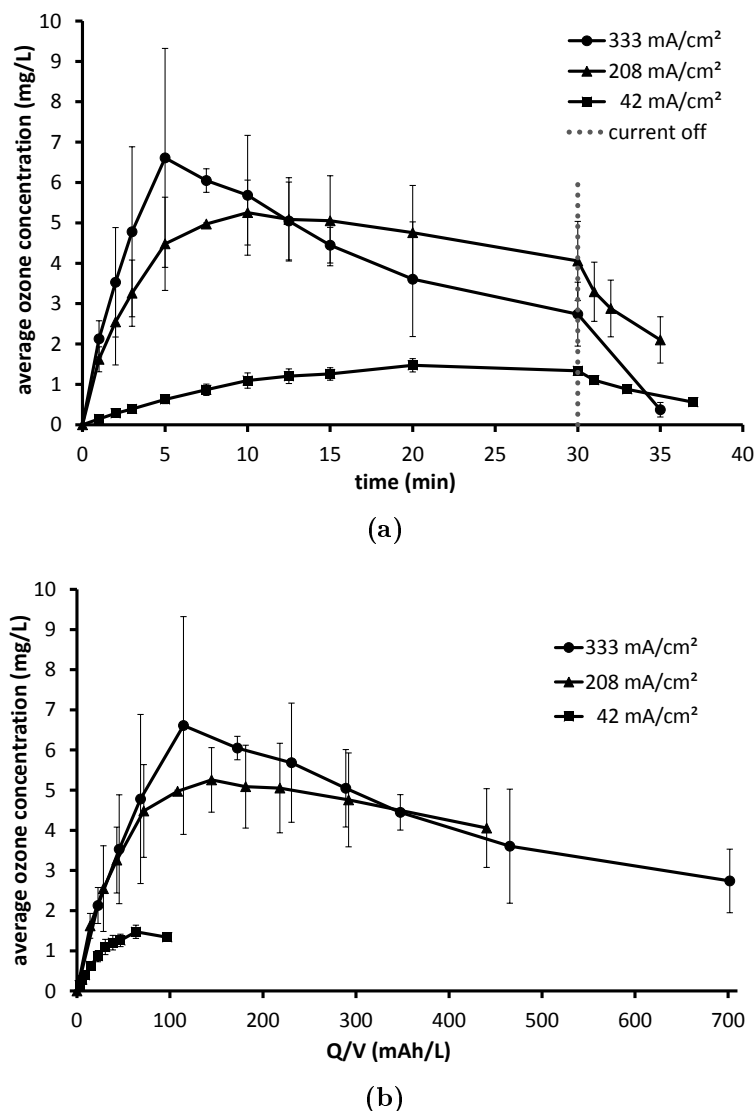


Figure 4.3 – Ozone concentrations in deionised water at $20 \pm 1^\circ\text{C}$ in dependence of (a) the time or (b) the charge input.

tion. It took 5 min to reach a maximum of 6.6 mg/L at 333 mA/cm² and 10 min at 208 mA/cm² to reach 5.3 mg/L. The curve at 42 mA/cm² showed a maximum ozone concentration of 1.4 mg/L after 20 min and slightly fell thereafter.

Figure 4.3b shows the same curves as Figure 4.3a but plotted against the charge input. It becomes clear that up to 50 mAh/L the achieved ozone concentration per unit of charge for 208 and 333 mA/cm² was identical. A representation over time (Figure 4.3a) appears more favourable for the higher current, but it is rather a kinetic advantage and not a higher efficiency. For the same amount of charge, the ozone values at 42 mA/cm² in Figure 4.3b were lower. The electrode favoured the generation of HO[•] at lower j values, so that electrolysis yielded less ozone. At higher j values, ozone formation was only dependent on the charge input.

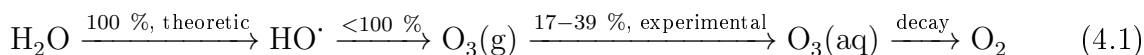
As can be seen in Figure 4.3, the ozone concentration increased to a maximum after which it began to decrease. This indicates that following the maximum point, ozone decayed more quickly than it accumulated in the water. There are two reasons

for this course. During the operation of the BDD electrode, it was noticeable that more heat generated in deionised water than when working with more laden waters (Chapter 5). This effect was very pronounced because deionised water is a medium of very low electrical conductivity, requiring higher potentials and operational energy ($E_{E,pro}$, see also Figure 5.5), which dissipates as heat. The local temperature of the solution flowing past the electrode must have been higher than 20 °C, thus promoting the decay of ozone (Kraft et al., 2006b). In Figure 4.3a after 30 min, the decay of the ozone concentrations after the current was turned off is shown. Although ozone decay was not precisely monitored, the fast decay rates measured suggest a strong local temperature rise (see also Table 1.2) which was more pronounced at higher current densities.

Besides temperature, the charge being fed into the system produced not only ozone, but also other oxidants that are not captured by the ozone measurement such as oxygen. The concentration of dissolved molecular oxygen rose from 7.8 to 14.9 mg/L and to 16.9 mg/L after 30 min of electrolysis at 208 mA/cm² and 333 mA/cm², respectively. Recirculation alone (before starting the electrolytic process, eq. 1.8) did not increase the oxygen concentration. In addition, the formation and accumulation of hydrogen peroxide in BDD electrolytic systems has been reported as a further cause for ozone instability during electrolysis (Kraft et al., 2006b). In fact, the combination of ozone and hydrogen peroxide is used as an AOP (*peroxone*) following eq. 1.14 and 1.15. These two factors are also likely to have caused the slight deviation from linearity in the O₃ + ROS curve (flattening for higher j values, Figure 4.1a).

Table 4.1 contrasts the measured ozone concentrations in deionised water after 1 min with the cumulative measurements and the expected concentration values derived from a theoretical standpoint. In all cases, the measured values were about five times as high as those from the cumulative measurements, yet lower than those expected theoretically. Due to the hydrodynamics of the electrolytic system used (short contact time with ozone and low contact ratio of the water with the electrode surface), it is comprehensible that some ozone escaped to the surroundings before it dissolved. Indeed, there was a permanent, strong odour of ozone near the reactor (therefore the ventilation hood).

Equation 4.1 summarises the ozone production process. The need for optimisation is present at yielding ozone from hydroxyl radicals and dissolving it in the water.



4.3 Energetic Considerations

The energy consumption of the BDD electrolytic system can be partitioned in process-intrinsic (specifically: the consumption of the electrode only) and non-process-intrinsic energy (the consumption of mixing, display and further devices, refer to Chapter 3). In Figure 4.4 the process-intrinsic energy consumption of the electrode is displayed. The energy increase was directly proportional to the current with linear fits above 0.99. Note that for a given j , consumption was always higher

for the radical determination than it was for ozone plus $\text{HO}\cdot$. Whereas IC is a disodium salt and produces ions in solution, RNO is a non-ionic compound thus giving rise to a solution with higher resistivity.

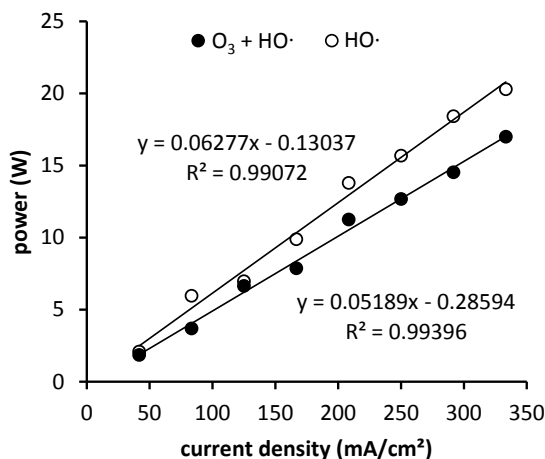


Figure 4.4 – Measured power of the BDD electrode (electrode only, $E_{E,pro}$) during the cumulative experiments at various current densities.

Table 4.2 offers a comparison of the ozone yield achieved with the BDD electrode in comparison to commercial, laboratory-scale ozone generators. Merely **Nano** by *Absolute Ozone* represents a technical plant with a very high (*state-of-the-art*) ozone output. The other ozonators are smaller, laboratory-scale devices with lower outputs. The data in Table 4.2 were obtained from the homepages of the producers, based on maximum ozone yield (employing pure oxygen instead of air for generation). The data for the BDD electrode represent maximum ozone yields as well (measurements in deionised water).

When considering the process-intrinsic consumption of the electrode, 22.0 and 18.7 g O_3/kWh were achieved at 208 and 333 mA/cm^2 , respectively. This is well in the lower range of other ozone generators. If we bear in mind that commercial devices generate gaseous ozone, which has to be dissolved in water by a contactor and that the ozone-transfer efficiency of such devices is well below 100% (often in the range of 30–40% Gottschalk et al., 2010, p. 141), the efficiency of BDD increases to mid-high-range. In addition, the oxidising potential of BDD is higher than that considered only for ozone because it produces further strong oxidants (see Section 1.3.3).

4.4 Summary

In the performed experiments, the BDD electrode generated hydroxyl radicals, ozone, oxygen and probably further oxidising agents. The cumulative measurements showed a more pronounced increase in the generation of ozone than in the generation of hydroxyl radicals with current density in the range from 42 to 333 mA/cm^2 . This indicates a shift in the equilibrium of ROS on the electrode surface toward ozone.

Table 4.2 – Comparative power data of selected laboratory-scale ozone generators and BDD.

device	company	ozone production		
		g/h	power W	ozone yield g/kWh
Nano (technical scale)	Absolute Ozone	20	200	100
Laboratory Ozonizer 300.5	Sander	4	60	67
802 N	BMT	4	80	50
OG 150	AquaCare	0.3	6	50
Thioxx Pool 1.4	KOI	1.4	28	50
OZX-300AT	Enaly	0.5	15	33
BDD 208 mA/cm ²	CONDIAS, Esau&Hueber	0.29	13.0	22.0*
OZ-1000 OZ3	OCS.tec	1	75	3.9*
BDD 333 mA/cm ²	CONDIAS, Esau&Hueber	0.38	20.3	18.7*
ACP 200	AirClimo	0.2	11	4.6*
Pressurized electrochemical ozone generator (PbO ₂ /SPE) (Stucki et al., 1987)				15*
Alternate current corona discharge of liquids (Suarasan et al., 2002)				9*

Gray background: BDD, electricity consumption for the electrode only, $E_{E;pro}$; *Italics*: BDD, total electricity consumption (electrode, pumps and displays; $E_{E;tot}$). * Dissolved ozone (at 20 °C) in contrast to gaseous ozone in other devices. SPE: solid polymer electrolyte.

Hence, the generation of ozone and hydroxyl radicals is governed by the current density.

The maximum yield attained by both approaches, the cumulative ozone determination and the ozone measurements in pure water, was 39.1 % of the theoretical value. One reason for the medium yield were the hydrodynamic conditions of the electrolytic chamber used. Preliminary experiments with a new, narrower electrolytic chamber showed increased yields. Nevertheless, in comparison to commercial ozone generators, the employed BDD electrode produced ozone quantities in the middle range (22.0 g O₃/kWh). Considering that commercial ozonators generate gaseous ozone that needs dissolving in water, whereas the electrolytic system produces and concomitantly dissolves the produced ozone, BDD has the potential of becoming a competitive technology in the near future.

Chapter 5

Effect of the Water Matrix on Ozone Formation and Degradation Efficiency¹

The formation potential of hydroxyl radicals and ozone on BDD was described in Chapter 4 for deionised water. This chapter focuses on two aspects of the treatment of model real waters with BDD. Continuing with Chapter 4, the formation of ozone is examined, but in dependence of the water matrix and the current density. And secondly, the treatment of CBZ as a target pollutant in these model waters is studied and the required operational energy is reported.

5.1 Ozone Concentration in Different Water Matrices

In order to analyse the effect of the water matrix on oxidant production, six different waters were utilised. Besides deionised water and STPE, two model drinking water matrices whose compositions resembled German soft and hard potable waters, were prepared (*soft* and *hard*). Two additional water matrices based on these model potable waters were utilised, the difference being some organic content (*SORG* and *HORG*). The compositions of all water matrices can be found in Table 2.1. Not only was the work with these waters useful because they simulate potable or typical industrial process waters, but also because they offer a systematic transition from deionised water to STP effluents. Owing to the fact that the matrix components would compete with the dyes used in Chapter 4 for the reactive species, it is not possible to use a cumulative approach in real waters. Therefore, the measurements were restricted to ozone as described in Section 2.3.2. Measuring the ozone consumption (as the complement of the residual ozone) is fairly complex. The residual ozone offers a means to at least estimate how much is reacting.

Figure 5.1 shows the measured residual ozone concentrations in the different wa-

¹Parts of this chapter were published in *Brewing Science*, **2011**, *64*, 83–88

Table 5.1 – Initial accumulation rate of ozone in water (first 3 minutes, for STPE first 10 min) at different current densities in dependence of the water matrix (R^2 shown in parentheses). Measurements at 20 °C.

water matrix	Ozone accumulation rate (mg/(L·min))					
	42 mA/cm ²		208 mA/cm ²		333 mA/cm ²	
deionised	0.135	(0.995)	1.178	(0.948)	1.680	(0.976)
<i>soft</i>	0.044	(0.985)	0.468	(0.896)	0.834	(0.906)
<i>hard</i>	0.031	(0.986)	0.367	(0.983)	0.594	(0.934)
<i>SORG</i>			0.260	(0.936)	0.550	(0.883)
<i>HORG</i>	0.029	(0.762)	0.155	(0.994)	0.420	(0.995)
STPE	0.002	(0.723)	0.034	(0.931)	0.094	(0.999)

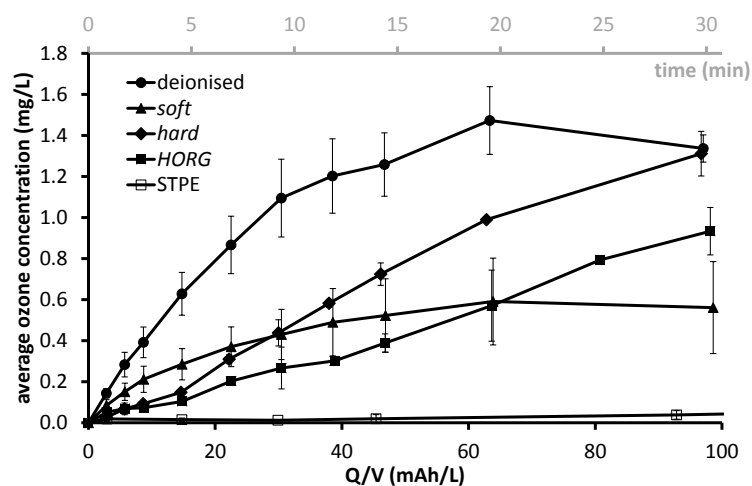
ters studied for 30 min ozonation. The curves are plotted against the charge input into the system; the time axis is additionally presented as a reference. After 30 min of electrolysis, the charge input for a j of 42 mA/cm² was between 93 and 98 mAh/L (Figure 5.1a), depending on the sampling volumes in each experiment. Ozone showed a logarithmic-like course: a large increase at the beginning that flattened with time (Beltrán, 2004).

5.1.1 Inorganic Water Components

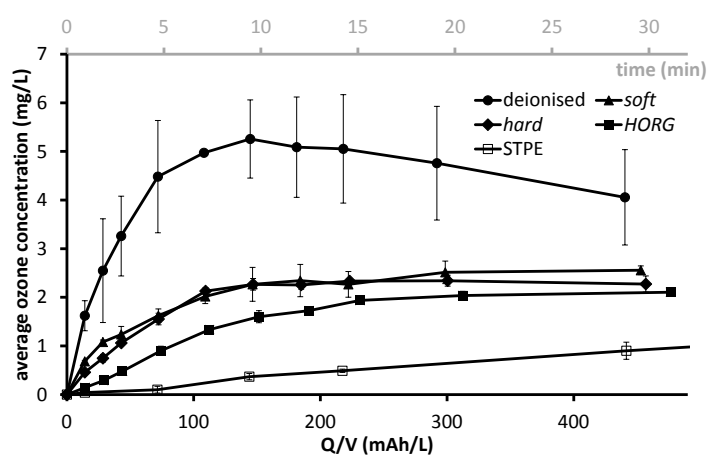
The presence of inorganic salts in the model potable waters had a considerable effect on the measured ozone concentrations. In comparison to deionised water, the ozone values in *soft* and *hard* were roughly halved (Figure 5.1). For instance at 208 mA/cm², the maximum measured ozone concentration in deionised water was 5.3 mg/L, whereas in *soft* and *hard* it reached values of 2.6 and 2.3 mg/L, respectively. Higher ozone concentrations were observed in *soft* compared to *hard*. This order was reversed only at 42 mA/cm² for Q/V values above 30 mAh/L, when other factors, not just consumption by water matrices, come into play.

The matrix effect was clearly observable in the first moments of the process. Table 5.1 shows the rates for ozone accumulation in water in the first 3 minutes. In parentheses, the correlation coefficients (R^2) for straight lines are presented (a linear fit was deemed accurate enough with R^2 mostly greater 0.90). The employed waters are sorted after the observed ozone accumulation rate in them.

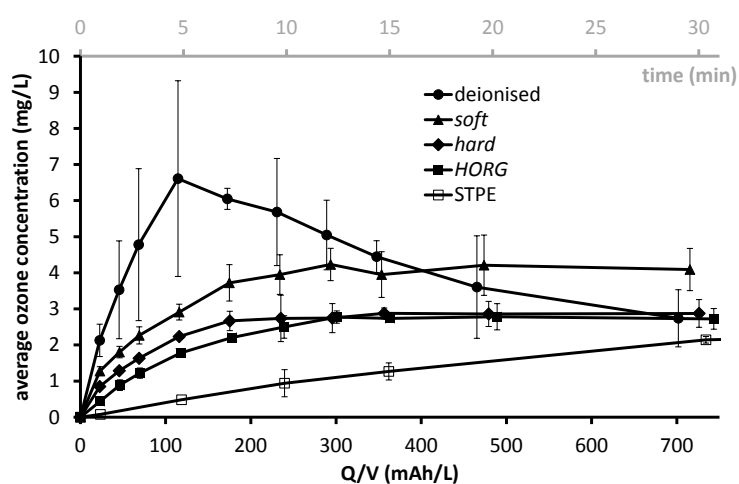
The accumulation rates decreased in the following order: deionised > *soft* > *hard*. As a consequence of the reactivity of ozone with inorganic substances, the basic inorganic compounds contained in the water matrix used up some of the ozone being produced, leading to lower residual ozone concentrations (see for instance the chloride consumption in Figure 6.1a). In *hard*, with its higher salt concentrations, the ozone consumption was more significant. In addition, less ozone formed in hard water because HO[•], the precursors of ozone, were more readily scavenged by the matrix.



(a) 42 mA/cm²



(b) 208 mA/cm²



(c) 333 mA/cm²

Figure 5.1 – Residual ozone concentrations measured in deionised water, model water matrices and STPE at 20 °C during the electrolyses with BDD. The data are plotted against the charge input per unit volume, the time axis is only referential.

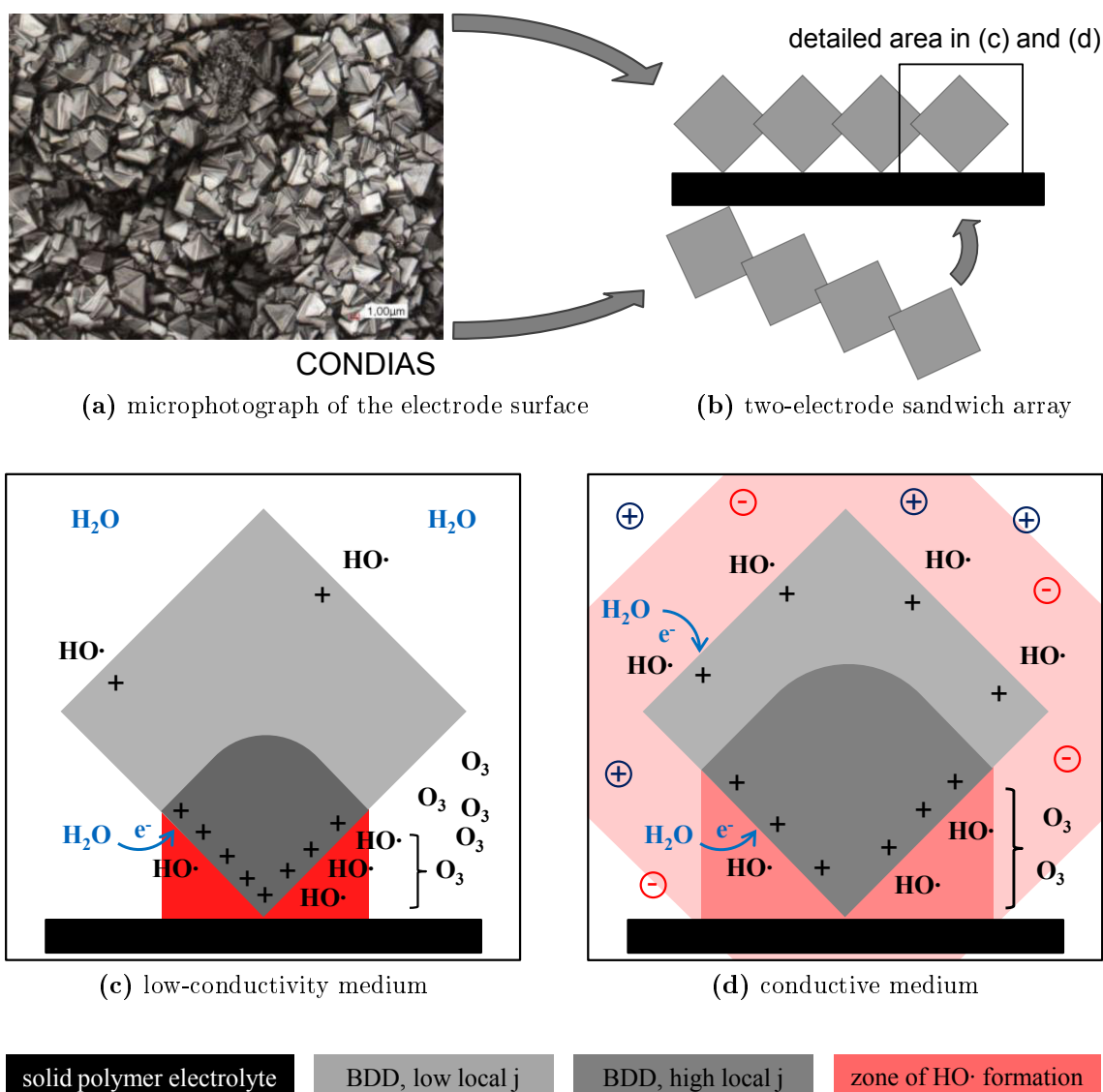


Figure 5.2 – Influence of the electrical conductivity of a medium on the ozone yield at identical nominal current density.

(a) **Laser scanning microscope photograph of the deposited diamond layer** (Behrendt-Fryda, 2012). Single crystals can be distinguished.

(b) **Two-electrode sandwich array around the polymer electrolyte.** Two electrode plates are placed in direct contact with the polymer electrolyte. As a result of the single crystal microstructure from (a), contact zones and gaps emerge at the interface.

(c) **In poorly conductive media,** the passage of an electrical current concentrates at the juncture electrode-polymer electrolyte. As a result, j is locally increased and the generated hydroxyl radicals are confined to a small space. Thus the further reaction of $\text{HO}\cdot$ to ozone is favoured.

(d) **In conductive media,** the passage of current to the medium is more likely, so that the region of higher local current and $\text{HO}\cdot$ density expands and weakens. Consequently, BDD produces comparatively more $\text{HO}\cdot$ in a greater space, so that ozone formation becomes less favourable.

The intensities of the colours are indicative of the level of current (gray) or $\text{HO}\cdot$ (red) density.

Furthermore, the electric conductivity of water plays an important role in ozone formation. Not only does the produced ozone react with matrix components, but also less ozone forms at higher conductivities (Figure 5.2). When working with deionised water, the electron density concentrates at the juncture of the BDD and the polymer electrolyte membrane, so that the local j is very high at the contact points and very low on the rest of the electrode surface due to the low conductivity of water (Figure 5.2c). When the electrical conductivity is increased, the electron density begins to expand from the junctures to the surroundings, as the passage of electrons through the matrix becomes more favourable (Figure 5.2d). This means that j at the junctures locally shrinks and ozone formation is less favoured (Kraft et al., 2006b).

Note that a lower ozone concentration in *hard* can at the same time imply a higher free chlorine concentration (as a result of radical scavenging by chloride or direct chloride oxidation). Free chlorine is a very effective disinfectant. Thus, the oxidising potential of electrolysed chloride-rich waters can be very high (see *e.g.* Lacasa et al. 2013), notwithstanding lower ozone concentrations.

The results obtained were in good agreement with the solubility tendencies for ozone described by Sotelo et al. (1989). Using gaseous ozone, Sotelo et al. reported lower dissolved ozone concentrations for higher ionic strengths and lower ozone dosages. The latter corresponds to j in this study because more ozone is produced at higher j values.

5.1.2 Organic Water Components

The water matrices *SORG* and *HORG* contained, in addition to the same inorganic ions in *soft* and *hard*, 2 mg/L and 5 mg/L organic matter, respectively. Table 5.1 shows that the ozone accumulation rates in *SORG* and *HORG* were between those in *hard* and STPE. The presence of organic material led to an increased ozone consumption. In the more laden water *HORG*, the ozone rates measured were lower than in *SORG*.

The organic content seemed to use up ozone more readily than the inorganic ions. The comparison between *SORG* and *hard* is especially interesting. In comparison to *soft*, *hard* contained around 500 mg/L more inorganic compounds, whereas *SORG* contained only 2 mg/L more organic compounds. Even so, the measured ozone accumulation rates in *SORG* were lower than those for *hard*. The two sources of organic matter, BSA and humic acid, readily reacted with ozone because they bear nucleophilic moieties in their structures. Double bonds, activated aromatic systems and non-protonated amines can react with ozone at rates of up to the $10^6 \text{ M}^{-1}\text{s}^{-1}$ range and with HO^\cdot at rates in the order of $10^9 \text{ M}^{-1}\text{s}^{-1}$ (von Gunten, 2003a). These functional groups can be found in BSA and humic acid (vanLoon and Duffy, 2010).

In brief, the more compounds that were present in a water matrix, the less ozone was available in solution. Ozone reacted with organic compounds more readily than with inorganic compounds, a trend only valid in the first minutes of the process.

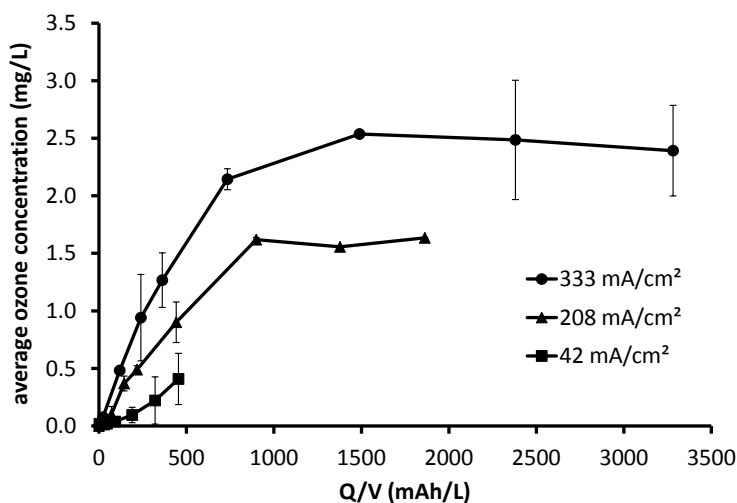


Figure 5.3 – Ozone concentrations against the charge input measured in STPE over 120 min of treatment with BDD at different current densities.

5.1.3 Ozone Concentrations in Real Wastewater

The effluent of the sewage treatment plant in Garching was the component-richest water matrix in this study. Besides inorganic ions, it contained the organic materials which were not degraded in the previous treatment processes (DOC: 6–13 mg/L). Additionally, pathogens (bacteria, viruses) and trace pollutants (pharmaceuticals and personal care products, heavy metals) should be present (Metcalf & Eddy, Inc., 2003). Although STPE was the most variable water matrix used (no fixed composition), the ozone concentrations measured in it were very stable, which translates into small standard deviations (compare bars in Figure 5.1).

Figure 5.3 shows the ozone concentrations in STPE against the charge input. The lower the j , the less ozone was measured per unit charge. Upon treatment of STPE, ozone was only very slowly enriched in solution (Table 5.1). The low R^2 for STPE resulted from the fact that ozone and HO^\cdot immediately reacted with the effluent components, so that fluctuations near zero were recorded. After one minute at 333 mA/cm^2 , only 0.08 mg/L were measured. In contrast, 2.13 mg/L were present in deionised water. The difference, 2.05 mg/L , must have been immediately scavenged by the wastewater components. The lower j of 42 mA/cm^2 needed more than 60 min to surpass 0.1 mg/L , whereas deionised water required less than 1 min.

Interestingly, after 60 min ($= 200 \text{ mAh/L}$) at 42 mA/cm^2 , ozone began to accumulate in the system (Figure 5.3). Though the DOC did not noticeably decrease during the process, it seems that after one hour all easily oxidisable molecular moieties were exhausted, so that the ozone demand of the solution was reduced.

Buffle et al. (2006) reported ozone consumptions of up to 4.0 mg in the effluent of a Swiss STP in around two minutes, with 75 % of this consumption in the first twelve seconds. Although it was an effluent with quite different properties than the one used here, it illustrates the ozone depleting potential of the matrix components.

STPE was the most laden water used in this study and clearly the matrix with

the highest ozone demand. Nevertheless, ozone accumulated to plateau values of 0.10, 1.63 and 2.39 mg/L for 42, 208 and 333 mA/cm², respectively, after one hour of electrolysis. These values represent an oxidising potential even in polluted water matrices.

5.1.4 Summarising Remarks - Matrix and Current Effect

Independent of the working j , one trend was noticeable. The ozone accumulation rate decreased with increasing matrix load (deionised > *soft* > *hard* > *SORG* > *HORG* > STPE). The influence of the current density can be seen when the columns of Table 5.1 are compared. A fivefold increment in current density from 42 to 208 mA/cm² brought about on average an elevenfold increase in the ozone build-up rate ($\times 11/5 = 2.20$ proportionality factor). In this range of j , the electrochemically favoured species stopped being HO[•] and became ozone (Chapter 4). A further current increase to 333 mA/cm² only doubled the build-up rates ($\times 2/1.6 = 1.25$ proportionality factor). The magnitude of the increase was not as pronounced because in the j range 208 to 333 mA/cm² there was no substantial mechanistic shift and the current increment only caused an intensification of ozone formation.

5.2 Fate of the Organic Matter

5.2.1 Transformation of the Bulk Organic Matter

For those waters containing organic matter, the TOC of the matrices was not reduced in a time span of 30 min (120 min for STPE), regardless of the j applied (450 to 3500 mAh/L total charge input). After the end of the electrolytic process, the pH slightly fell below the original value (before treatment). Furthermore, the DOC of *HORG* rose from 1.6 to 2.2 mg/L, which is an increase of 0.6 ± 0.04 mg/L in 30 min at both 208 and 333 mA/cm². In addition, the COD of STPE was reduced from 21.7 to 8.8 mg/L (by 60 %) in 180 min at 208 mA/cm². From these results it can be derived that an incipient oxidation was taking place. Several bonds of humic acid and even the undissolved humin (present in the native soil extract employed) were being oxidised and broken down, so that the resulting smaller molecules (Kerc et al., 2004) were partially converted to carboxylic acids (pH reduction) and hence passed from the undissolved solid state into the liquid phase (DOC increment). Kraft et al., 2006a observed an analogous oxidation behaviour with benzyl alcohol.

5.2.2 Degradation of a Target Compound

The purpose of the quaternary cleaning stage in STPs shall be the targeted elimination of persistent pollutants contained in a more complex water matrix. In fact, the oxidation of all bulk compounds would be bound to a very elevated energy consumption. In order to find out what happens to a target compound during electrolysis in the presence of different water loads, carbamazepine was spiked to the water matrices in Table 2.1 (except to *SORG*).

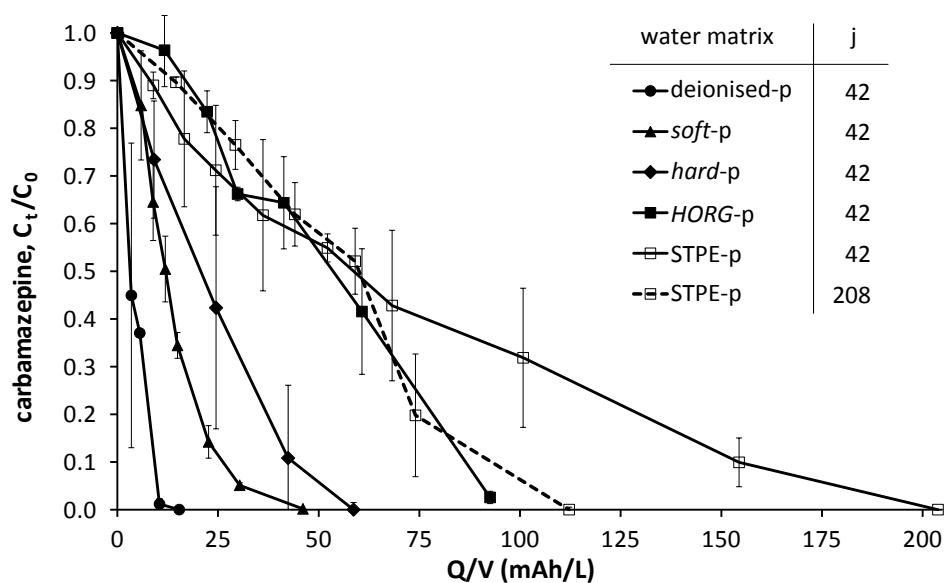


Figure 5.4 – Carbamazepine degradation with BDD in different water matrices at 20 ± 1 °C.

Figure 5.4 shows the relative concentration of CBZ over the charge input upon treatment with BDD. The degradation of CBZ took place more quickly in pure water than in all other matrices. Only 15 mAh/L were required to oxidise it completely. In *soft-p*, the charge input until degradation tripled (46 mAh/L). *hard-p* followed *soft-p*, then *HORG-p* and finally *STPE-p*. The more ions in the solution, the longer (and the more energy) it took to degrade CBZ (deionised-p < *soft-p* < *hard-p*). Also the presence of further organic materials worsened the electrolytic efficiency for the targeted CBZ degradation (*hard-p* < *HORG-p* < *STPE-p*). CBZ is known to undergo complexation with humic acids (Mirza et al., 2011), so in addition to competitive reactions, a shielding effect is likely to be present in *HORG-p*. Although there was no noticeable reduction in the TOC of the solution (Section 5.2.1), oxidation of the target compound was effective. It follows that CBZ was not mineralised during the experiment, but only partly degraded.

When j was increased to 208 mA/cm² ($\times 5$), the degradation time of CBZ in *STPE-p* to a concentration under the detection limit (t_{PC_0} , LOD ≈ 5 μ g/L) was shortened from 60 to 7.5 min ($\times 8$). This pronounced fall translated into a reduction of the charge input from 204 to 112 mAh/L (Figure 5.4). Recall that a depiction against the charge input is a means of normalisation. A reduction of the required charge is indicative of a different mechanism of oxidant formation. Whereas primarily hydroxyl radicals were produced at lower j , ozone generation was enhanced when j rose (Chapter 4). The extension of the active reaction volume from the electrode vicinity ($\text{HO}\cdot$) to the bulk (O_3) significantly contributed to the efficiency and reduced the energy input for the full CBZ degradation (Table 5.2). In addition, many *STPE* components are not prone to oxidation by ozone, *e.g.* chloride (Rosal et al., 2010; von Gunten, 2003b). Carbamazepine had more competitors for hydroxyl radicals at 42 mA/cm² than at 208 mA/cm², when the production of oxidants shifted to favour ozone, causing a more selective oxidation. Thus the energy input for complete CBZ

Table 5.2 – Energy consumption (E_{PC_0} , electrolysis only) for single-step oxidation of CBZ (1.3 mg/L, total volume: 3L) in different water matrices at 42 and 208 mA/cm².

water matrix	j	charge input	t_{PC_0}	power	E_{PC_0}
		mAh/L	min	W	Wh/L
deionised-p	42	15	4	2.23	0.05
<i>soft</i> -p	42	46	15	1.98	0.16
<i>hard</i> -p	42	59	20	1.59	0.18
<i>HORG</i> -p	42	≈ 93	30	1.45	0.24
STPE-p	42	204	60	1.52	0.51
STPE-p	208	112	7.5	8.04	0.33

degradation at the higher j (Table 5.2) was lowered.

In short, the j applied to the electrode not only regulated the oxidant species produced (HO[•] and O₃), but as a consequence also the elimination efficiency of trace pollutants such as CBZ (note that CBZ is likely to be partly oxidised and not fully mineralised). Even the efficiency of disinfection processes can be regulated with j, as the disinfection potential of these oxidants is different (Chapter 7).

5.3 Energy Consumption

During all previous experiments, it was observed that the energy consumption of the electrode varied not only with the j applied (Figure 4.4), but also with the matrix being electrolysed (Figure 5.5). According to Ohm's Law, the higher the electrical conductivity of a matrix, the lower the energy consumption of the electrode ($E_{E,pro}$). Deionised water, with a very low electrical conductivity, displayed a consumption of 13 W. The presence of ions in solution drastically decreased consumption. *soft* and the 22.5 μM solution of IC used in Chapter 3 were in the range of 11.5 W. The ion-richer matrix *hard* presented consumptions slightly above 9 W. The presence of organic materials reduced the power to a small extent (see pairs *soft/SORG* and *hard/HORG*), which can be attributed to the fact that proteins and humic substances also produce ions in solution. The effect of a non-ionic organic compound is more clearly seen with RNO (refer to Chapter 4), whose consumption was even higher than that of deionised water.

Figure 5.5 only presents the consumption of the electrode during operation. The amount of energy required for the elimination of CBZ as a target compound (E_{PC_0}) can be seen in Table 5.2. Although the electrolytic process was more energy-intensive in deionised water, the elimination of CBZ needed less energy (0.05 Wh/L) because of the shorter treatment time. The abatement of CBZ in STPE-p needed ten times as much energy as in deionised-p at 42 mA/cm² owing to competition reactions. It means that the lower electrolytic consumption in STPE-p in comparison to deionised-p was largely compensated by the longer treatment time required. The current increase to 208 mA/cm² accelerated the reaction and reduced consumption

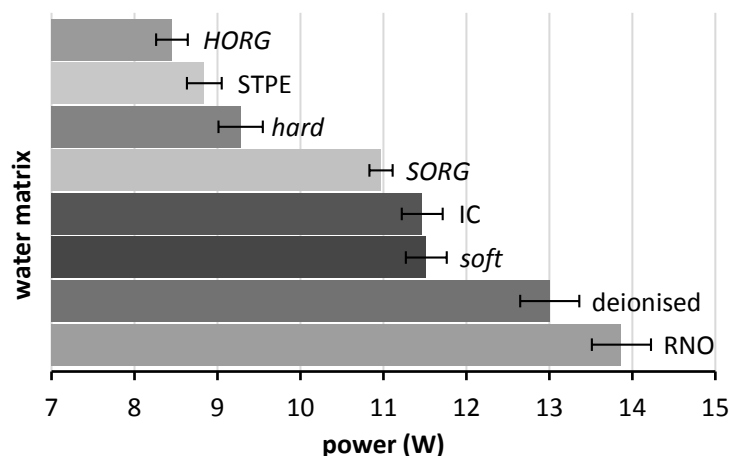


Figure 5.5 – Measured power of BDD (electrode only) during the electrolysis at 208 mA/cm^2 and 20°C in different water matrices.

RNO: N,N-dimethyl-4-nitrosoaniline, IC: indigo carmine (refer to Chapter 4).

by 34 %.

The average STP in Germany treats 80 m^3 of wastewater per person and year (DWA Deutsche Vereinigung für Wasserwirtschaft, Abwasser und Abfall e.V., 2012). Electricity costs for wastewater treatment including mechanical, microbiological and nutrient removal stages are around $8.6 \text{ €/}(\text{person}\cdot\text{annum})$. For completely eliminating CBZ (the parent compound) at 208 mA/cm^2 , an additional fee of 6.6 €/p.a. (+ 77 %) would result under the assumptions made here. In reality, CBZ and other xenobiotics do not occur in STPE at a concentration of 1.3 mg/L , but some 10^3 times lower. If the BDD electrode finds an application in STPs, it would probably not be a stand-alone technique, but part of a synergy with further water treatment processes steps, which could take up the more readily degradable substances coming from BDD treatment for further processing. These complementary processes could be of physical (membrane technology), chemical (chemical oxidation) and/or biological nature (biodegradation). In this way, the overall energy consumption could be reduced.

5.4 Summary

The ozone yield was strongly influenced by the water matrix. Of the six model matrices, highest ozone concentrations were measured in deionised water for all j values. The gradual addition of inorganic salts and organic material impaired the ozone accumulation in the water due to enhanced consumption of the arising oxidants by the matrix components. Organic matter was a more effective ozone consumer than inorganic ions were. Nevertheless, even in STPE there was considerable oxidising potential through ozone concentrations as high as 2.4 mg/L . Such potential enabled the elimination of the target molecule CBZ even at low j , when the measured residual ozone concentration was only around 0.002 mg/L .

The abatement of CBZ took place in all five water matrices tested in a time span of

3 to 60 min at 42 mA/cm² and followed the same kinetic trend observed for ozone generation (deionised-p > *soft-p* > *hard-p* > *HORG-p* > STPE-p). A *j* increment to 208 mA/cm² brought about an acceleration of the reaction from 60 to 7.5 min resulting in a reduction of energy consumption.

The formation of different oxidants, especially HO[•] and O₃, was shown to be adjustable over the current density. Furthermore, due to the different stabilities of these oxidant species, the elimination efficiency of target pollutants can be controlled with *j* as well, on the ground of the different specific reactivities of the oxidants formed.

Chapter 6

Formation of Organic By-Products

This chapter deals with the effect of the current density on by-product formation in water matrices with increasing chemical load. Only organic by-products, namely AOX and THMs, are addressed. Inorganic by-products such as chlorate, perchlorate and bromate are part of a partner research.

6.1 Inorganic Water Components

In Section 5.1.1, it was shown that the inorganic compounds present in a water matrix use up ozone (and additionally the emerging $\text{HO}\cdot$) to some degree. Ozone concentrations were thus lower in *soft* and *hard* than in deionised water. Halide anions are common matrix components that are readily oxidised by the ROS generated on BDD. Halides are of concern because once they are oxidised to a reactive form such as chlorine atoms ($\text{Cl}\cdot$), free chlorine (Cl_2) or hypochlorite (HOCl/OCl^-) for chlorine, they can halogenate the organic matter thus producing persistent and toxic by-products (according to eqs. 1.31 and 1.32 or analogous, Schwarzenbach et al., 2006). Furthermore, halides are ultimately oxidised to known health hazards at higher oxidation states such as chlorate, perchlorate and bromate (von Gunten, 2003b; Bergmann et al., 2009, 2011).

The chloride concentration was monitored during the electrolysis in STPE and *HORG* (Figure 6.1a). All measurements in *HORG* and STPE taken as a whole lay on a straight line with slope -0.0101 mgCl/mAh and a linear fit of 0.90. In absolute terms, the slope of the curve implies that only 0.77 % of the electrolytic power effected this reaction. Since chloride ($E_{\text{ox}}^\ominus = -2.59 \text{ V}$) is oxidised by $\text{HO}\cdot$ ($E_{\text{red}}^\ominus = 2.80 \text{ V}$) but not by ozone ($E_{\text{red}}^\ominus = 2.08 \text{ V}$, see Section 1.5), the reaction was confined to the thin reaction cage above the electrode surface. It was shown in Chapter 4 that the employed system suffered transport limitations. The hydrodynamic conditions in the reactor did not bring the matrix components effectively to the electrode surface. In this specific case, this was a desirable side-effect which reduced chlorine formation, but this may be detrimental for the degradation of ozone-refractory compounds requiring direct exposure to $\text{HO}\cdot$.

Also the chloride measurements for the individual water matrices followed linear

kinetics, but there was one significant difference between them. The lowest current density (42 mA/cm^2) was very efficient in eliminating chloride ions (slope $-0.0349 \text{ mg Cl/mAh}$). The higher the j , the less chloride ions were transformed per unit charge. Because at 42 mA/cm^2 the relative yield of hydroxyl radicals was highest (Chapter 4), more chloride underwent oxidation.

Bromide was consumed during electrolysis as well (not shown).

6.2 Organic Water Components

6.2.1 Adsorbable Organically Bound Halogens

The oxidation of halide ions produces halogen radicals which can halogenate the organic matter (following eq. 1.31 or equivalently for chlorine). Halogenated compounds are measured by the sum parameter AOX. No organic by-products formed in *soft* nor in *hard*, as these contained no precursor organic matter. In STPE, values as high as $254 \mu\text{g/L}$ were measured working at 42 mA/cm^2 (Figure 6.1b). In contrast, working at higher j produced between 50 and $75 \mu\text{g/L}$ at up to 3500 mAh/L . Recall from Table 5.2 that a charge input of 204 mAh/L was sufficient to oxidise CBZ, so treating the water with 3500 mAh/L was of scientific interest. Similarly for *HORG*, whose AOX concentrations are shown in more detail in Figure 6.1c. The current densities 42 (red) and 83 mA/cm^2 (black) produced more AOX (37 to $49 \mu\text{g/L}$) than higher j values for the same charge input. At 208 (green) and 333 mA/cm^2 (blue), a time span three to four times as long was required to reach comparable AOX concentrations, which is illustrated by the fact that the steepness of the lines flattened with increasing j .

The AOX formation rates for different waters in dependence of j are shown in Table 6.1. The AOX formation rate at 42 mA/cm^2 in comparison to that at 333 mA/cm^2 was seven times as high for *HORG* and 36 times as high for STPE. Every j increment brought about a reduction of the formation rate, being this most pronounced in the region below 100 mA/cm^2 (red + black). This is in agreement with the finding that at 42 mA/cm^2 comparatively more hydroxyl radicals (Chapter 4) and thus more atomic chlorine forms. At higher j , oxidant production shifted towards ozone, which is incapable of oxidising chloride. Nevertheless, the magnitude of the chloride reductions did not match the AOX concentrations measured. Halides must have been oxidised to further compounds as well, such as chlorate, perchlorate and bromate.

In the presence of $5.5 \mu\text{M}$ CBZ ($\approx 1 \text{ mg DOC/L}$), AOX formation remained unaltered in STPE-p at both current densities tested (no experiment was carried out at 333 mA/cm^2). Though CBZ should increase the organic content, its addition to STPE produced a dilution of the matrix, which explains the constant AOX formation. On the other hand, in *HORG*-p, carbamazepine did add an additional mg TOC/L to the 5 mg/L it contained without causing dilution, and AOX formation was therefore enhanced in comparison to *HORG* without CBZ. The measurement would appear in Figure 6.1c at the coordinates (95 mAh/L ; $69 \mu\text{g/L}$). In *hard*-p the presence of CBZ as an organic compound and thus an AOX precursor enabled the

Table 6.1 – Average AOX formation rate in dependence of the charge input in *HORG* and STPE at different current densities (R^2 shown in parentheses).

j (mA/cm ²)	AOX formation rate (µg/mAh)			
	<i>HORG</i>		STPE	
42	0.397	(0.993)	0.460	(0.710)
83	0.242	(0.996)		
208	0.075	(0.608)	0.034	(0.975)
333	0.057	(0.751)	0.013	(0.667)

formation of AOX and produced on average the coordinate (99 mA/L ; 18 µg/L), only a fraction of the measurements in *HORG*.

6.2.2 Trihalomethanes

The current effect had consequences on THM formation as well. For all j values and sampling times, the measurements in *SORG* were below the LOD. In *HORG*, a linear correlation became apparent when the sum of the THMs was taken (Figure 6.2a). An enhanced THM production took place at the lower current (208 mA/cm²) in comparison to 333 mA/cm² (8.64 vs. 3.91 ng/mAh, respectively).

A very illustrative phenomenon was observed when measuring the concentrations of individual THMs – chloroform, bromodichloromethane, dibromochloromethane and bromoform – in *HORG*. Figure 6.2b shows that bromoform and dibromochloromethane were the two products that more readily formed (2.0 and 0.85 µg/L, respectively, after 437 mA/L) although bromide was present at a concentration 250 times lower than chloride. The same phenomenon was observed by Al-Rasheed et al. (1997) when ozonating sea water. At 208 mA/cm², predominantly O₃ formed, which is able to oxidise bromide but not chloride. As a consequence, only little amounts of chlorinated THMs emerged, resulting from the direct exposure to HO· in the diffusion zone near the electrode. Chloroform and bromodichloromethane were found in a concentration range of 0.1 to 0.5 µg/L. With the current density, the oxidant species produced by the electrode can be regulated and this has profound consequences on the type of BPs formed.

The maximum THM concentration measured (3.7 µg/L) was well below the drinking water limit of 50 µg/L set by the German Drinking Water Ordinance 2012 (The US EPA (2012) is with 80 µg/L more admissible). In comparison to the AOX values reported in Figure 6.1c, the THMs represented between 5 and 9 % of the total amount. This means that up to 95 % of the AOX were different than the four individual THMs determined. The formation of further small halogenated by-products (*e.g.* haloacetonitriles, haloketons) was verified by Anglada et al. (2011). In the case of *HORG*, the halogenation of the large humic molecules is most likely to occur.

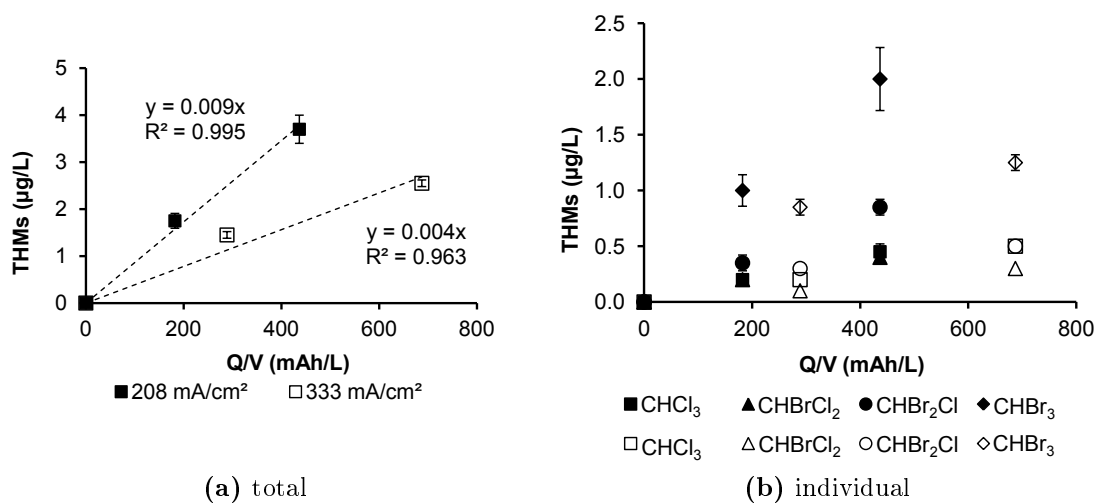


Figure 6.2 – THM formation in *HORG* upon BDD treatment at 20 °C. Black squares: 208 mA/cm². Open squares: 333 mA/cm². Where standard deviation is not shown, it equals zero.

6.2.3 Comparison to literature data

In comparison to the work by other authors utilising the same reactor type (CONDIAS) and the effluent of a municipal STP, the AOX values presented here were lower. Table 6.2 shows the AOX concentrations measured by various authors. The results by Haaken et al. (2010) are comparable to those measured in this study at 42 mA/cm². Bewersdorff (2005) (after conversion, because no charge input was reported) measured concentrations three times as high as those presented here for 208 mA/cm². Finally, Schmalz et al. (2009) reported a linear increase of AOX with charge input. The steepness of the line was 2 µg AOX/mAh, that is four times larger than that reported in Table 6.1 for 42 mA/cm² in STPE (highest value). Furthermore, Schmalz et al. measured an AOX concentration up to 1 mg/L at 1000 mAh/L. Such high concentrations are likely to have emerged as a result of the utilisation of even lower current densities as in this work, and also the fact that the BDDE employed in his work has experienced an optimisation in the last years toward enhanced ozone yields and thus lower AOX formation (due to the utilisation of an SPE, see Figure 5.2). In the past, BP concentrations were not directly linked to j , which is necessary in view of the electrolytic mechanism and its strong repercussions on water treatment.

In waters rich in chloride and organic substances, the AOX concentration may become critical. For highly polluted wastewaters, such as those in metal hardening plants, AOX values up to 2 mg/L have been reported (Table 6.2). In Germany, there are no discharge limit values for AOX from municipal wastewater treatment. However, a maximum AOX concentration of 1 mg/L for the metal and coating resin industry, 0.5 mg/L for *e.g.* the leather industry and 0.1 mg/L for the ceramic production have been stipulated in the Wastewater Ordinance from 2012 (German Federal Ministry of Justice, 2012) for direct discharge.

Table 6.2 – Comparison of AOX measurements in this study and literature in dependency of the applied current density.

AOX $\mu\text{g/L}$	Q/V mAh/L	j mA/cm^2	type of wastewater	reference
189	189	42	STPE	this study
224	450			
53	898	208	STPE	this study
75	1862			
64	1488	333	STPE	this study
64	3477			
25-112	100	15-90	STPE	Haaken et al. (2010)
170	900	155	STPE	Bewersdorff (2005)
210	1862			
200	20	2.5-120	STPE	Schmalz et al. (2009)
1000	1000			
2000	15000	8-66	hardening plant	Schmalz et al. (2008)

6.3 Summary

The inorganic water components underwent reactions with the organic material upon electrolysis. Reductions of chloride and bromide concentrations and simultaneous increases in halogenated compounds (AOX) were observed. By-product formation was found to be dependent on both water matrix, enhanced by the presence of organic compounds and halides, and current density. The lower the j , the more hydroxyl radicals emerged and the more AOX/THM were generated for a given charge input. Even at low j values, the concentrations measured ($< 254 \mu\text{g/L}$) were low and would not endanger compliance with any existing water ordinances. The concentration of several THMs ($3.7 \mu\text{g/L}$) accounted for between 5 and 9% of the AOX measured ($\approx 55 \mu\text{g/L}$).

A j of 208 mA/cm^2 can be considered most favourable for treatment. Not only was it more energy-efficient in the elimination of a target compound (Chapter 5), but it also generated less halogenated by-products.

Chapter 7

Inactivation of waterborne bacteria

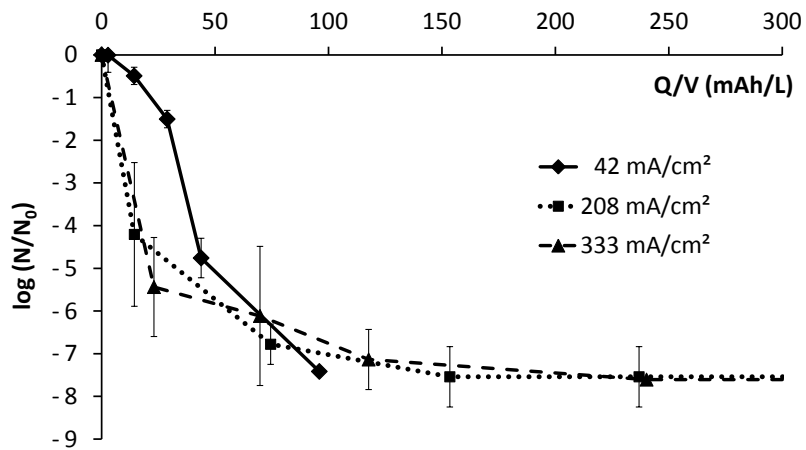
In Chapter 4, it was shown that different ROS form on BDD depending on the current density. These ROS display various oxidation potentials. Thus, j should not only influence oxidant generation, but also the disinfection efficiency and mechanism. This chapter focuses on the effect of j and the water matrix on bacteria inactivation.

7.1 Current Effect on Bacteria Inactivation

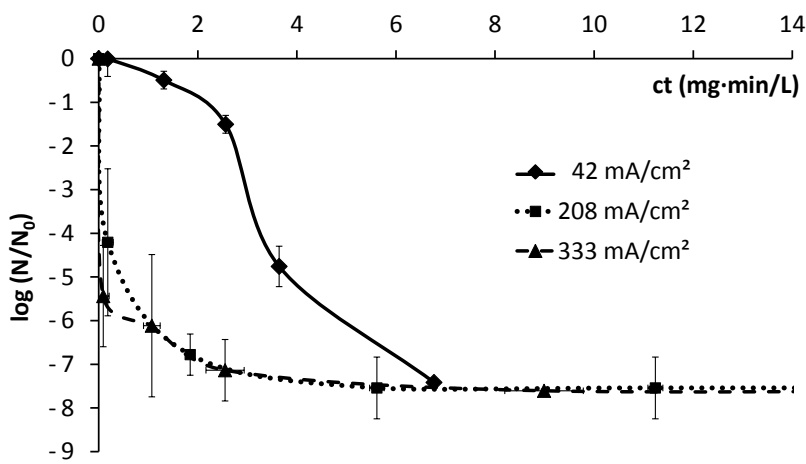
The inactivation of *E. coli* was tested in *soft-b* at various current densities in order to determine the optimum electrode conditions for disinfection. Since the entirety of oxidative agents brought into the system during electrolysis cannot be measured, determination of residual ozone concentrations was the method of choice to trace the reaction (Section 2.3.2).

Figure 7.1a shows the decrease of the survival ratios against the charge input per volume. Initial bacteria numbers varied between 10^7 and 10^8 CFU/mL, and for each current density complete inactivation of about 7–8 log units could be observed with a strong initial reduction and a slower decrease of bacteria counts afterwards. Variations of j led to different treatment times. Complete inactivation of *E. coli*, which was achieved at about 100 mAh/L, took less than 5 minutes at a current density of 333 mA/cm^2 , whereas it took 30 minutes at 42 mA/cm^2 . Recall from Section 2.3.8 that the parameter *charge input per volume* (Q/V) normalises time and thus relates to electrolytic efficiency. It can be seen that the curve for 42 mA/cm^2 displayed a remarkable deviation regarding the inactivation rates below 30 mAh/L in Figure 7.1a. This means that the lower j was less efficient for disinfection. Nevertheless, as soon as j surpassed 100 mA/cm^2 and predominantly ozone formed, inactivation depended on the total charge input instead of j (the disinfection efficiency at 208 mA/cm^2 was comparable to that at 333 mA/cm^2).

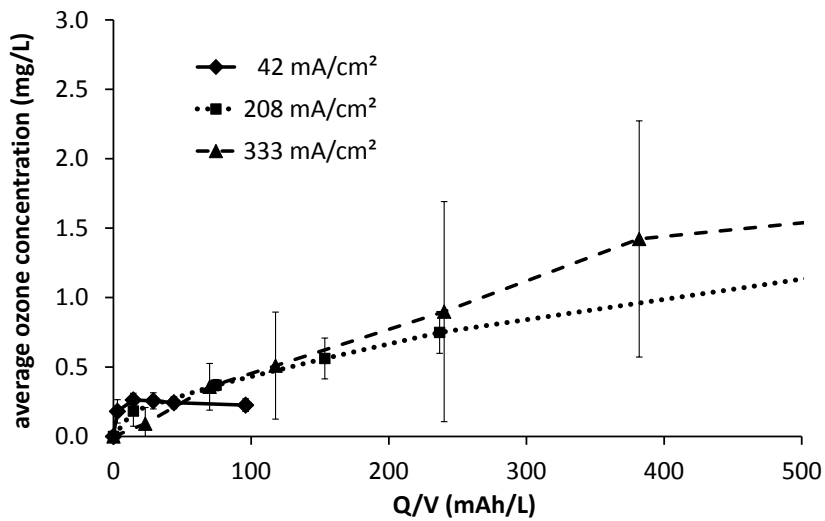
To find an explanation for this observation, the exposure of *E. coli* to ozone was quantified. Figure 7.1c displays the residual ozone concentrations in the bacteria suspension. In Table 5.1 a linear correlation between j and residual ozone concentrations in various waters was described. The same tendency could be observed during the disinfection experiments. In the bacteria-spiked *soft-b*, ozone concentra-



(a) inactivation efficiency



(b) inactivation in dependence of ozone exposure



(c) O₃ concentrations

Figure 7.1 – *E. coli* inactivation in *soft-b* at various current densities and 20°C. (a) inactivation vs. the charge input per volume, (b) inactivation vs. *ct* (based on O₃ only), (c) ozone concentrations during disinfection.

tions between 0.25 mg/L at 42 mA/cm² and 1.5 mg/L at 333 mA/cm² were measured. Thereby, *soft-b* presented a behaviour in between *HORG* and *STPE* in Figure 5.1.

In a subsequent step, the measured residual ozone concentrations were multiplied with the treatment time to obtain the ozone exposures (*ct*). Figure 7.1b illustrates the same curves as Figure 7.1a but in dependency of the ozone concentration and disinfection time (*ct*) according to the Law of Chick and Watson (Gottschalk et al., 2010, Chapter 3). Thus, these curves do not represent efficiency any more (normalisation to Q/V). Instead, they display the dependency of inactivation rates on ozone exposure alone. Inactivation of 4.2 log units could be achieved at a *ct* value of 0.18 mg·min/L at both 208 mA/cm² and 333 mA/cm². The *ct* curves at those current densities became identical and reflect the strong dependency of bacterial inactivation on ozone concentrations. The low *j* of 42 mA/cm² differed from that tendency with a delayed reduction of *E. coli*. A *ct* value of approximately 3.5 mg·min/L clearly indicates another, less effective disinfection mechanism in this case.

Since for current densities below 100 mA/cm² the efficiency of ozone formation was found to be significantly lower (Chapter 4 and Kraft et al., 2006b), while the generation of HO· was favoured, it can be postulated that bacterial inactivation at low *j* was not predominantly driven by ozonation but by the attack through hydroxyl radicals. HO· could instantly and non-selectively react with cellular components of the microorganisms and cause damage rather to the outer cell membrane. However, major damage and bacterial inactivation are achieved through reactions with the DNA (von Gunten, 2003b). In contrast to ozone, HO· are not able to penetrate into the cells, and, as a consequence of their short-lived existence, their reaction radius is strongly limited. Therefore, the disinfecting potential of HO· has been reported to be lower than that of ozone, independent of the water matrix (Wolfe et al., 1989; Cho et al., 2003).

The depicted *ct* values lie in the range of other literature data (Tanner et al., 2004). However, no comparison can be drawn in terms of the applied current densities as a different technology was used for electrochemical ozone generation.

7.2 Energy Consumption

Higher current densities did not only result in more ozone but also in a higher energy consumption (Table 7.1). Operation of the electrode at 42 mA/cm² resulted in the lowest energy requirement regarding process-intrinsic energy. However, since the treatment time until inactivation was extended compared to higher current densities, the total energy consumption was highest for the low *j*. As seen in Chapter 3, $E_{E,mix}$ had a considerable impact at prolonged treatment times. The most advantageous configuration was 208 mA/cm² with a total energy consumption of 1.09 Wh/L for a log 5 removal and 4.83 Wh/L for a log 7.4 removal of *E. coli*. A further *j* increase yielded higher energy values for both, process-intrinsic and total energy consumption.

Since both 208 mA/cm² and 333 mA/cm² were shown to be equally efficient in dis-

Table 7.1 – Calculated energy consumption for log 5 and log 7.4 (complete) *E. coli* inactivation in *soff*-b in dependence of j.

water matrix	j	log 5 removal					complete inactivation				
		Q/V	t_{log5}	$E_{E,log5,pro}$	$E_{E,log5,tot}$	Wh/L	Q/V	$t_{log7.4}$	$E_{E,log7.4,pro}$	$E_{E,log7.4,tot}$	Wh/L
<i>soff</i> -b	42	49	20	0.14	8.69	96	30	0.25	15.72		
	208	34	2.5	0.17	1.09	143	10	0.75	4.83		
	333	21	1	0.74	1.10	197	10	8.74	13.06		
STPE-b	208	61	5	0.27	2.13	127	10	0.63	5.05		

$E_{E,log5,pro}$ and $E_{E,log7.4,pro}$: process-intrinsic electrical energy for log 5 removal and complete inactivation, $E_{E,log5,tot}$ and $E_{E,log7.4,tot}$: total electrical energy for log 5 removal and complete inactivation, respectively.

infection per unit charge, while 208 mA/cm² displayed a lower energy consumption, this j was chosen as standard configuration for further disinfection experiments. The election is backed by the reported low energy consumptions, $E_{E,pro}$, for this j from Chapter 3.

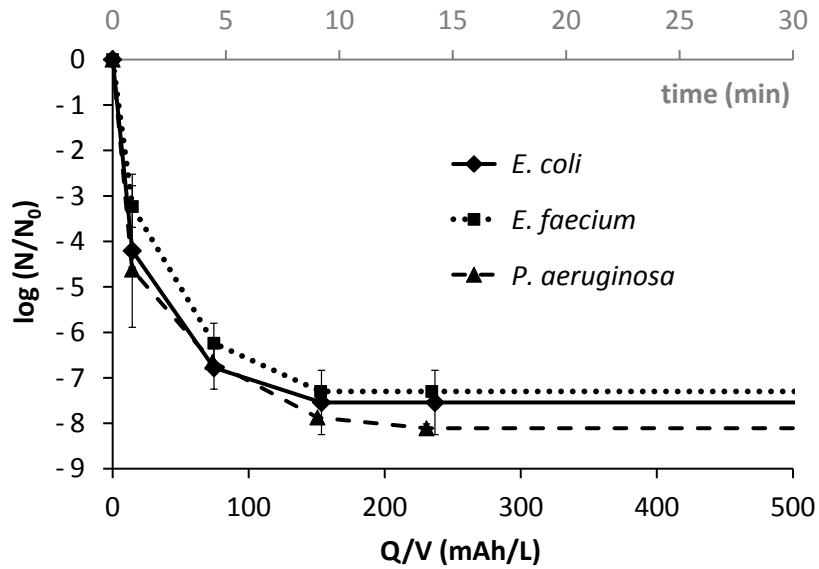
7.3 Different Bacteria Strains

Different bacteria species can show variable sensitivity towards disinfectants. To test whether BDD is effective against further microorganisms, electrochemical inactivation of the gram-negative model bacteria *E. coli* and *P. aeruginosa* and the gram-positive *E. faecium* in *soft-b* was determined in comparison.

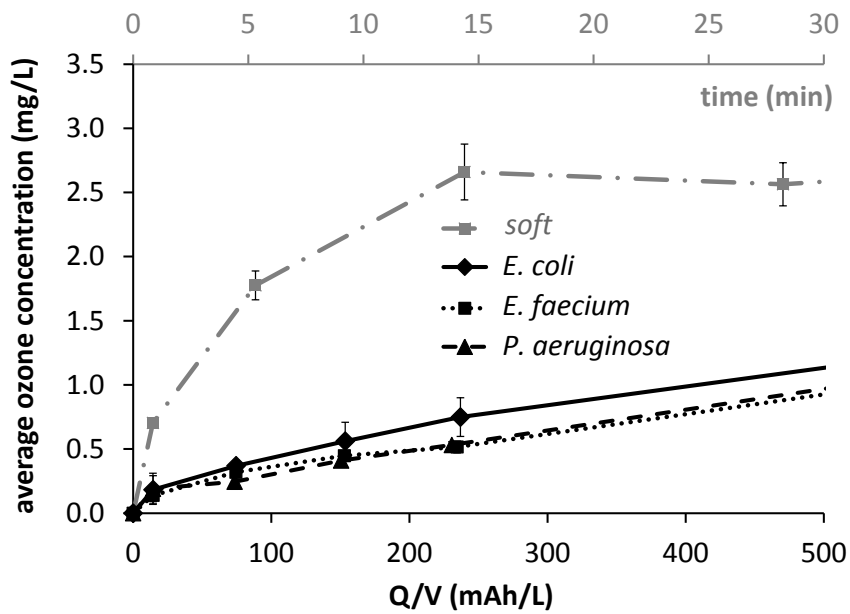
Inactivation curves of the three model organisms are displayed in Figure 7.2a. Since all experiments were conducted at 208 mA/cm², the specific charge input, and therefore also the disinfection progress can be directly linked to disinfection time. Bacterial reduction rates of at least 5 log units could be observed for all three model organisms during the first 75 mAh/L (5 min), followed by a continuous but slower inactivation afterwards. Complete inactivation was achieved within 150 mAh/L (10 min).

The sensitivity of the different species towards disinfection was comparable but appeared slightly higher for *E. coli* and *P. aeruginosa*, whereas the gram-positive *E. faecium* showed more resistant against oxidation. The outer cell wall of gram-positive bacteria such as *E. faecium* has been described to be less penetrated and damaged by oxidising agents than that of gram-negative bacteria (*E. coli* and *P. aeruginosa*) due to its complex composition (Restaino et al., 1995; Khadre et al., 2001). The cell walls of gram-positive bacteria consist of a thick structure of several peptidoglycan layers, whereas gram-negative species are characterised by an outer membrane containing lipoproteins, lipopolysaccharides and a thin layer of peptidoglycans. It was reported that N-acetylglucosamine present in the peptidoglycan layer could not be oxidised by ozone in aqueous solution (Khadre et al., 2001). The data in Figure 7.2a account for minor disparities as a consequence of different cell wall constitutions in gram-positive and gram-negative bacteria. Due to the fact that bacterial reduction of at least 5 log units could be observed within the first minutes for both gram-positive and gram-negative bacteria, BDD seems to be applicable for various disinfection purposes.

Ozone showed a continuous increase during disinfection (Figure 7.2b). The residual ozone concentrations in solutions of the three bacteria strains were almost identical. Only for *E. coli* disinfection did the ozone curve slightly differ from those measured for *P. aeruginosa* and *E. faecium*. Ozone measurements in *soft* (without addition of microorganisms) were significantly higher for the whole analysis period compared to those in the bacteria-spiked solutions. Even after complete bacteria inactivation (from 150 mAh/L onwards) ozone was consumed by residual cell material in the solution. The amounts of residual ozone in the sample solutions can be expected to approach that of pure *soft* when the oxidation of the cell material as well as other organic and inorganic matter is completed (mineralisation).



(a) Inactivation of different bacteria strains



(b) Residual ozone concentrations during bacteria inactivation

Figure 7.2 – (a) Inactivation of *E. coli*, *P. aeruginosa* and *E. faecium* and (b) corresponding ozone concentrations during electrolysis in *soft-b* at 208 mA/cm² and 20 °C. The time axis is only referential.

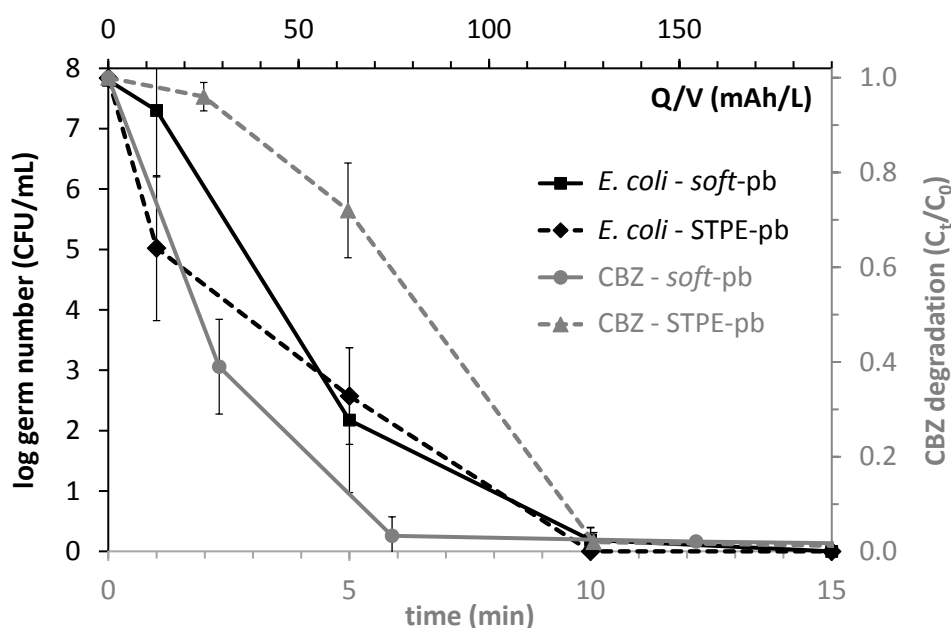


Figure 7.3 – *E. coli* inactivation and simultaneous CBZ degradation in *soft*-pb and STPE-pb at 208 mA/cm².

7.4 Matrix Effect on Disinfection

It was shown in Chapter 5 that the matrix components of water compete with target compounds for oxidative species. To examine the matrix effect on disinfection, inactivation rates of *E. coli* in *soft*-pb were compared with those in STPE-pb (-pb: pharmaceutical and bacteria-spiked). To gain further insights into the disinfection mechanism, the experiments were performed in the presence of the target compound CBZ. Disinfection of *E. coli* and CBZ degradation were simultaneously carried out at a current density of 208 mA/cm².

Carbamazepine degradation was observed, as in Chapter 5, to be strongly dependent on the complexity of the water matrix (Figure 7.3). Whereas about 70 mAh/L (6 min) were required to almost fully oxidise CBZ in *soft*-pb, 120 mAh/L (10 min) were required in STPE-pb to reach the same level of degradation. In contrast, complete bacteria inactivation could be observed in both water matrices at around 120 mAh/L (\approx 10 min). The initial disinfection rate even appeared quicker in STPE-pb when compared to *soft*-pb. This means that the reduced oxidation rates observed for CBZ degradation could not be noted during disinfection. As the matrix effect is still expected to be present in STPE-pb, bacteria inactivation must have been governed by a different mechanism, one that compensated for the matrix effect described in Chapter 5.

In chloride-rich water, chlorine and hypochlorite, both commonly used disinfectants, are by-products that result from reactions with HO \cdot (eqs. 1.25 and 1.26, von Gunten, 2003b). STPE-pb had a higher chloride concentration (216.6 mg/L) than *soft*-pb (40.7 mg/L). It is thus likely that those disinfectants formed at higher concentrations in STPE-pb and compensated for the lower ozone yield. A clear increase of

inactivation ratios at higher chloride concentrations has been shown in studies with varying chloride concentrations in water (Schmalz et al., 2009; Liu et al., 2012; Yao et al., 2011). Furthermore, Wolfe et al. (1989) detected a greater bactericidal effect of free chlorine in wastewater compared to ozone. In the present investigation, the role of HO \cdot in STPE-pb probably was negligible owing to the fact that the reactive radicals cannot diffuse away from the electrode and immediately react with other water components.

The electrolysis in STPE-pb almost doubled the energy values for disinfection-grade inactivation in *soft*-pb, but was comparable for the complete inactivation (Table 7.1). The energy expenditure in STPE-pb (2.13 Wh/L for *E. coli* disinfection) corresponded with literature data which reported a total consumption of 2.0–2.6 Wh/L for a 5 log reduction of *E. coli* (Haaken et al., 2012).

7.5 Fate of Organic Matter

It was observed in Section 7.1 that the residual ozone concentrations in the bacteria-spiked *soft*-b were comparable to measurements in *HORG* and STPE. Bacterial cell membranes and inner cell components used up ozone and ROS in the same fashion as proteins and humic acids in *HORG* and STPE did. Consequently, very similar trends in DOC values were measured. Table 7.2 presents measurements of DOC concentrations before and after disinfection. DOC values increased after treatment (see also Section 5.2.1). These findings represent the conversion of complex organic matter during the oxidation process. For instance, residual cellular material that is filtered out during the preparation for DOC measurement is oxidised to better degradable and more soluble compounds that remain in solution (Kerc et al., 2004).

The variation in DOC concentrations indicates to which degree organic matter was transformed during the oxidation process. In *soft*-b, DOC concentrations rose from 3.8 to 6.6 mg/L, while in STPE-b only a slight increase from 5.4 to 6.0 mg/L was observed (Table 7.2). According to literature data, it typically requires a minimum of 3 g of O $_3$ to remove 0.2 g of DOC (Gottschalk et al., 2010). Since residual ozone concentrations in the current experiments were around 2.5 mg/L for non-spiked *soft* (containing few ozone consuming compounds, recall Figure 5.1b), this relatively low ozone excess was insufficient for the removal of all organic material in the bacteria-spiked solutions, considering that initial DOC values were about 5.4 mg/L.

The conversion of complex organic matter to better degradable compounds carries the risk of bacterial regrowth, as those compounds can be more easily consumed by microorganisms. Excess ozone as well as residuals of other disinfectants such as chlorine in the aqueous solution will, in contrast, act preventively. Already minimum amounts of excess ozone were found to successfully inactivate bacteria from aqueous solutions. How much ozone remains in solution depends in turn on the water matrix (Lazarova et al., 1999; Khadre et al., 2001; Kowalski et al., 1998).

Table 7.2 – DOC, AOX and chloride concentrations in *soft*-b and STPE-b before and after disinfection at 208 mA/cm².

time point	<i>soft</i> -b ^a			STPE-b ^b		
	DOC mg/L	AOX µg/L	Cl ⁻ mg/L	DOC mg/L	AOX µg/L	Cl ⁻ mg/L
before disinfection	3.8	<LOD	40.7	5.4	13.3	216.6
after disinfection	6.6	<LOD	36.5	6.0	157.7	190.2

disinfection duration: ^a 30 min, ^b 60 min.

7.6 By-Product Formation

AOX and chloride concentrations were measured in both bacteria-spiked water matrices before and after disinfection (Table 7.2). In *soft*-b, AOX concentrations were always below the detection limit of 10 µg/L, although here, in contrast to Chapter 6, the cell material provided organic precursors of AOX. In STPE-b, AOX levels were found to increase from 13.3 up to 157.7 µg/L after electrolysis. These concentrations are in a non-critical range (refer to Chapter 6).

As a result of AOX and BP formation in STPE and *HORG*, chloride levels decreased in both water matrices. However, as observed in Chapter 6, AOX concentrations in STPE were in the µg/L-range, while chloride losses were in the mg/L-range. The formation of both free chlorine as well as ClO₃⁻, ClO₄⁻ and ClO⁻ by the oxidation of chloride ions could account for the apparent chloride losses. Their determination should be topic of further research.

7.7 Summary

The presented data show that inactivation mechanisms of *E. coli*, *E. faecium* and *P. aeruginosa* can be influenced by variations of electrode parameters on the one hand and the water matrix on the other hand. In *soft*-b, the applied *j* defined whether the disinfection was ozone or radical-driven. The ozone mechanism (*j* > 100 mA/cm²) was more efficient, as ozone is able to penetrate the cell wall and directly attack DNA. Hydroxyl radicals, on the contrary, are scavenged on the cell wall. The more complex matrix STPE-b exhibited a different, probably chlorine-driven disinfection mechanism, so that disinfection efficiency remained comparable to that in *soft*-b. Significant differences between three bacteria strains could not be observed and all of them were inactivated in a time span of 5–10 min at 208 mA/cm².

Chapter 8

Degradation Pathways of Organic Compounds as a Tool for the Characterisation of Advanced Oxidation Processes

The idea of having tailor-made oxidants for different applications is appealing, but at the same time hard to achieve in practise. Ozone, for instance, decays to hydroxyl radicals upon reaction. Furthermore, electrochemical AOPs such as BDD do not just produce radicals but also ozone. Thus, pure radicalarian or ozonolytic processes may not always occur. Moreover, secondary oxidants may derive from ozone and hydroxyl radicals. The superoxide ion (O_2^-) forms upon ozone decay (von Gunten, 2003a), while hydroxyl radicals are able to oxidise chloride to chlorine (Refer to Chapter 6). In view of this situation, a characterisation of the species generated during the operation of different AOPs is of utmost importance.

The application of different AOPs can lead to diverse oxidation products (Christensen et al., 2009). This can be shown by two representative examples. Sulfamethoxazole, an antibiotic compound, has been treated with ozone (Beltrán et al., 2008; Rodayan et al., 2010; Gómez-Ramos et al., 2011), a combination of ozone and a hydroxyl radical scavenger to suppress secondary reactions (Abellán et al., 2008) as well as with AOPs (hydrogen radicals) such as TiO_2 photocatalysis (Hu et al., 2007), solar photo-Fenton (Trovó et al., 2009a), photocatalytic ozonation (Beltrán et al., 2008, 2009), O_3/H_2O_2 (Gómez-Ramos et al., 2011), direct photolysis (Trovó et al., 2009b) and electro-Fenton with a boron-doped diamond electrode (Dirany et al., 2010). These investigations resulted in the identification of a great variety of *transformation products*, TPs. In some instances, the reaction mixture containing TPs became more toxic than the parent compound alone (Abellán et al., 2008; Gómez-Ramos et al., 2011; Trovó et al., 2009b).

Furthermore, the oxidation of CBZ with ozonation (with a radical scavenger, McDowell et al., 2005) and with UV/ H_2O_2 (Vogna et al., 2004) has been characterised. The kinetics and mechanisms are known and differ from one another.

It was this fact that made the idea of a *back-to-front investigation* as a character-

isation tool plausible. By looking at the degradation products resulting from an oxidative treatment, one should be able to deduce whether the oxidation was caused by ozone or hydroxyl radicals. Since the chemical structure of SMX considerably differs from that of CBZ, it is oxidised differently so that the utilisation of these two substances as model compounds could offer complementary information on oxidation mechanisms.

The characterisation of AOPs should include the energetic component to better evaluate which technology is suitable for a certain application. The energetic demand of an AOP depends on the total amount of energy and chemicals consumed. By monitoring the TPs, it should be possible to keep track of the extent of the reaction and link it to the energetic demand of the related technology.

In this chapter, the TPs of CBZ and SMX resulting from three different AOP technologies, namely UV/H₂O₂, DD* and BDD, are compared with each other and with the existing literature. The comparison should demonstrate which oxidising agents are formed by these technologies, so they can be better understood and characterised.

8.1 Oxidation Pathways

An extensive literature research was initially carried out to identify all relevant TPs of SMX and CBZ resulting from ozone and hydroxyl radical exposure. Radical pathways were found for solar photo-Fenton, electro-Fenton, photodegradation, photocatalytic ozonation, O₃/H₂O₂ and TiO₂ photolysis in the case of SMX and for UV/H₂O₂ in the case of CBZ. Since the main oxidant species in AOPs should be HO[•] regardless of the specific technology, all TPs from literature were considered meaningful, even if the reported methods differed from the AOPs used for this research. With these TP ions as well as their possible H, Na and K adducts and the dimer clusters of the parent compounds, a mass spectrometric database was set up (Appendix A). The exact masses (four decimal places) of all species were fed into the database.

In a subsequent step, the experimentally recorded mass spectra from the UV/H₂O₂, DD* and BDD treatments were screened in the database for the TPs and their adduct ions. The masses were corrected either with the standards from the mass correction kit or with the Na or K adducts of the parent compounds, depending on the visibility of the mass spectrometric signals. The corrected masses showed a very good agreement with the theoretical masses (Table 8.2 in page 113 and Table 8.3 in page 114). The deviation was in most cases below 10 ppm, thus leading to empirical formulas for molecules up to 1000 Da.

The *ozone products* in literature originated from conventional ozonation and not from in-situ ozonation (as in the case of BDD). For a mechanistic investigation, this is only a technical difference.

Figure 8.1 and Figure 8.2 show the degradation products from Tables A1 and A2 that were experimentally found in this study. Many products from both the ozone and HO \cdot pathways, as well as some adduct ions were encountered. Every molecule is labelled with the oxidation technology for which it was found. Noticeably, the labels for the four different methods / conditions used (HP, DD*, DD', DD'') are spread throughout the pathways and even within single reaction routes. Furthermore, Figure 8.1a is already an assortment of different pathways reported in literature. Such an intertwining is a hint that the reaction mechanisms are mostly hydroxyl-radical-driven and thus comparable, regardless of the specific technology utilised. Moreover, this is proof that the reactive species in all technologies are equal.

Figure 8.1 presents the degradation pathways of SMX. Nine transformation products belonging to the *SMX-radical pathway* from literature were found in this study (**A-J**). Additionally, a new mass trace with m/z 262.0569 was observed. A structure that suits this mass trace (**F**, Figure 8.1a) is postulated for the new TP based on reported oxidation mechanisms (García-Galán et al., 2012). As for the *SMX-ozone pathway*, four species (**K-N**, Figure 8.1b) reported in literature (Abellán et al., 2008) could be detected.

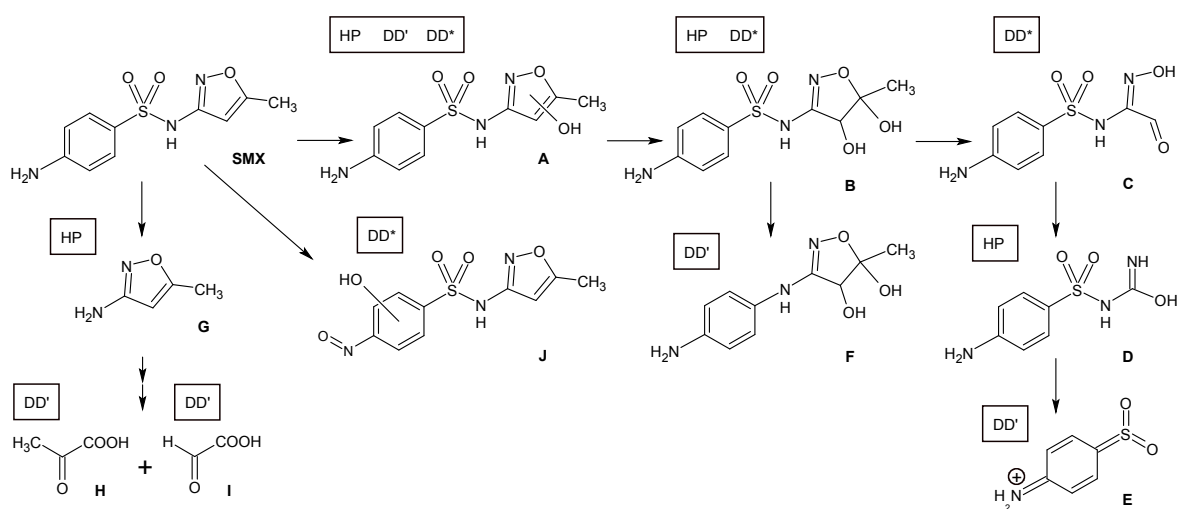
Figure 8.2 shows the degradation pathways of CBZ for both hydroxyl radicals and ozone adapted from literature. For the reaction with HO \cdot , there was only one rather complete pathway known for CBZ, whose adaptation is shown in Figure 8.2a. The CBZ-ozone pathway in Figure 8.2b was extended for the hydrated precursor of 1-(2-benzaldehyde)-4-hydro-(1*H*,3*H*)-quinazoline-2-one (BQM), preBQM, which was visible in this study. However, due to its low concentration, no structure validation could be performed by tandem MS or nuclear magnetic resonance (NMR). This molecule was postulated by McDowell et al. (2005) but could not be detected in their study.

Several unknown mass traces were found as well. Their relevance should be further evaluated with non-target analytic methods to decide whether they originate from the pharmaceutical substances and if they can also be found in real waters.

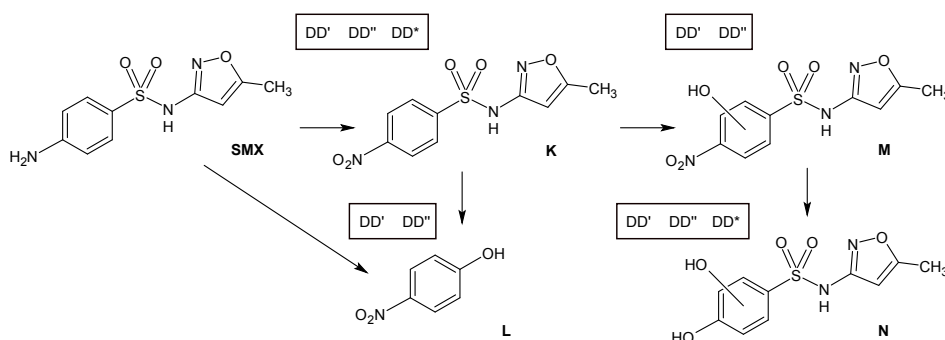
8.2 Characterisation of Hydrogen Peroxide Photolysis (UV/H $_2$ O $_2$)

Hydrogen peroxide photolysis was the only homogeneous AOP used in this study. During the operation of homogeneous AOPs, hydroxyl radicals emerge in the bulk of the solution at comparatively lower concentrations than with heterogeneous AOPs such as BDD or photocatalysis (TiO $_2$ / $h\nu$ /O $_2$).

In the experiments, predominantly species from the radical pathways of SMX and CBZ were detected (Figure 8.1 and Figure 8.2). However, there was some level of crossover: *ozone products* were found for the UV/H $_2$ O $_2$ treatment of CBZ, although this technique is supposed to produce only HO \cdot . Ozone is known to decay in water



(a) hydroxyl radical pathway



(b) ozone pathway

Figure 8.1 – Degradation pathways and detected degradation products of SMX upon (a) HO[•] attack and (b) ozonation according to literature.

Two-letter abbreviations stand for the method from which the molecule stemmed: HP: hydrogen peroxide photolysis, DD' and DD'': electrolysis with BDD at 42 and 208 mA/cm² respectively, DD*: electrolysis by a micro BDD directly coupled to MS. Species **A** to **D** were reported for solar photo-Fenton (Trovó et al., 2009a), species **E** for photodegradation with a solar simulator (Trovó et al., 2009b), species **G** for both of these treatments (Trovó et al., 2009a,b), compounds **H** and **I** were found for electro-Fenton with BDD (Dirany et al., 2010), compound **J** for O₃/H₂O₂ (Gómez-Ramos et al., 2011), species **K** to **N** were reported for ozone treatment (Abellán et al., 2008) and compound **F** is postulated in the present work.

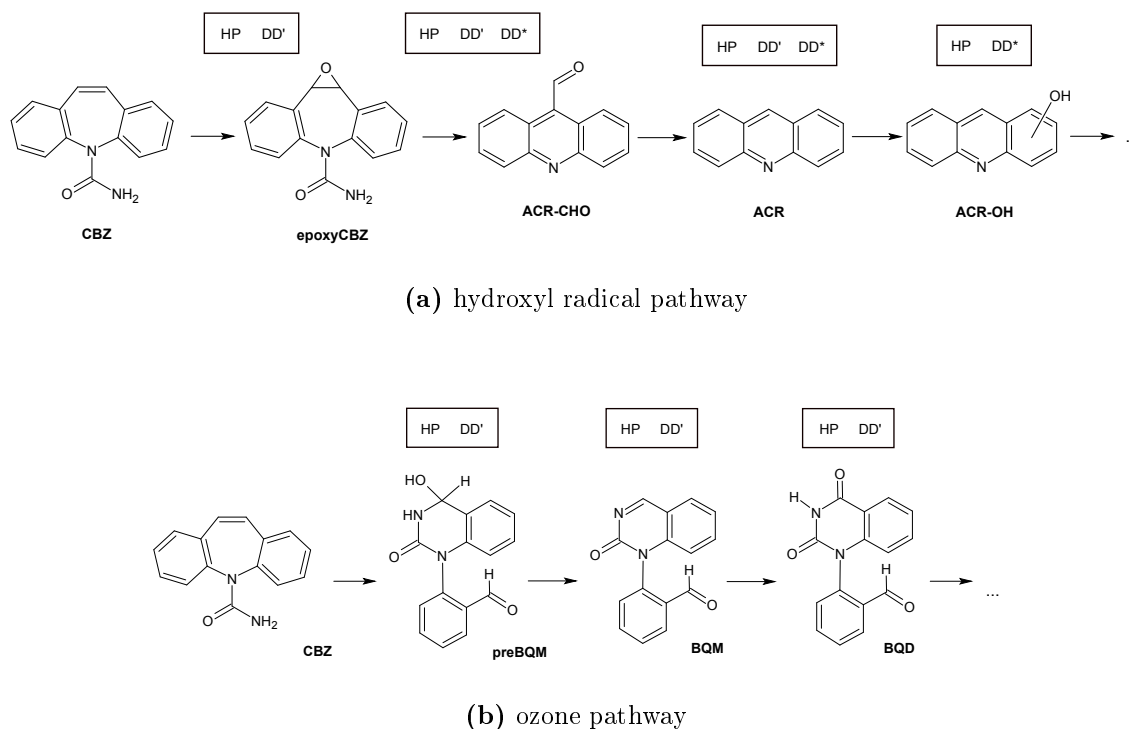


Figure 8.2 – Degradation pathways and detected degradation products of CBZ upon (a) HO[•] attack (Vogna et al., 2004) and (b) ozonation (McDowell et al., 2005).

Two-letter labels stand for the method from which the molecule stemmed: HP: hydrogen peroxide photolysis, DD': electrolysis with BDD at 42 mA/cm², DD*: electrolysis by a micro BDD directly coupled to MS.

to hydroxyl radicals (von Gunten, 2003a). Thus, *radical products* can be expected to an extent during ozonation. In this study, the opposite situation was observed.

Ozone measurements (according to Bader and Hoigné, 1981) of the reacting mixture in the UV/H₂O₂ reactor showed that an ozone-equivalent species emerged, which behaved similarly to ozone in that it decoloured indigo carmine. This species must have been different than HO[•] due to a seven second delay between sample taking and pouring into the flask containing indigo carmine. HO[•] are not produced in the absence of ultraviolet light and decay within a fraction of a second. The equivalent concentration of the ozone-equivalent species was between 0.05 and 0.1 mgO₃/L (enriching in time).

8.3 Characterisation of the Micro Diamond Electrode Coupled to Mass Spectrometry (DD*)

The coupling of a micro-scaled electrochemical cell with MS is a novel technique that has been described as a powerful tool for the study of the oxidative (and reductive) treatment of environmental pollutants (Baumann and Karst, 2010; Hoffmann et al., 2011). An important advantage that it offers is the in-line injection of the

electrolysed solution into the analytic device. As a result, instantaneous changes can be recorded and sampling, as well as sample preparation, becomes unnecessary. Since the potential can be varied throughout the run, the method is a means of studying the electrochemistry of the substances. As the system was equipped with a BDD electrode, the formation of hydroxyl radicals from direct water electrolysis was expected and thus, AOP conditions should have been reproduced. However, owing to the system scale and the direct coupling to MS, DD* alone is not an AOP, but rather a miniaturised adaptation of an electrochemical AOP. This technique should be explorable with the approach developed in this study.

Unlike UV/H₂O₂, the treatment with DD* is a heterogeneous AOP. The hydroxyl radicals form on the surface of the electrode at comparatively high concentrations, but are localised and unable to diffuse into the bulk volume. Nevertheless, treatment with DD* was comparable to that with UV/H₂O₂. Primarily *radical products* were observed (Figure 8.1 and Figure 8.2). The potential increased continually, starting at 0 V and rising up to around 2.4 V. The measured current density rose from 0 to 69 mA/cm² in the case of SMX and to 49 mA/cm² in the case of CBZ. Though the water used was completely deionised (very low conductivity), ozone can theoretically form through the reaction of HO· with each other. Indeed, for SMX the compounds **K** and **N** stemming from the ozone pathway were detected at a higher 69 mA/cm².

8.4 Characterisation of the Boron-Doped Diamond Electrode (DD)

The treatment with BDD was in principle very similar to that with (DD*), as the electrode material was identical, but in laboratory scale. The differences were the applied potential on the one hand and the electrode stack on the other hand. Whereas the potential was raised to 2.4 V during DD* and the current was a non-adjusted result of the potential, for BDD j was set to 42 or 208 mA/cm² and the potential was left unadjusted. It reached values of 1.7 and 4.0 V respectively. The employed electrode stack comprised an SPE between anode and cathode, whose role was to locally increase the hydroxyl radical density at the interface junctures. This in turn promoted the formation of ozone. Tests showed that ozone formed from 20 to 40 mA/cm² upwards with this electrode stack (internal communication with Mr. Fryda, CONDIAS). In contrast, the DD* system produced only limited amounts of ozone between 49 and 69 mA/cm² (Section 8.3).

Transformation products of both pathways (HO· and O₃) were observed for the two test compounds when working at 42 mA/cm² (DD', Figure 8.1 and Figure 8.2). The target compounds SMX and CBZ were exposed to hydroxyl radicals every time they were pumped onto the surface of the BDD electrode (recirculation) and to ozone in the bulk of the solution.

For SMX, an additional, higher current density of 208 mA/cm² was tested (DD''). Only products from the ozone pathway were detectable at this higher j (Figure 8.1). Above the ozone formation threshold (20 to 40 mA/cm²), a current increment brings about a higher ozone production in comparison to HO· (Chapter 4). An increase

from 42 to 208 mA/cm² was so pronounced that virtually all SMX was subjected to ozonation and almost no radical attack. At 208 mA/cm², hydroxyl radicals must still have formed, but at such spatial density that they probably swiftly collided with one another to form ozone before getting the chance of encountering and oxidising SMX molecules. Furthermore, whilst radicals are confined to the electrode surface, ozone can be transported into the aqueous phase, thus increasing its volume of action. The exposure of SMX to the radicals was virtually suppressed at 208 mA/cm².

8.5 Conclusive Remarks on AOP Characterisation

In conclusion, hydroxyl radical pathways were confirmed for UV/H₂O₂, DD* and DD'. Additionally, ozone pathways were only detected at all times for DD' and DD'', indicating that BDD simultaneously generates both oxidising agents (HO· and O₃). With j variations, it was possible to steer the mechanism of the reaction at BDD. That is a promising characteristic of this technology which would make it suitable for both disinfection and oxidation of micropollutants.

Interestingly, the exposure to oxidants on DD* was not equal to that on DD. The different set-up of DD, which included a polymer electrolyte, caused a reduction of the ozone formation threshold from 49–69 to 20–40 mA/cm².

The use of the known degradation pathways of two well-studied model compounds provided valuable information about the oxidants generated by two AOPs (UV/H₂O₂ and BDD) and one oxidation module (DD*). The *back-to-front* analysis was successful in the characterisation of these technologies and could be used in a similar fashion for studying further AOPs. The procedure only requires that the chosen model compounds display diverse degradation pathways for the different oxidants.

8.6 Time Courses of the Transformation Products

All TPs detected in the experiments were monitored until they were totally consumed. The corresponding reaction time (t_{TP_0}) was set as the reaction endpoint for the experiments. Unknown reaction products were not further investigated.

Figure 8.3 shows the intensities of SMX and its TPs over time. The absolute intensities do not represent concentrations, but rather are referential for individual species; an interspecies comparison is not possible. The time required for the total abatement of the parent compound (t_{PC_0}) was 10 min with DD'. When the current was increased (DD''), the oxidation was complete after only 3 min due to enhanced ozone production. UV/H₂O₂ also required 3 min to eliminate SMX.

However, the TPs of SMX needed longer treatment times than SMX itself. The intensities of the TPs were close to their maxima the moment SMX disappeared (t_{PC_0}) and only when the time had doubled did they reach the base line ($t_{TP_0} \geq 2 \times t_{PC_0}$). Table 8.1 shows the t_{PC_0} and t_{TP_0} for SMX.

The courses of the TPs evidenced some disparities between the ozone and radical

pathways. It was found that **L** reached its maximum concentration later than **K**, **M** and **N**, pointing to a lower reactivity of **L** (Figures 8.3a and 8.3b). **L** is a smaller molecule than **K**, **M** and **N** (Figure 8.1b) and has fewer functional groups. Besides, the aromatic ring is electron-poor due to the presence of a nitro substituent. Its higher resistance against electrophilic attack is plausible, especially due to the fact that ozone is a selective oxidant. For radical products (Figures 8.3a and 8.3c), no special differentiations were observed. Hydroxyl radicals are non-selective oxidants which display reaction constants in the order of 10^7 – 10^9 $\text{M}^{-1}\text{s}^{-1}$ (nearly diffusion controlled) with organic matter (von Gunten, 2003a). It is worth mentioning that the product **I** (oxoethanoic acid) began to emerge after 15 min of treatment and its concentration increased until 30 min (not shown). The reaction was stopped even if **I** was still measurable because it is a non-toxic TP in a very advanced oxidation stage. This shows that the time spans reported here do not represent the times required for mineralisation of the treated compounds.

The TPs of CBZ behaved similarly to those of SMX and are shown in Figure B1 (Appendix B).

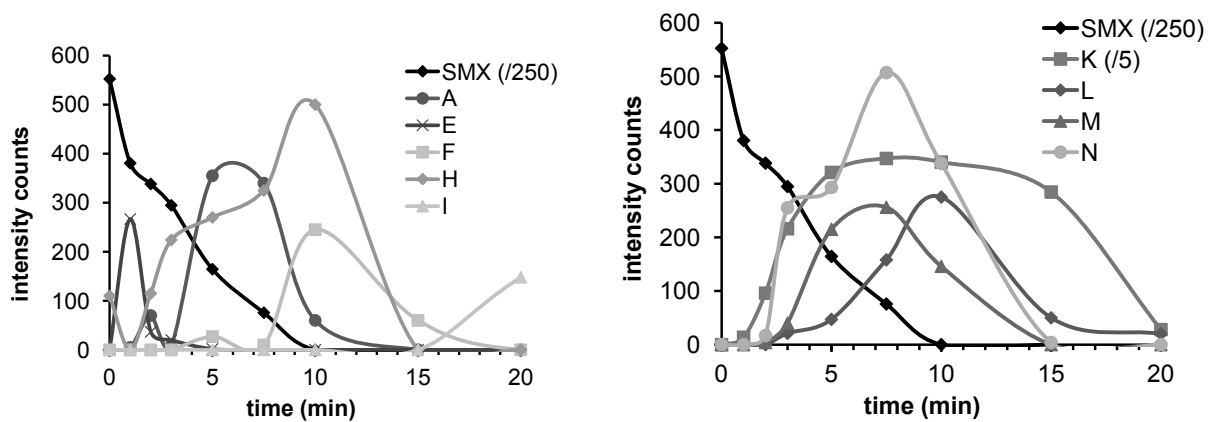
In short, the model compounds used were degraded before their TPs, which required longer treatment times to be consumed. Depending on their chemical structure, some TPs were more resistant to oxidative treatment than others. Oxoethanoic acid emerged only in advanced oxidation stages and remained in solution even after the reaction was stopped.

8.7 Energetic Considerations

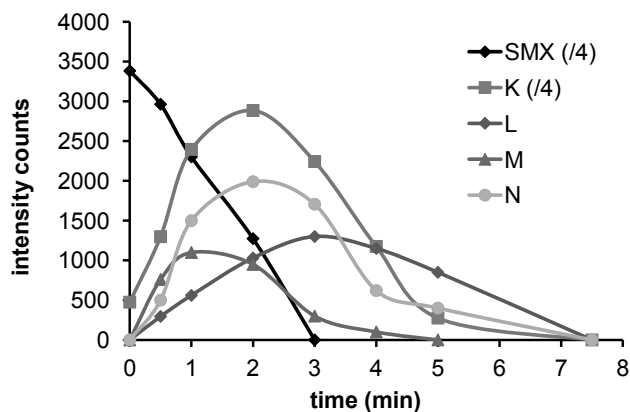
As the courses of the TPs could be monitored so well, they were taken as the basis for another calculation. The various AOPs and configurations employed required different treatment times before the complete abatement of the model substances or TPs occurred (Section 8.6). Because every configuration was associated with a certain energetic demand, it was possible to calculate, analogously to Section 5.2.2 and Section 7.2, the amount of energy required for the treatment of the model compounds up to a definite reaction extent. The energetic calculations were carried out for SMX, as most methods were tested for this substance. DD* was not considered because it is an analytical tool and not an oxidative method for bulk volumes.

An overview of the energetic consumption of the employed systems is given in Table 8.1. Oxidation of SMX with DD' required 10 min of treatment (t_{PC_0}), which translates into 3.55 Wh/L total energy. Of this amount, only 0.09 Wh/L were caused by electrolytic demand. As BDD does not require the use of any chemicals, the electrolytic energy alone made up the effective energy consumption. For the abatement of the known TPs of SMX (t_{TP_0}) 20 min of treatment were necessary. Hence, the energy consumption doubled (7.10 and 0.19 Wh/L).

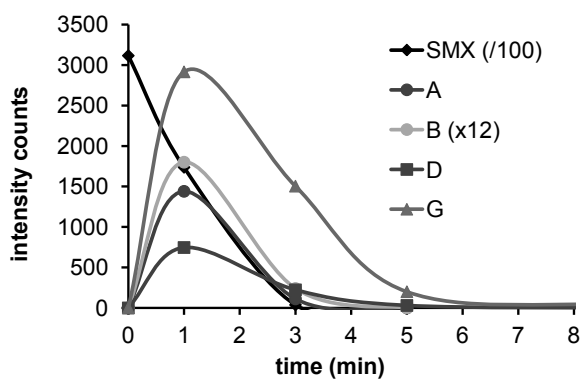
A j increment to 208 mA/cm² (DD'') produced a shortening of the treatment time of SMX to 3 min (t_{PC_0}) and it took 7.5 min to oxidise SMX and its transformation products **K**–**N** (t_{TP_0}) (see Figure 8.3). Owing to the considerable reduction of operation time, the overall consumption until t_{TP_0} was reduced from 7.10 to 3.07 Wh/L.



(a) DD' (at 42 mA/cm²)



(b) DD' (at 208 mA/cm²)



(c) UV/H₂O₂

Figure 8.3 – Course of SMX and selected degradation products during the (a) DD' (42 mA/cm²), (b) DD' (208 mA/cm²) and (c) UV/H₂O₂ experiments in deionised-p. The intensity counts of SMX and **K** were divided and that of **B** multiplied for visualisation.

Table 8.1 – Energy consumption for the treatment until total elimination of SMX (t_{PC_0}) and full abatement of its known transformation products (t_{TP_0}) in deionised-p.

parent compound	AOP	$E_{E,pro}$	$E_{E,chem}$	$E_{E,mix}$	t_{PC_0}	$E_{E,tot}$	$E_{E,pro} + E_{E,chem}$	t_{TP_0}	$E_{E,tot}$	$E_{E,pro} + E_{E,chem}$
		Wh/(L·min)	Wh/L	Wh/(L·min)	min	Wh/L	Wh/L	min	Wh/L	Wh/L
SMX	DD ¹	0.01	0	0.35	10	3.55	0.09	20	7.10	0.19
SMX	DD ²	0.06	0	0.35	3	1.23	0.19	7.5	3.07	0.48
SMX	UV/H ₂ O ₂	0.20	1.39	0.44	3	3.31	2.00	7	5.86	2.81

[SMX]_{*i*} = 10 µM. Methods shown: electrolysis with a diamond electrode (DD¹: 42 mA/cm², DD²: 208 mA/cm²) and hydrogen peroxide photolysis (UV/H₂O₂). $E_{E,mix}$: electrical energy for mixing; $E_{E,pro}$: process-intrinsic electrical energy; $E_{E,chem}$: cost of chemicals converted to energy; $E_{E,tot}$: total electrical energy; $E_{E,pro} + E_{E,chem}$: effective energy.

Nonetheless, the electrolysis at 208 mA/cm² needs more energy than at 42 mA/cm² which led to an increase in $E_{E,pro}$ from 0.19 to 0.48 Wh/L.

When working with UV/H₂O₂, an $E_{E,tot}$ of 3.31 Wh/L was measured for the oxidation of SMX. For the abatement of the TPs, the treatment time increased from 3 to 7 min, but the energy did not double because no further addition of chemicals was necessary. In other words, the high $E_{E,chem}$ (1.39 Wh/L) is a one-time hurdle for the initiation of the UV/H₂O₂ process, but once the process is running, the energy consumption is of electric nature only. In comparison to BDD, the $E_{E,tot}$ was in a similar range (compare 3.31 to 3.55 and 1.23 Wh/L for t_{PC_0} and 5.86 to 7.10 and 3.07 Wh/L for t_{TP_0} in Table 8.1). Nevertheless, when considering only effective energy, UV/H₂O₂ had values that were an order of magnitude higher than BDD (compare *e.g.* for t_{TP_0} 2.81 Wh/L to 0.19 or 0.48 Wh/L).

In the case of CBZ, instead of a concentration of 10 μM (as for SMX), 5.5 and 1 μM were chosen. Table B1 in Appendix B shows the same trend for CBZ as for SMX. Consequently, the calculations can be satisfactorily applied over at least one order of magnitude.

The total toxicity of SMX solutions, understood as the toxicity of the parent drug plus that of its degradation products, has been reported to increase upon ozonation (Abellán et al., 2008; Gómez-Ramos et al., 2011) and photodegradation (Trovó et al., 2009b). For CBZ, acridine (ACR), a human carcinogen, has been found among its degradation products (Vogna et al., 2004). Therefore, an incipient or partial oxidation of SMX and CBZ may be risky. Treating these compounds not only for t_{PC_0} but for t_{TP_0} could be meaningful to prevent inflicting more severe damage to the environment unknowingly.

Briefly, the courses of the TPs allowed for an energetic comparison of the AOPs. The energetic consumption strongly depended on the aim of the treatment. If the target pollutant should be oxidised, approximately half of the energy was required than if the resulting TPs should be degraded as well. The overall energy consumption was similar for BDD and UV/H₂O₂, but one order of magnitude lower for BDD if only process-energy was considered.

8.8 Summary

This chapter presented a novel approach for the elucidation of the oxidation mechanisms of different AOPs. By observing the organic degradation products of two model compounds and comparing them to literature data, the oxidising agents produced by any AOP could be inferred. The tested AOPs were UV/H₂O₂, a BDD electrode and a micro electrochemical cell equipped with a BDD electrode (DD*). It could be proven that the technologies UV/H₂O₂ and DD* primarily produce HO· as reactive species. In contrast, oxidant production on BDD could be regulated with current density. At 42 mA/cm² a mixture of radicals and ozone was observed, whilst at 208 mA/cm² virtually only ozone was produced.

A comparison of the experimentally obtained products from the various AOPs with the database demonstrated that the products resulting from radical attack are in-

dependent of the specific technology in use. In other words, the radicals involved in oxidation are identical among different technologies. It was the variety of techniques that rendered the overall picture of radical products.

Finally, the time courses of the detected TPs were linked to the energy consumption of the systems, thus allowing for an energetic comparison. The energy required to oxidise a model compound was roughly one half of that needed to additionally degrade its TPs. In general terms, the energy consumptions of UV/H₂O₂ and BDD were in a similar range. The treatment target should be determined based upon the specific toxicity of the compound in question and its related TPs.

Table 8.2 – SMX degradation products observed in deionised-p with mass spectrometry and sorted after AOP.

ion	mode	m/z	UV/H ₂ O ₂	Δ	DD'	Δ	DD''	Δ	DD*	Δ
SMX+H	+	254.0600	254.0597	-1.2	254.0601	0.1	254.0599	-0.6	RM	0
SMX+Na	+	276.0420	RM	0	RM	0	RM	0	276.0408	-4.1
SMX+K	+	292.0159	292.0163	1.5	292.0161	0.6	292.0160	0.2	292.0142	-5.9
2*SMX+Na	+	529.0942	529.0932	-1.9	RM	0	RM	0	529.0862	-15.1
A+H	+	270.0549							270.0519	-11.3
A+K	+	308.0108	308.0127	6.2	308.0098	-3.3			308.0067	-13.2
B+K	+	326.0214	326.0219	1.8					326.0124	27.6
C+K	+	281.9951							282.0037	30.2
D+Na	+	238.0263	238.0266	1.4						
E+K	+	156.0120			156.0134	9.1				
F+K	+	262.0595			262.0569	-10.1				
G+H	+	99.0559	99.0539	-20.0						
H-H	-	72.9925			72.9928	4.6				
I-H	-	87.0082			87.0085	3.5				
J+K	+	321.9900							321.9972	22.2
K-H	-	282.0185			282.0187	0.8	282.0185	0	282.0161	-8.5
L-H	-	138.0191			138.0186	-3.7	138.0196	3.5		
M-H	-	298.0134			298.0141	2.4	298.0173	13.1		
N-H	-	269.0232			269.0238	2.1	269.0255	8.3	269.0242	3.7

UV/H₂O₂: hydrogen peroxide photolysis, DD' and DD'': electrolysis with a boron-doped diamond electrode at 42 and 208 mA/cm² respectively, DD*: electrolysis by a micro diamond electrode directly coupled to mass spectrometry. Δ represents the deviation from the theoretical value (m/z) in parts per million (ppm). RM: used as referential mass for mass correction (see Section 2.3.5). Refer to Figure 8.1 for the chemical structures of compounds **A-N**.

Table 8.3 – CBZ degradation products observed in deionised-p with mass spectrometry in positive mode and sorted after AOP.

ion	mode	m/z	UV/H ₂ O ₂	Δ	DD'	Δ	DD*	Δ
CBZ+H	+	237.1029	RM	0	237.1027	-0.7	RM	0
CBZ+Na	+	259.0848	259.0852	1.3	259.0844	-1.5	259.0856	3.0
CBZ+K	+	275.0588	275.0585	-0.9	275.0591	1.4	275.0592	1.4
2*CBZ+Na	+	495.1799	RM	0	495.1794	-1.0	495.1831	6.5
2*CBZ+K	+	511.1538	511.1538	0	511.1573	6.8	511.1544	2.0
epoxyCBZ+H	+	253.0978	253.0978	0	253.0940	-15.2		
epoxyCBZ+K	+	291.0537	291.0567	10.6	291.0591	18.6		
ACR-CHO+H	+	208.0763	208.0766	1.5	208.0761	-0.9	208.0757	-2.9
ACR+H	+	180.0814	180.0817	1.4	180.0814	0.1	180.0807	-3.9
ACR-OH+H	+	196.0763	196.0770	3.7			196.0754	-4.6
preBQM+H	+	269.0927	269.0937	3.9	269.0924	-1.0		
preBQM+Na	+	291.0746			291.0733	-4.4		
preBQM+K	+	307.0486	307.0522	11.8	307.0479	-2.0		
BQM+H	+	251.0821	251.0825	1.6	251.0818	-1.2		
BQM+Na	+	273.0641	273.0649	3.0	273.0637	-1.2		
BQM+K	+	289.0380			289.0383	1.2		
BQD+H	+	267.0770	267.0820	18.6	267.0764	-2.2		
BQD+Na	+	289.0590	289.0516	-25.6				
BQD+K	+	305.0329	305.0352	7.5	305.0368	12.9		

UV/H₂O₂: hydrogen peroxide photolysis, DD': electrolysis at 42 mA/cm² with a boron-doped diamond electrode, DD*: electrolysis by a micro diamond electrode directly coupled to mass spectrometry. Δ represents the deviation from the theoretical value (m/z) in parts per million (ppm). RM: used as referential mass for mass correction (see Section 2.3.5). See Figure 8.2 for the chemical structures of the compounds.

Chapter 9

Conclusions

This work studied a new electrochemical AOP: the utilisation of a boron-doped diamond electrode for the elimination of persistent pollutants from water and disinfection. The focus was set on the characterisation of BDD, that is, the conditions at which the formation of different oxidising agents are favoured. Furthermore, the various repercussions of the variable oxidant generation were analysed by means of the disinfection efficiency, the by-product formation potential and the energy consumption of the system. In the course of the research, three new approaches were developed that could be used beyond the work with BDD electrodes.

9.1 Characterisation of the Diamond Electrode

The generation of oxidants on BDD was shown to be strongly dependent on the current density. At a j of 42 mA/cm^2 both hydroxyl radicals and ozone formed. Every j increment contributed to the displacement of the chemical equilibrium toward ozone formation because the hydroxyl radical density increased and promoted their condensation to form ozone (*current effect*). At 208 mA/cm^2 , the equilibrium shifted to the ozone side. These results could be confirmed with two completely different approaches. The first one was a direct determination which measured the decolouration of two dyes caused by radicals or radicals plus ozone. The second approach was an indirect determination consisting in the comparison of the TPs of two model compounds with the degradation pathways for radicals and ozone reported in literature. Hence, the production of oxidising agents on BDD could be regulated with j .

The dye decolouration experiments evidenced one shortcoming of the reactor set-up used. The water to treat was not effectively brought into contact with the electrode surface, so that the oxidising potential of the hydroxyl radicals was not exploited. On the other hand, ozone is less reactive than $\text{HO}\cdot$ and could be successfully used to exert oxidation in the bulk of the solution. Boron-doped diamond produced $22 \text{ g O}_3/\text{kWh}$, which is well in the middle range of conventional, laboratory-scale ozonators. The fact that this ozone concentration was measured *in solution* means that BDD is actually even more efficient, but an improved reactor set-up should

enhance ozone dissolution and the exposure to hydroxyl radicals. Current density increments beyond 208 mA/cm^2 were not advantageous, as the increased heat transfer into solution contributed to ozone decay.

Nevertheless, the employed BDD was shown to be optimised for ozone production. Experiments with a miniaturised BDD which was directly coupled to MS, showed that the use of a solid polymer electrolyte lowered the ozone formation threshold. As mentioned above, already at 42 mA/cm^2 was ozone produced. When no solid electrolyte was used, ozone started to emerge only at current densities between 49 and 69 mA/cm^2 .

When working in water matrices of variable composition, it was observed that both the organic and the inorganic components used up the radicals and ozone, so that lower oxidant concentrations resulted and the oxidising potential in those waters was lessened (*matrix effect*). Organic matter was hundreds of times more efficient in scavenging ozone than inorganic matter was. Consequently, the degradation of a model compound took place most quickly in deionised water and turned slower with increasing matrix load. In STPE it took the longest time and most energy to degrade the target compound.

In comparison to other AOPs, which were shown to generate predominantly $\text{HO}\cdot$, BDD excelled in that it was an extremely flexible technology. The diamond electrode would be adaptable to specific applications. For instance, it could be used in industry to disinfect a reactor (with ozone) one moment and to degrade toxic organic wastes (with radicals) the moment after.

9.2 Consequences of Different Oxidising Agents on Water Treatment

The treatment with BDD in different configurations, and thus with diverse oxidising species, had a number of implications, especially on the efficiency of the different cleaning tasks (pollutant abatement, disinfection), energy consumption and by-product formation. Figure 9.1 presents a graphical overview. The explanations follow in the text.

It was known from literature that ozone is a more effective disinfectant than hydroxyl radicals. Accordingly, it was observed that treatment at low current densities ($\text{HO}\cdot$) was less effective than at high current densities (O_3). The *ct* curves showed how strongly disinfection depended on ozone concentration. At 208 and 333 mA/cm^2 , the disinfection efficiency was purely subject to ozone exposure because the current value from which predominantly ozone emerges ($\approx 100 \text{ mA/cm}^2$) had been amply surpassed. At 42 mA/cm^2 , the inactivation was slower than expected from the energy input, which was caused by the higher radical yield. However, because chlorine is a powerful disinfectant and it forms through radical oxidation, the matrix effect was almost eliminated in chloride-rich waters for disinfection.

The higher the current density, the more energy was consumed for the operation of BDD, but also the more ozone was produced. Since ozone can penetrate into the aqueous phase and thus extend the volume of reaction, an acceleration of degra-

dation and inactivation rates was observed. It follows that the overall treatment times for degradation and disinfection were reduced and energy consumption was diminished. Even so, the *effective energy* consumption (for the electrolytic process alone) increased.

Due to the fact that HO \cdot is able to oxidise both chloride and bromide whereas O $_3$ can only oxidise bromide, the operation of BDD at low current densities resulted in significantly higher BP concentrations. A current of 42 mA/cm 2 very rapidly eliminated chloride from solution and led to the highest AOX formation rates. At 208 and 333 mA/cm 2 , predominantly brominated THMs were measured, although the bromide concentration was 250 times lower than that of chloride, confirming that very few radicals were available for oxidation at high current densities.

9.3 Pragmatic Recommendation

If we combine the individual phenomena observed, a moderate current density that favours O $_3$ formation would be recommended for operation, when possible. On the one hand, pollutant abatement and bacteria inactivation were more efficient than at lower j ; on the other hand, the energy required was lowered (shorter duration) and by-product formation reduced. Of the tested current densities, 208 mA/cm 2 would comply with these requirements. Table 9.1 offers an overview of the energy required for the elimination of CBZ and that of its TPs. In addition, it predicts AOX formation and bacteria inactivation for those treatment times and conditions based on the results from Chapters 6 and 7. If the pollutants to treat are ozone-resistant, operating conditions that favour radical attack (< 100 mA/cm 2) would be preferred, although costs and by-product concentrations would be higher.

A sensible way to reduce costs for the real application in STPs would be to combine the BDD electrolysis with other, less costly technologies. Müller et al. (2013) reported on the biodegradation of SMX by activated sludge. They identified two stable metabolites that could not be oxidised further by the microorganisms. The structures of the stable metabolites resemble those for **G** and **N** in Figure 8.1. BDD could assist in the breakage of stable species for their further microbiological or chemical degradation.

9.4 New Approaches for Water Treatment

To facilitate the comparison between different AOP technologies and reactor set-ups, the partition of total energy into three constituents was worked out (Chapter 3). The constituents comprise the process-intrinsic energy, chemical energy and mixing energy. Only the first two components are directly responsible for reaction. This calculation made it possible to compare three completely different reactors with different volumes carrying out diverse chemical reactions. The total energy consumption of BDD was comparable to that of UV/H $_2$ O $_2$. The photo-Fenton reaction showed higher energy requirements. Nonetheless, the process-intrinsic energy consumption of BDD was at least one order of magnitude lower than that of the other

technologies. There are two reasons for this. Firstly, BDD needs no chemicals to perform the reaction, it generates oxidants in situ directly from water. And secondly, the electrolytic process is more efficient than light absorption as it is not subject to quantum yields.

The pathway comparison illustrated the feasibility of performing a *back-to-front investigation* for determining the oxidant species on BDD (Chapter 8). By looking at the TPs resulting from well-established reactions in literature, such as ozonation and radical attack, it was possible to indirectly uncover the mechanisms of BDD. Notwithstanding the fact that it is a time-consuming procedure, it was above all an extremely useful technique. Beside the indirect determination of oxidants, it opened the possibility of monitoring TPs and enabled the identification of novel degradation products. In the course of this research, two new TPs were detected for the first time: **F** for SMX (Figure 8.1a) and **preBQM** for CBZ (Figure 8.2b).

The pathway investigation for the characterisation of the oxidants formed on BDD involved the observation of TPs. These were monitored until they were completely consumed. It was found that the degradation of the TPs of the two model compounds (SMX and CBZ) needed at least twice as much energy as the complete abatement of the parent compounds. It is often the case that the TPs of pharmaceuticals and other refractory substances display a higher toxicity than the parent compounds. If that should be the case, treatment ought to eliminate TPs as well. The monitoring of TPs should therefore belong to standard procedures when assessing the cost or efficiency of oxidative technologies.

These three approaches are not circumscribed to BDD research and could be relevant for the broader field of water treatment.

Table 9.1 – Calculated energy consumption (electrolysis only), AOX concentration and bacteria inactivation for the complete oxidation of CBZ (t_{PC_0}) or its TPs (t_{TP_0}) in STPE-pb at 42 and 208 mA/cm².

	j mA/cm ²	CBZ abatement				TPs _{CBZ} abatement				
		Q/V mAh/L	t_{PC_0} min	E_{PC_0} Wh/L	log(N/N ₀) -	AOX µg/L	Q/V mAh/L	t_{TP_0} min	E_{TP_0} Wh/L	log(N/N ₀) -
CBZ	42	204	60	0.54	94	408	120	1.09	-	188
CBZ	208	112	7.5	0.37	-6.7	224	15	0.74	-8.7	8



Figure 9.1 – Graphical (simplified) representation of (a) the current effect and (b) the matrix effect.

Chapter 10

Outlook

10.1 Research Topics for the Future

There are a number of important issues that should be covered in order to get a clear picture of the BDD electrode. The formation of inorganic disinfection by-products (*e.g.* BrO_3^- , ClO_3^- , ClO_4^-) should be studied, especially in dependence of the current density. If the direct contact between the wastewater components and the electrode promotes the formation of inorganic DBPs, an alternative could be given by using a by-pass system, *i.e.* electrolysing a cleaner water and mixing it with the wastewater. Such an approach would squander the oxidising potential of HO^\bullet though. As inorganic DBPs are more stringently regulated than AOX, compliance with limiting values should be ensured.

The diamond electrode is currently being modified by its producers to further enhance ozone yields and simultaneously suppress by-product formation. New geometries for the electrolytic cell ought to be evaluated as well, so that the oxidants can be better used. Further pollutants should be treated with BDD. Of special importance would be ozone-resistant substances. Since both SMX and CBZ readily react with ozone, this remains a gap of knowledge. Could they be degraded at 208 mA/cm^2 , when predominantly ozone forms? Are the new, nano-modified BDD electrodes also effective for the degradation of compounds refractory to ozonation?

Once the questions on the realm of chemistry are answered, research should move on to the up-scaling of the systems, to bring the electrodes a step further toward their application in STPs. Large-scale systems would have to be optimised in terms of flow conditions, hydraulic retention time at the electrode surface (related to radical exposure) and current configurations. The optimisation would replace the AOP reactor comparison based on $E_{E,pro}$.

Diamond electrodes will have to be characterised in STPE anew. The databases provided in this work could be used to screen electrolysed wastewater for the TPs of the treated substances. It would be important to find out if the same TPs detected in deionised water form in STPE and if the presence of chloride and further organic and inorganic matter has an effect on the oxidation mechanisms. The current developments in analytical techniques such as HILIC-LC-MS will enable the non-target

screening of complex matrices such as STPE or industrial effluents. By separating both polar and non-polar compounds according to hydrophobicity and acquiring their exact masses, so-called chemical fingerprints could be measured. With the fingerprints, it would be possible to rapidly check for transformations of a complex water matrix and its constituents; looking for *a tiny flower in a dense forest*.

When working with STPE, the disinfection mechanisms could be better investigated. This research suggested the involvement of chloride (as free chlorine) in disinfection as the cause for a weakened matrix effect. If chlorine could be measured, directly or indirectly, it would help identify the optimum conditions for bacteria inactivation.

10.2 Practical Approaches to Follow

Beside chemical solutions to the problem, a preventive approach should be followed as well. The general public should be made aware of the problem of micropollutants in water and the easy measures it can take to cut the entry of pharmaceuticals into the environment. Not flushing medicine rests away, not abusing of the use of pharmaceuticals, not interrupting antibiotic treatments before completion are easy things we could do. But also taking an eye on what we eat. If meat comes from industrial farms, it will have been likely produced with the aid of pharmaceutical products and conventional agriculture uses pesticides, herbicides and further chemicals, which cannot be treated owing to the large areas affected.

Research should slightly move away from its current focus of identifying new transformation products for the sake of science. If the focus was set on the toxicity of chemical compounds, much time could be saved by carefully studying only those cases in which toxicity increases. If substances with very toxic TPs are found, they should be monitored until they are completely oxidised. The precursor parent compounds could be categorised in order of risk. Eventually, a different disposal method would have to be found, and in the long term, a *green* equivalent of the problematic compounds may be synthesised to take up their niches. Green pharmaceuticals are those which can be perfectly biodegraded after their passage through the body.

If BDD successfully passes the next tests, it would represent a practical tool for more applications besides wastewater treatment. They could be used in medical equipment for the cleaning and disinfection of instruments; in the beverage industry for disinfecting bottles or reactors; they could be embedded into portable devices for the disinfection of drinking water in developing countries. Rain water could be electrochemically polished with BDD for its use in the household. Maybe diamond electrodes replace conventional ozonators one day, if the energy consumption of water electrolysis per gram of ozone becomes comparable to that of corona discharge.

References

- Abellán, M. N., Gebhardt, W., Schröder, H. F., 2008. Detection and identification of degradation products of sulfamethoxazole by means of LC/MS and -MS(n) after ozone treatment. *Water Science and Technology* 58 (9), 1803–1812.
- Absolute Ozone, accessed in May 2012.
URL <http://absoluteozone.com>
- AirClino, accessed in May 2012.
URL <http://www.jrrozon.eu>
- Al-Rasheed, R., Sahul, K., Thankachan, T., Oct 1997. Ozonation of Al-Jubail sea water - formation potential, speciation and kinetics of trihalomethanes and bromate. In: IDA Conference Book, Madrid, Spain. pp. 1532–1555.
- Aleboye, A., Moussa, Y., Aleboye, H., 2005. The effect of operational parameters on UV/H₂O₂ decolourisation of Acid Blue 74. *Dyes and Pigments* 66 (2), 129–134.
- Ammar, S., Abdelhedi, R., Flox, C., Arias, C., Brillas, E., 2006. Electrochemical degradation of the dye indigo carmine at boron-doped diamond anode for waste-waters remediation. *Environmental Chemistry Letters* 4 (4), 229–233.
- Andreozzi, R., Caprio, V., Insola, A., Marotta, R., 1999. Advanced oxidation processes (AOP) for water purification and recovery. *Catalysis Today* 53 (1), 51–59.
- Anglada, A., Urtiaga, A., Ortiz, I., Mantzavinos, D., Diamadopoulos, E., 2011. Boron-doped diamond anodic treatment of landfill leachate: Evaluation of operating variables and formation of oxidation by-products. *Water Research* 45, 828–838.
- AquaCare, accessed in May 2012.
URL <http://www.aquacare.de>
- Ash, R., Mauck, B., Morgan, M., 2002. Antibiotic resistance of gram-negative bacteria in rivers, United States. *Emerging Infectious Diseases* 8 (7), 713–716.
- Babak, A., Amadelli, R., Battisti, A. D., Fateev, V., 1994. Influence of anions on oxygen/ozone evolution on PbO₂/*spe* and PbO₂/Ti electrodes in neutral pH media. *Electrochimica Acta* 39 (11/12), 1597–1602.
- Bader, H., Hoigné, J., 1981. Determination of ozone in water by the indigo method. *Water Research* 15 (4), 449–456.

- Baumann, A., Karst, U., 2010. Online electrochemistry/mass spectrometry in drug metabolism studies: principles and applications. *Expert Opinion on Drug Metabolism & Toxicology* 6 (6), 715–731.
- Bechtold, T., Turcanu, A., Schrott, W., 2006. Electrochemical decolourisation of dispersed indigo on boron-doped diamond anodes. *Diamond and Related Materials* 15 (10), 1513–1519.
- Behrendt-Fryda, B., 2012. 3rd partial report on the project NADINE – Nanomodifizierte Diamantelektroden für Inlinedesinfektionsprozesse in unterschiedlichen Einsatzgebieten. Tech. rep., CONDIAS – Conductive Diamond Products.
- Beltrán, F. J., 2004. *Ozone Reaction Kinetics for Water and Wastewater Systems*. Lewis Publishers, Boca Raton, USA.
- Beltrán, F. J., Aguinaco, A., García-Araya, J. F., 2009. Mechanism and kinetics of sulfamethoxazole photocatalytic ozonation in water. *Water Research* 43 (5), 1359–1369.
- Beltrán, F. J., Aguinaco, A., García-Araya, J. F., Oropesa, A., 2008. Ozone and photocatalytic processes to remove the antibiotic sulfamethoxazole from water. *Water Research* 42 (14), 3799–3808.
- Bergmann, H., 2010. Zur Bewertung von Diamantelektroden für die Wasserdesinfektionselektrolyse. *GWF Wasser Abwasser* 6, 604–613.
- Bergmann, M. E. H., Iourtchouk, T., Rollin, J., 2011. The occurrence of bromate and perbromate on BDD anodes during electrolysis of aqueous systems containing bromide: first systematic experimental studies. *Journal of Applied Electrochemistry* 41 (9, SI), 1109–1123.
- Bergmann, M. E. H., Rollin, J., Iourtchouk, T., 2009. The occurrence of perchlorate during drinking water electrolysis using BDD anodes. *Electrochimica Acta* 54 (7), 2102–2107.
- Bewersdorff, I., March 2005. Investigation of the mode of action of boron-doped diamond electrodes for advanced water treatment. Master's thesis, Institute of Water Quality Control - Technical University of Berlin.
- BMT, accessed in May 2012.
URL <http://www.bmt-berlin.de>
- Bolton, J., Bircher, K., Tumas, W., Tolman, C., 2001. Figures-of-merit for the technical development and application of advanced oxidation technologies for both electric- and solar-driven systems - (IUPAC technical report). *Pure and Applied Chemistry* 73 (4), 627–637.
- Boudreau, J., Bejan, D., Li, S., Bunce, N. J., 2010. Competition between electrochemical advanced oxidation and electrochemical hypochlorination of sulfamethoxazole at a boron-doped diamond anode. *Industrial & Engineering Chemistry Research* 49 (6), 2537–2542.

- Brachvogel, F., March 2011. Musterhaushalt für Strom 2011: 46 Prozent des Strompreises sind Steuern und Abgaben. Tech. rep., BDEW.
- Bradl, H., 2005. Chapter 1: Sources and origins of heavy metals. In: Bradl, H. (Ed.), Heavy Metals in the Environment: Origin, Interaction and Remediation. Vol. 6 of Interface Science and Technology. Elsevier, pp. 1–27.
- Buffle, M., Schumacher, J., Salhi, E., Jekel, M., von Gunten, U., 2006. Measurement of the initial phase of ozone decomposition in water and wastewater by means of a continuous quench-flow system: Application to disinfection and pharmaceutical oxidation. *Water Research* 40 (9), 1884–1894.
- Cañizares, P., Paz, R., Sáez, C., Rodrigo, M. A., 2009. Costs of the electrochemical oxidation of wastewaters: A comparison with ozonation and Fenton oxidation processes. *Journal of Environmental Management* 90 (1), 410–420.
- Cañizares, P., Sáez, C., Lobato, J., Rodrigo, M., 2004. Electrochemical oxidation of polyhydroxybenzenes on boron-doped diamond anodes. *Industrial & Engineering Chemistry Research* 43 (21), 6629–6637.
- Camarero, L. M., Peche, R., Collado, A., 1997. Kinetic study of the oxidation of indigocarmine by hydrogen peroxide with ferrous and ferric ions in acid medium. *International Journal of Chemical Kinetics* 29 (8), 575–578.
- Cho, M., Chung, H., Yoon, J., 2003. Disinfection of water containing natural organic matter by using ozone-initiated radical reactions. *Applied and Environmental Microbiology* 69 (4), 2284–2291.
- Cho, M., Kim, J., Kim, J. Y., Yoon, J., Kim, J.-H., 2010. Mechanisms of *Escherichia coli* inactivation by several disinfectants. *Water Research* 44 (11), 3410–3418.
- Christensen, A., Gurol, M. D., Garoma, T., 2009. Treatment of persistent organic compounds by integrated advanced oxidation processes and sequential batch reactor. *Water Research* 43 (16), 3910–3921.
- Cleuvers, M., 2003. Aquatic ecotoxicity of pharmaceuticals including the assessment of combination effects. *Toxicology Letters* 142 (3), 185–194.
- Comninellis, C., Chen, G., 2009. *Electrochemistry for the Environment*. Springer, New York, Dordrecht, Heidelberg, London.
- Cooper, E. R., Siewicki, T. C., Phillips, K., 2008. Preliminary risk assessment database and risk ranking of pharmaceuticals in the environment. *Science of the Total Environment* 398 (1-3), 26–33.
- Costa, C. R., Montilla, F., Morallon, E., Olivi, P., 2009. Electrochemical oxidation of acid black 210 dye on the boron-doped diamond electrode in the presence of phosphate ions: Effect of current density, pH, and chloride ions. *Electrochimica Acta* 54, 7048–7055.
- da Silva, L., Santana, M., Boodts, J., 2003. Electrochemistry and green chemical processes: Electrochemical ozone production. *Química Nova* 26 (6), 880–888.

- Dirany, A., Sires, I., Oturan, N., Oturan, M. A., 2010. Electrochemical abatement of the antibiotic sulfamethoxazole from water. *Chemosphere* 81 (5), 594–602.
- DVGW Deutsche Vereinigung des Gas und Wasserfaches e.V. (Ed.), 2012. German Drinking Water Ordinance (Trinkwasserverordnung, TrinkwV).
- DWA Deutsche Vereinigung für Wasserwirtschaft, Abwasser und Abfall e.V. (Ed.), 2012. Performance Comparison of Municipal Sewage Treatment Plants 2012 (25. Leistungsvergleich kommunaler Kläranlagen).
- Elovitz, M. S., von Gunten, U., 1999. Hydroxyl radical ozone ratios during ozonation processes. I - The R_{ct} concept. *Ozone: Science & Engineering* 21 (3), 239–260.
- Enaly, accessed in May 2012.
URL <http://www.enaly.com>
- Frontistis, Z., Brebou, C., Venieri, D., Mantzavinos, D., Katsaounis, A., 2011. BDD anodic oxidation as tertiary wastewater treatment for the removal of emerging micro-pollutants, pathogens and organic matter. *Journal of Chemical Technology and Biotechnology* 86 (10), 1233–1236.
- Fryda, M., Matthée, T., Mulcahy, S., Hampel, A., Schäfer, L., Tröster, I., 2003. Fabrication and application of Diachem[®] electrodes. *Diamond and Related Materials* 12 (10-11), 1950–1956.
- Fujishima, A., Einaga, Y., Rao, T. N., Tryk, D. A., 2005. *Diamond Electrochemistry*. BKC, Elsevier; Tokyo.
- Gälli, R., Ort, C., Schärer, M., 2009. Micropollutants in the aquatic environment. Assessment and reduction of the pollutant load due to municipal waste water. No. 0917 in *Umwelt-Wissen*. Federal Office of Environment (FOEN), Bern.
- García-Galán, M. J., Díaz-Cruz, M. S., Barceló, D., 2012. Kinetic studies and characterization of photolytic products of sulfamethazine, sulfapyridine and their acetylated metabolites in water under simulated solar irradiation. *Water Research* 46 (3), 711–722.
- German Federal Ministry of Justice (Ed.), 24th, Feb 2012. Wastewater Ordinance (Verordnung über Anforderungen an das Einleiten von Abwasser in Gewässer (Abwasserverordnung - AbwV)). No. BGBl.IS.212.
- Gilbert, N., 2011. Drug waste harms fish. *Nature* 476 (7360), 265.
- Gómez-Ramos, M. d. M., Mezcuca, M., Agüera, A., Fernández-Alba, A. R., Gonzalo, S., Rodríguez, A., Rosal, R., 2011. Chemical and toxicological evolution of the antibiotic sulfamethoxazole under ozone treatment in water solution. *Journal of Hazardous Materials* 192 (1), 18–25.
- Gottschalk, C., Libra, J., Saupe, A., 2010. *Ozonation of Water and Waste Water - A Practical Guide to Understanding Ozone and its Applications*, 2nd Edition. Wiley-VCH, Weinheim.

- Gujer, W., 2007. Siedlungswasserwirtschaft, 3rd Edition. Springer-Verlag, Berlin, Heidelberg.
- Haaken, D., Dittmar, T., Schmalz, V., Worch, E., 2012. Influence of operating conditions and wastewater-specific parameters on the electrochemical bulk disinfection of biologically treated sewage at boron-doped diamond (BDD) electrodes. *Desalination and Water Treatment* 46 (1-3), 160–167.
- Haaken, D., Schmalz, V., Dittmar, T., Worch, E., 2010. Use of diamond electrodes for the production of service water by electrochemical disinfection of biologically treated waste water. *Chemie Ingenieur Technik* 82 (10), 1781–1788.
- Halling-Sørensen, B., Nielsen, S., Lanzky, P., Ingerslev, F., Lützhøft, H., Jørgensen, S., 1998. Occurrence, fate and effects of pharmaceutical substances in the environment - a review. *Chemosphere* 36 (2), 357–394.
- Hammami, S., Oturan, M. A., Oturan, N., Bellakhal, N., Dachraoui, M., 2012. Comparative mineralization of textile dye indigo by photo-Fenton process and anodic oxidation using boron-doped diamond anode. *Desalination and Water Treatment* 45 (1-3), 297–304.
- Harris, D. C., 2007. *Quantitative Chemical Analysis*, 7th Edition. W. H. Freeman and Company, New York.
- Heim, C., Glas, K., 2011. Ozone I: Characteristics/generation/possible applications. *BrewingScience* 64, 8–12.
- Heim, C., Ureña de Vivanco, M., Rajab, M., Glas, K., Horn, H., Helmreich, B., Letzel, T., 2011. Ozone II: Characterization of in situ ozone generation using diamond electrodes. *BrewingScience* 64, 83–88.
- Hoffmann, T., Hofmann, D., Klumpp, E., Kueppers, S., 2011. Electrochemistry-mass spectrometry for mechanistic studies and simulation of oxidation processes in the environment. *Analytical and Bioanalytical Chemistry* 399 (5), 1859–1868.
- Holleman, A., Wiberg, E., Wiberg, N., 2007. *Lehrbuch der anorganischen Chemie*, 102nd Edition. Walter de Gruyter, Berlin, New York.
- Honda, Y., Ivandini, T. A., Watanabe, T., Murata, K., Einaga, Y., 2013. An electrolyte-free system for ozone generation using heavily boron-doped diamond electrodes. *Diamond and Related Materials* 40, 7–11.
- Hu, L., Flanders, P. M., Miller, P. L., Strathmann, T. J., 2007. Oxidation of sulfamethoxazole and related antimicrobial agents by TiO₂ photocatalysis. *Water Research* 41 (12), 2612–2626.
- Ikehata, K., Naghashkar, N. J., Ei-Din, M. G., 2006. Degradation of aqueous pharmaceuticals by ozonation and advanced oxidation processes: A review. *Ozone Science & Engineering* 28 (6), 353–414.

- Isse, A. A., Lin, C. Y., Coote, M. L., Gennaro, A., 2011. Estimation of standard reduction potentials of halogen atoms and alkyl halides. *Journal of Physical Chemistry B* 115 (4), 678–684.
- Jones, O., Lester, J., Voulvoulis, N., 2005. Pharmaceuticals: a threat to drinking water? *Trends in Biotechnology* 23 (4), 163–167.
- Kapałka, A., Foti, G., Comninellis, C., 2009. The importance of electrode material in environmental electrochemistry formation and reactivity of free hydroxyl radicals on boron-doped diamond electrodes. *Electrochimica Acta* 54 (7), 2018–2023.
- Kerc, A., Bekbolet, M., Saatci, A., 2004. Effects of oxidative treatment techniques on molecular size distribution of humic acids. *Water Science and Technology* 49 (4), 7–12.
- Khadre, M., Yousef, A., Kim, J., 2001. Microbiological aspects of ozone applications in food: A review. *Journal of Food Science* 66 (9), 1242–1252.
- Kidd, K. A., Blanchfield, P. J., Mills, K. H., Palace, V. P., Evans, R. E., Lazorchak, J. M., Flick, R. W., 2007. Collapse of a fish population after exposure to a synthetic estrogen. *Proceedings of the National Academy of Sciences of the United States of America* 104 (21), 8897–8901.
- KOI, accessed in May 2012.
URL <http://www.koicompetence.de>
- Kowalski, W., Bahnfleth, W., Whittam, T., 1998. Bactericidal effects of high airborne ozone concentrations on *Escherichia coli* and *Staphylococcus aureus*. *Ozone: Science & Engineering* 20 (3), 205–221.
- Kraft, A., 2007. Doped diamond: A compact review on a new, versatile electrode material. *International Journal of Electrochemical Science* 2 (5), 355–385.
- Kraft, A., Stadelmann, M., Blaschke, M., 2003. Anodic oxidation with doped diamond electrodes: a new advanced oxidation process. *Journal of Hazardous Materials* 103 (3), 247–261.
- Kraft, A., Stadelmann, M., Wunsche, M., Blaschke, M., 2006a. Electrochemical destruction of organic substances in deionized water using diamond anodes and a solid polymer electrolyte. *Electrochemistry Communications* 8 (1), 155–158.
- Kraft, A., Stadelmann, M., Wunsche, M., Blaschke, M., 2006b. Electrochemical ozone production using diamond anodes and a solid polymer electrolyte. *Electrochemistry Communications* 8 (5), 883–886.
- Kraljić, I., Trumbore, C., 1965. p-nitrosodimethylaniline as an OH radical scavenger in radiation chemistry. *Journal of the American Chemical Society* 87 (12), 2547–2550.
- Kümmerer, K., 2010. Pharmaceuticals in the environment. In: Gadgil, A and Liverman, DM (Ed.), *Annual Review of Environment and Resources*. Vol. 35. pp. 57–75.

- Lacasa, E., Tsolaki, E., Sbokou, Z., Rodrigo, M. A., Mantzavinos, D., Diamadopoulos, E., 2013. Electrochemical disinfection of simulated ballast water on conductive diamond electrodes. *Chemical Engineering Journal* 223, 516–523.
- Lazarova, V., Savoye, P., Janex, M., Blatchley, E., Pommepuy, M., 1999. Advanced wastewater disinfection technologies: State of the art and perspectives. *Water Science and Technology* 40 (4-5), 203–213.
- Lenntech, accessed in May 2012.
URL <http://www.lenntech.com>
- Liu, F., He, G., Zhao, M., Huang, L., Qu, M., 2012. Study on the wastewater disinfection at the boron-doped diamond film electrode. *Procedia Environmental Sciences* 12, Part A (0), 116–121.
- Marselli, B., Garcia-Gomez, J., Michaud, P., Rodrigo, M., Comninellis, C., 2003. Electrogeneration of hydroxyl radicals on boron-doped diamond electrodes. *Journal of the Electrochemical Society* 150 (3), D79–D83.
- Matilainen, A., Sillanpää, M., 2010. Removal of natural organic matter from drinking water by advanced oxidation processes. *Chemosphere* 80 (4), 351–365.
- May, P. W., 2008. Materials science - the new diamond age? *Science* 319 (5869), 1490–1491.
- McDowell, D., Huber, M., Wagner, M., von Gunten, U., Ternes, T., 2005. Ozonation of carbamazepine in drinking water: Identification and kinetic study of major oxidation products. *Environmental Science & Technology* 39 (20), 8014–8022.
- Méndez-Arriaga, F., Torres-Palma, R. A., Pétrier, C., Esplugas, S., Gimenez, J., Pulgarin, C., 2009. Mineralization enhancement of a recalcitrant pharmaceutical pollutant in water by advanced oxidation hybrid processes. *Water Research* 43 (16), 3984–3991.
- Metcalf & Eddy, Inc., 2003. *Wastewater Engineering: Treatment and Reuse*, 4th Edition. McGraw-Hill Education, Boston.
- Michaud, P., Panizza, M., Ouattara, L., Diaco, T., Foti, G., Comninellis, C., 2003. Electrochemical oxidation of water on synthetic boron-doped diamond thin film anodes. *Journal of Applied Electrochemistry* 33, 151–154.
- Mirza, M. A., Ahmad, N., Agarwal, S. P., Mahmood, D., Anwer, M. K., Iqbal, Z., 2011. Comparative evaluation of humic substances in oral drug delivery. *Results in Pharma Sciences* 1 (1), 16–26.
- Muff, J., Bennedsen, L. R., Søgaaard, E. G., 2011. Study of electrochemical bleaching of p-nitrosodimethylaniline and its role as hydroxyl radical probe compound. *Journal of Applied Electrochemistry* 41 (5), 599–607.
- Müller, E., Schüssler, W., Horn, H., Lemmer, H., 2013. Aerobic biodegradation of the sulfonamide antibiotic sulfamethoxazole by activated sludge applied as co-substrate and sole carbon and nitrogen source. *Chemosphere* 92 (8), 969–978.

- Müller, L., Jekel, M., 2001. Comparison of advanced oxidation processes in flow-through pilot plants (Part I). *Water Science and Technology* 44 (5), 303–309.
- National Institute of Standards and Technology, accessed in Nov 2012. Material measurement laboratory - ozone.
URL <http://webbook.nist.gov/cgi/cbook.cgi?ID=C10028156&Mask=10#Solubility>
- Oaks, J., Gilbert, M., Virani, M., Watson, R., Meteyer, C., Rideout, B., Shivaprasad, H., Ahmed, S., Chaudhry, M., Arshad, M., Mahmood, S., Ali, A., Khan, A., 2004. Diclofenac residues as the cause of vulture population decline in Pakistan. *Nature* 427 (6975), 630–633.
- OCS.tec, accessed in May 2012.
URL <http://www.top-messtechnik.com>
- Owen, R., Jobling, S., 2012. The hidden costs of flexible fertility. *Nature* 485 (7399), 441.
- Panizza, M., Cerisola, G., 2005. Application of diamond electrodes to electrochemical processes. *Electrochimica Acta* 51 (2), 191–199.
- Pleskov, Y., 2002. Electrochemistry of diamond: A review. *Russian Journal of Electrochemistry* 38 (12), 1275–1291.
- Polcaro, A. M., Vacca, A., Mascia, M., Ferrara, F., 2008. Product and by-product formation in electrolysis of dilute chloride solutions. *Journal of Applied Electrochemistry* 38 (7), 979–984.
- Polcaro, A. M., Vacca, A., Mascia, M., Palmas, S., Ruiz, J. R., 2009. Electrochemical treatment of waters with BDD anodes: kinetics of the reactions involving chlorides. *Journal of Applied Electrochemistry* 39 (11), 2083–2092.
- Reemtsma, T., Jekel, M., 2007. *Organic Pollutants in the Water Cycle*. John Wiley & Sons, Weinheim.
- Restaino, L., Frampton, E., Hemphill, J., Palnikar, P., 1995. Efficacy of ozonated water against various food-related microorganisms. *Applied and Environmental Microbiology* 61 (9), 3471–3475.
- Rodayan, A., Roy, R., Yargeau, V., 2010. Oxidation products of sulfamethoxazole in ozonated secondary effluent. *Journal of Hazardous Materials* 177 (1-3), 237–243.
- Rodrigo, M., Cañizares, P., Sánchez-Carretero, A., Sáez, C., 2010. Use of conductive-diamond electrochemical oxidation for wastewater treatment. *Catalysis Today* 151, 173–177.
- Rosal, R., Rodríguez, A., Antonio Perdigón-Melón, J., Petre, A., García-Calvo, E., José Gómez, M., Agüera, A., Fernández-Alba, A. R., 2010. Occurrence of emerging pollutants in urban wastewater and their removal through biological treatment followed by ozonation. *Water Research* 44 (2), 578–588.

- Rote Liste Service GmbH (Ed.), 2012. Rote Liste 2012 – Arzneimittelverzeichnis für Deutschland (einschließlich EU-Zulassungen und bestimmter Medizinprodukte).
- Roth, J., Sullivan, D., 1981. Solubility of ozone in water. *Industrial & Engineering Chemistry Fundamentals* 20 (2), 137–140.
- Sanchez, W., Sremski, W., Piccini, B., Palluel, O., Maillot-Maréchal, E., Betoulle, S., Jaffal, A., Aït-Aïssa, S., Brion, F., Thybaud, E., Hinfray, N., Porcher, J.-M., 2011. Adverse effects in wild fish living downstream from pharmaceutical manufacture discharges. *Environment International* 37 (8), 1342–1348.
- Sander, accessed in May 2012.
URL <http://www.sander-ozon.de>
- Schmalz, V., Dittmar, T., Haaken, D., Worch, E., 2009. Electrochemical disinfection of biologically treated wastewater from small treatment systems by using boron-doped diamond (BDD) electrodes – Contribution for direct reuse of domestic wastewater. *Water Research* 43 (20), 5260–5266.
- Schmalz, V., Dittmar, T., Worch, E., Fischer, D., 2008. Diamantelektroden in der dezentralen Abwasserbehandlung – elektrochemischer Abbau des chemischen Sauerstoffbedarfs organisch hochbelasteter Härtereiabwässer. *Chemie Ingenieur Technik* 80 (10), 1545–1550.
- Schwarzenbach, R. P., Escher, B. I., Fenner, K., Hofstetter, T. B., Johnson, C. A., von Gunten, U., Wehrli, B., 2006. The challenge of micropollutants in aquatic systems. *Science* 313 (5790), 1072–1077.
- Sedlak, D. L., von Gunten, U., 2011. The chlorine dilemma. *Science* 331 (6013), 42–43.
- Sehested, K., Holcman, J., Hart, E., 1983. Rate constants and products of the reactions of e_{aq}^- , O_2^- , and H with ozone in aqueous solutions. *Journal of Physical Chemistry* 87 (11), 1951–1954.
- Sies, H., 1993. Strategies of antioxidant defense. *European Journal of Biochemistry* 215 (2), 213–219.
- Soriano, D., October 2010. Photo-Fenton reaction, University of Pittsburgh-Bradford. Internet broadcast, accessed in Nov 2012.
URL <http://www.youtube.com/watch?v=3m7-vS6yEOo>
- Sotelo, J., Beltrán, F., Benitez, F., Beltrán-Heredia, J., 1987. Ozone decomposition in water: Kinetic study. *Industrial & Engineering Chemistry Research* 26 (1), 39–43.
- Sotelo, J., Beltrán, F., Benitez, F., Beltrán-Heredia, J., 1989. Henry's law constant for the ozone-water system. *Water Research* 23 (10), 1239–1246.
- Stackelberg, P., Furlong, E., Meyer, M., Zaugg, S., Henderson, A., Reissman, D., 2004. Persistence of pharmaceutical compounds and other organic wastewater contaminants in a conventional drinking-water-treatment plant. *Science of the Total Environment* 329 (1-3), 99–113.

- Stucki, S., Baumann, H., Christen, H., Kotz, R., 1987. Performance of a pressurized electrochemical ozone generator. *Journal of Applied Electrochemistry* 17 (4), 773–778.
- Suarasan, I., Ghizdavu, L., Ghizdavu, I., Budu, S., Dascalescu, L., 2002. Experimental characterization of multi-point corona discharge devices for direct ozonation of liquids. *Journal of Electrostatics* 54, 207–214.
- Switzer, J., Rajasekharan, V., Boonsalee, S., Kulp, E., Bohannon, E., 2006. Evidence that monochloramine disinfectant could lead to elevated Pb levels in drinking water. *Environmental Science & Technology* 40 (10), 3384–3387.
- Tanner, B., Kuwahara, S., Gerba, C., Reynolds, K., 2004. Evaluation of electrochemically generated ozone for the disinfection of water and wastewater. *Water Science and Technology* 50 (1), 19–25.
- Ternes, T., 1998. Occurrence of drugs in German sewage treatment plants and rivers. *Water Research* 32 (11), 3245–3260.
- Tröster, I., Schäfer, L., Fryda, M., Matthée, T., 2004. Electrochemical advanced oxidation process using DiaChem[®] electrodes. *Water Science and Technology* 49 (4), 207–212.
- Trovó, A. G., Nogueira, R. F. P., Agüera, A., Fernández-Alba, A. R., Sirtori, C., Malato, S., 2009a. Degradation of sulfamethoxazole in water by solar photo-Fenton. Chemical and toxicological evaluation. *Water Research* 43 (16), 3922–3931.
- Trovó, A. G., Nogueira, R. F. P., Agüera, A., Sirtori, C., Fernández-Alba, A. R., 2009b. Photodegradation of sulfamethoxazole in various aqueous media: Persistence, toxicity and photoproducts assessment. *Chemosphere* 77 (10), 1292–1298.
- US EPA, 2012. 2012 edition of the drinking water standards and health advisories. Tech. Rep. EPA 822-S-12-001, Office of Water, U.S. Environmental Protection Agency, Washington, DC.
- vanLoon, G. W., Duffy, S. J., 2010. *Environmental chemistry: a global perspective*, 3rd Edition. Oxford University Press: Oxford.
- Vogna, D., Marotta, R., Andreozzi, R., Napolitano, A., d'Ischia, M., 2004. Kinetic and chemical assessment of the UV/H₂O₂ treatment of antiepileptic drug carbamazepine. *Chemosphere* 54 (4), 497–505.
- von Gunten, U., 2003a. Ozonation of drinking water: Part I. oxidation kinetics and product formation. *Water Research* 37, 1443–1467.
- von Gunten, U., 2003b. Ozonation of drinking water: Part II. disinfection and by-product formation in presence of bromide, iodide or chlorine. *Water Research* 37, 1469–1487.

- von Sonntag, C., von Gunten, U., 2012. *Chemistry of Ozone in Water and Wastewater Treatment: From Basic Principles to Applications*, 1st Edition. IWA Publishing, Glasgow.
- Wolfe, R., Stewart, M., Liang, S., McGuire, M., 1989. Disinfection of model indicator organisms in a drinking-water pilot-plant by using PEROXONE. *Applied and Environmental Microbiology* 55 (9), 2230–2241.
- Yao, Y., Kubota, Y., Murakami, T., Ochiai, T., Ishiguro, H., Nakata, K., Fujishima, A., 2011. Electrochemical inactivation kinetics of boron-doped diamond electrode on waterborne pathogens. *Journal of Water and Health* 9 (3), 534–543.
- Yates, R., Stenstrom, M., 2000. Gravimetric sampling procedure for aqueous ozone concentrations. *Water Research* 34 (4), 1413–1416.
- Zollinger, H., 2003. *Color chemistry: syntheses, properties and applications of organic dyes and pigments*, 3rd Edition. VHCA; Wiley-VCH.

Appendix A

Mass Spectrometric Databases

Table A1: SMX transformation product database - known TPs from literature for ozone treatment according to Abellán et al. (2008) [1] and Rodayan et al. (2010) [2], ozone hydrogen peroxide system according to Gómez-Ramos et al. (2011) [3], TiO₂ photocatalysis according to Hu et al. (2007) [4], solar photo-Fenton according to Trovó et al. (2009a) [5], photodegradation according to Trovó et al. (2009b) [6] and electro-Fenton with BDD according to Dirany et al. (2010) [7]. See Figure 8.1 for the experimentally found TPs. n.a.: not available due to negative detection mode. n.e.: not expected.

TP	molecular formula	formula weight	mode	m/z	x + Na	x + K
sulfamethoxazole (SMX)	C ₁₀ H ₁₁ N ₃ O ₃ S	253.0522	+	254.0600	276.0420	292.0159
2 x SMX	2xC ₁₀ H ₁₁ N ₃ O ₃ S	506.1044	+	507.1122	529.0942	545.0681
SMX'	C ₁₀ H ₁₁ N ₃ O ₃ S	253.0522	-	252.0444	n.a.	n.a.
SMX-SO2	C ₁₀ H ₁₁ N ₃ O	189.0903	+	190.0982	212.0801	228.0540
A (C8[5])	C ₁₀ H ₁₁ N ₃ O ₄ S	269.0471	+	270.0549	292.0369	308.0108
B (TP-288[3], Int2[4], C5[5])	C ₁₀ H ₁₃ N ₃ O ₅ S	287.0577	+	288.0655	310.0474	326.0214
C (C1[5])	C ₈ H ₉ N ₃ O ₄ S	243.0314	+	244.0393	266.0212	281.9951
D (C6[5])	C ₇ H ₉ N ₃ O ₃ S	215.0365	+	216.0444	238.0263	254.0002
E (C5[6])	C ₆ H ₆ NO ₂ S ⁺	n.e.	+	156.0120	n.e.	n.e.
F (postulated)	C ₁₀ H ₁₃ N ₃ O ₃	223.0958	+	224.1036	246.0856	262.0595
G (TP-99[3], Int3[4], C4[5], C3[6])	C ₄ H ₆ N ₂ O	98.0481	+	99.0559	121.0378	137.0118
H (2-oxopropanoic acid[7])	C ₂ H ₂ O ₃	74.0004	-	72.9925	n.a.	n.a.
I (oxoethanoic acid[7])	C ₃ H ₄ O ₃	88.0160	-	87.0082	n.a.	n.a.
J (TP-284a[3])	C ₁₀ H ₉ N ₃ O ₅ S	283.0263	+	284.0342	306.0161	321.9900
K (TP-284c[3])	C ₁₀ H ₉ N ₃ O ₅ S	283.0263	+	284.0342	306.0161	321.9900
K' (A[1])	C ₁₀ H ₉ N ₃ O ₅ S	283.0263	-	282.0185	n.a.	n.a.
L (B[1])	C ₆ H ₅ N ₁ O ₃	139.0270	-	138.0191	n.a.	n.a.
M (C[1])	C ₁₀ H ₉ N ₃ O ₆ S	299.0212	-	298.0134	n.a.	n.a.
N (D[1])	C ₁₀ H ₁₀ N ₂ O ₅ S	270.0311	-	269.0232	n.a.	n.a.

continued on next page

TP	molecular formula	formula weight	mode	m/z	x + Na	x + K
	<i>continued from previous page</i>					
E[1]	C ₁₀ H ₉ N ₃ O ₂	203.0696	+	204.0774	226.0593	242.0333
F[1]	C ₁₀ H ₁₁ N ₃ O ₄	237.0750	+	238.0829	260.0648	276.0387
G[1]	C ₁₀ H ₉ N ₃ O ₆ S	299.0212	+	300.0291	322.0110	337.9849
TP-270[3], Int1[4], C10[5], C6[6], C9[6]	C ₁₀ H ₁₁ N ₃ O ₄ S	269.0471	+	270.0549	292.0369	308.0108
Hu1[4], C2[6]	C ₆ H ₇ NO ₃ S	173.0147	+	174.0225	196.0044	211.9784
Hu2[4]	C ₆ H ₇ NO ₄ S	189.0096	+	190.0174	211.9993	227.9733
Hu3[4]	C ₁₀ H ₁₂ N ₂ O ₅ S	287.0577	+	288.0655	310.0474	326.0214
Hu4[4]	C ₁₀ H ₁₂ N ₂ O ₅ S	272.0467	+	273.0546	295.0365	311.0104
Hu5[4]	C ₄ H ₈ N ₂ O ₃	132.0535	+	133.0614	155.0433	171.0172
C2[5]	C ₇ H ₇ N ₃ O ₂ S	197.0260	+	198.0338	220.0157	235.9897
4-aminobenzene sulfonamide[2], C3[5]	C ₆ H ₈ N ₂ O ₂ S	172.0307	+	173.0385	195.0205	210.9944
C9[5]	C ₁₀ H ₁₀ N ₂ O ₅ S	270.0311	+	271.0389	293.0208	308.9948
C7[5], C8[6]	C ₁₀ H ₁₁ N ₃ O ₃ S	253.0522	+	254.0600	276.0420	292.0159
C1[6]	C ₆ H ₇ NO ₄ S	189.0096	+	190.0174	211.9993	227.9733
C4[6]	C ₇ H ₉ N ₃ O ₃ S	215.0365	+	216.0444	238.0263	254.0002
C7[6]	C ₁₀ H ₁₃ N ₃ O ₄ S	271.0628	+	272.0706	294.0525	310.0265
hydroxylated SMX[7]	C ₁₀ H ₁₀ N ₂ O ₄ S	254.0362	+	255.0440	277.0259	292.9999
p-benzoquinone[7]	C ₆ H ₄ O ₂	108.0211	+	109.0290	131.0109	146.9848
Z-butenedioic acid[7]	C ₄ H ₄ O ₄	116.0109	-	115.0031	n.a.	n.a.
hydroxybutanedioic acid[7]	C ₄ H ₆ O ₅	134.0215	-	133.0137	n.a.	n.a.
ethanedioic acid[7]	C ₂ H ₂ O ₄	89.9953	-	88.9874	n.a.	n.a.
3-amino-5-methylisoxazole[7]	C ₄ H ₇ N ₂ O	99.0559	-	98.0481	n.a.	n.a.
TP-284b[3]	C ₁₀ H ₁₀ N ₃ O ₅ S	283.0263	+	284.0342	306.0161	321.9900
N-(3-phenylpropyl)-acetamide[2]	C ₁₁ H ₁₅ NO	177.1155	+	178.1233	200.1052	216.0792

continued on next page

TP	molecular formula	formula weight	mode	m/z	x + Na	x + K
<i>continued from previous page</i>						
2-methyl-1-benzoxazole[2]	C ₈ H ₇ NO	133.0528	+	134.0606	156.0426	172.0165
phenol[2]	C ₆ H ₆ O	94.0419	+	95.0497	117.0316	133.0056
ethyl ethanoate[2]	C ₄ H ₈ O ₂	88.0524	+	89.0603	111.0422	127.0161
methyl ethanoate[2]	C ₃ H ₆ O ₂	74.0368	+	75.0446	97.0265	113.0005
ethanoic acid[2]	C ₂ H ₄ O ₂	60.0211	+	61.0290	83.0109	98.9848
ethanol[2]	C ₂ H ₆ O	46.0419	+	47.0497	69.0316	85.0056
methanol[2]	CH ₄ O	32.0262	+	33.0341	55.0160	70.9899

Table A2: CBZ transformation product database - known TPs from literature for hydrogen peroxide photolysis according to Vogna et al. (2004) [8] and ozone treatment according to McDowell et al. (2005) [9]. See Figure 8.2 for the experimentally found TPs. n.a.: not available due to negative detection mode.

TP	molecular formula	formula weight	mode	m/z	x + Na	x + K
carbamazepine (CBZ)	$C_{15}H_{12}N_2O$	236.0951	+	237.1029	259.0848	275.0588
2 x CBZ	$2xC_{15}H_{12}N_2O$	472.1901	+	473.1980	495.1799	511.1538
10,11-epoxycarbamazepine[8] (epoxyCBZ)	$C_{15}H_{12}N_2O_2$	252.0900	+	253.0978	275.0797	291.0537
acridine-9-carboxaldehyde[8] (ACR-CHO)	$C_{14}H_9NO$	207.0685	+	208.0763	230.0582	246.0322
acridine[8] (ACR)	$C_{13}H_9N$	179.0736	+	180.0814	202.0633	218.0373
1 or 2-hydroxyacridine[8] (ACR-OH)	$C_{13}H_9NO$	195.0685	+	196.0763	218.0582	234.0322
preBQM[9]	$C_{15}H_{12}N_2O_3$	268.0849	+	269.0927	291.0746	307.0486
BQM[9]	$C_{15}H_{10}N_2O_2$	250.0743	+	251.0821	273.0641	289.0380
BQD[9]	$C_{15}H_{10}N_2O_3$	266.0692	+	267.0770	289.0590	305.0329
Vogna1[8]	$C_{15}H_{12}N_2O_5$	300.0747	+	301.0825	323.0644	339.0384
Vogna1'[8]	$C_{15}H_{12}N_2O_5$	300.0747	-	299.0668	n.a.	n.a.
2-aminobenzoic acid[8]	$C_7H_7NO_2$	137.0477	-	136.0399	n.a.	n.a.
2-hydroxybenzoic acid[8]	$C_7H_6O_3$	138.0317	-	137.0239	n.a.	n.a.
2-hydroxyphenol[8]	$C_6H_6O_2$	110.0368	+	111.0446	133.0265	149.0005
Z or E-butenedioic acid[8]	$C_4H_4O_4$	116.0109	-	115.0031	n.a.	n.a.
2,3-dihydroxybutanedioic acid[8]	$C_4H_6O_6$	150.0164	-	149.0086	n.a.	n.a.
butanedioic acid[8]	$C_4H_6O_4$	118.0266	-	117.0188	n.a.	n.a.
hydroxybutanedioic acid[8]	$C_4H_6O_5$	134.0215	-	133.0137	n.a.	n.a.
oxobutanedioic acid[8]	$C_4H_4O_5$	132.0058	-	130.9980	n.a.	n.a.
propanedioic acid[8]	$C_3H_4O_4$	104.0109	-	103.0031	n.a.	n.a.
2-hydroxypropanedioic acid[8]	$C_3H_4O_5$	120.0058	-	118.9980	n.a.	n.a.
2-hydroxyethanoic acid[8]	$C_2H_4O_3$	76.0160	-	75.0082	n.a.	n.a.
ethanedioic acid[8]	$C_2H_2O_4$	89.9953	-	88.9874	n.a.	n.a.
BaQD[9]	$C_{15}H_{10}N_2O_4$	282.0641	-	281.0563	n.a.	n.a.
dibenzazepine (iminostilbene)	$C_{14}H_{11}N$	193.0892	+	194.0971	216.0790	232.0529

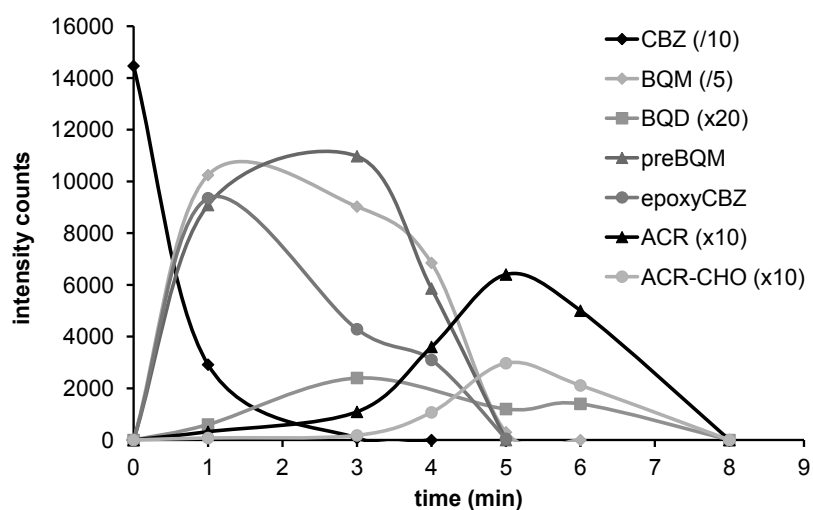
Appendix B

Time Courses and Energetic Requirements of CBZ

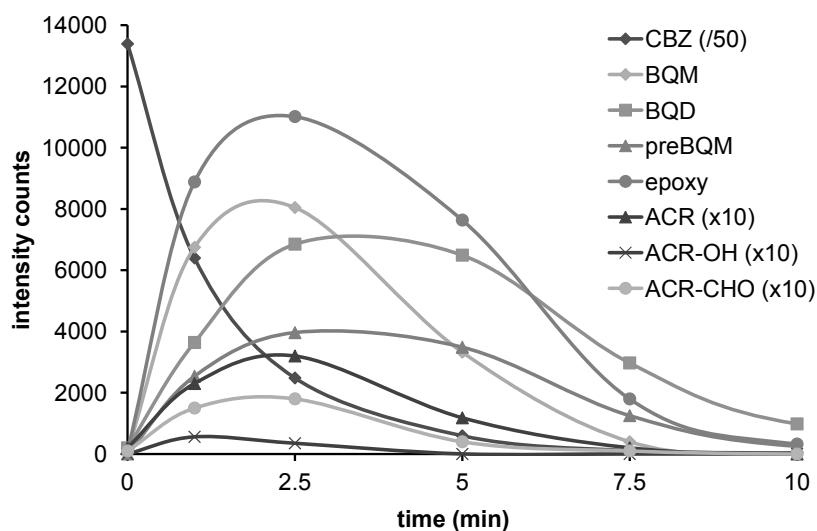
Table B1: Energy consumption for treatment until complete elimination of CBZ (t_{PC_0}) and full abatement of its known transformation products (t_{TR_0}) in deionised-p.

parent compound	AOP	$E_{E,pro}$	$E_{E,chem}$	$E_{E,mix}$	t_{PC_0}	$E_{E,tot}$	$E_{E,pro} + E_{E,chem}$	t_{TR_0}	$E_{E,tot}$	$E_{E,pro} + E_{E,chem}$
		Wh/(L·min)	Wh/L	Wh/(L·min)	min	Wh/L	Wh/L	min	Wh/L	Wh/L
CBZ	DD'	0.01	0	0.35	3	1.07	0.03	8	2.84	0.08
CBZ	UV/H ₂ O ₂	0.20	3.33	0.44	10	9.71	5.35	15	12.90	6.36

[CBZ]_{*i*}, $DD' = 1 \mu\text{M}$, [CBZ]_{*i*}, UV/H₂O₂ = 5.5 μM . Methods shown: electrolysis with a boron-doped diamond electrode (DD': 42 mA/cm²) and photolysis (UV/H₂O₂). $E_{E,mix}$: electrical energy for mixing; $E_{E,pro}$: process-intrinsic electrical energy; $E_{E,chem}$: cost of chemicals converted to energy; $E_{E,tot}$: total electrical energy; $E_{E,pro} + E_{E,chem}$: effective energy.



(a) DD' (at 42 mA/cm²)



(b) UV/H₂O₂

Figure B1: Course of CBZ and its identified degradation products during (a) the DD' and (b) the UV/H₂O₂ experiment.

CBZ was oxidised by DD' in the first 3 min to a concentration below the LOD. The courses of the individual products can be divided in three. The first group, consisting of **preBQM**, **BQM** and **epoxyCBZ** emerged as soon as treatment began, reached a maximum concentration after 1 to 3 min and vanished after 5 min. These species were described in literature as primary transformation products from both the HO[•] and ozone pathways (Figure 8.2). The second group, comprising **ACR** and **ACR-CHO**, arose more slowly and showed maxima after 5 min of treatment. Accordingly, their complete oxidation took place 3 minutes later than that of the first group (8 min). These species were reported to form from **epoxy-CBZ** (Vogna et al., 2004). Finally, **BQD** was in between, forming at the beginning, but being resilient to treatment up to 8 min. **BQD** forms from **BQM** by further ozonation (McDowell et al., 2005). For the oxidation products of UV/H₂O₂ no group differentiations were observed and all products behaved similarly to **preBQM**. Total oxidation of the identified products needed 15 min. The intensity counts of CBZ and **BQM** were divided, whereas those of **BQD**, **ACR**, **ACR-OH** and **ACR-CHO** were multiplied by the factors shown for visualisation.

Mateo Joaquín Ureña de Vivanco

Date of birth: January 5th 1984

Nationality: Peruvian

E-mail: urenadevivanco@gmail.com

Tel.: +49 (0)163 920 44 97



Education

08.2008 – 02.2013	Doctoral studies at the Technische Universität München <ul style="list-style-type: none">• Scholarship holder of the German Academic Exchange Service (DAAD)• Dissertation at the Institute of Water Quality Control under the supervision of Prof. Dr. Helmreich• Title: <i>Characterisation of a Boron-Doped Diamond Electrode and Applications for the Oxidation of Pharmaceutical Substances and Disinfection in Water</i>• Supervising Bachelor and Master students
09.2006 – 09.2007	Exchange year at the Technische Universität Berlin <ul style="list-style-type: none">• Scholarship holder of ALFA-Ingam (European-Latin American, technical cooperation for the environment)• Master thesis at the Chair of Water Quality Control under the supervision of Prof. Dr. Jekel• Title: <i>Kinetic and Mechanistic Investigation of the Degradation of the X-Ray Contrast Agent Iopromide with the aid of zerovalent iron</i>• Main courses – Environmental Engineering (waste water treatment, waste management), Chemical Engineering and Analytical Chemistry (instrumental analysis)
03.2001 – 12.2007	Degree in Chemistry at the Pontifical Catholic University of Peru (PUCP) Degree designation: <i>Licenciado en ciencias</i> (licentiate in science), score: 86 % (ranking: top 1.19 %)
03.1987 – 12.2000	High School Certificate <i>La Casa De Cartón</i> , Lima (score: 82 %)

Publications

See Preface on page 23

Teaching Experience

03.2008 – 07.2008	Lectured Chemistry at the PUCP (first general chemistry course for Science and Engineering students).
05.2004 – 07.2008	Tutored school classes at the Faculty of Chemistry (PUCP). With oral presentations and quick experiments, I motivated pupils to study chemistry.
08.2005 – 12.2005	Tutored the practical course <i>Experimental Chemistry</i> for 2nd-year chemistry students at the PUCP.
12.2003 – 04.2005	Conducted research on the project <i>Dye lasers and their pedagogic applications</i> at the Faculty of Physics (PUCP).
01.2001 – 03.2009	Gave private lessons in Mathematics, Spanish, English, German, natural sciences and analysis. Learners between 6 and 33 years. Over 400 teaching hours of experience.

Additional Skills

Languages

Spanish	native language
English	excellent command
German	excellent command (TestDAF, average score: 5/5)

Computer Skills

Microsoft Office (Word, Excel, Power Point), L^AT_EX, CorelDraw, ChemSketch, liquid chromatography and mass spectrometric software

Interests and Activities

Music: playing the guitar and panpipes, listening to classical music and opera, classical singing

Sports: cycling, TaeKwon-Do (member of the International TaeKwon-Do Federation)

Index

- t_{PC_0} , 78, 79, **107–112**, 119, 142
 t_{TP_0} , **107–112**, 119, 142
ct, **91–93**
- AOPs, **29–31**, 48, 53, 59, 66, 102
 characterisation, 49, **101–112**
 conventional, 29, 58
 electrochemical, 31, 101, 115
 heterogeneous, 31, 55, 103, 106
 homogeneous, 30, 55, 103
 reactor, 44, 45, 55, 56, 117, 121
- AOX, 37, 47, **84–89**, 99, 117, 119, 121
- carbamazepine, 27, 28, 41, 49, **77–80**, 80, 84, 97–98, 101–106, 111, 114, 117–119, 121, 139, 142, 143
- charge input, **51**, 62, 65, 72, 73, 76–79, 84, 86, 87, 89, 91, 119
- Chick and Watson’s Model, 93
- current
 density (j), 38, 56, 58–60, **61–69**, 71–81, 83–89, 91, 97, **106**, 107, 108, 111, 115, 116
 effect, **77**, 79, 86, **91–95**, 99, **120**
- disinfection, 29, 34, 37–39, 41, 50–51, 59, **91–99**, 107, 115–117, **120**, 122
- electrical conductivity, 41–43, 66, **74**, **75**, 79, 106
- energy consumption, 122
 $E_{E,chem}$, 52, 53, 102, 111
 $E_{E,mix}$, **56**, 58, 93
 $E_{E,pro}$, **56**, 58–60, 66–68, 79, 94, 102, **108**, 110, 117, **119**
 $E_{E,tot}$, 68, 94, **108**, 111, 117
 $E_{EO,rx}$, 59, **59**, 60
 $E_{EO,tot}$, 56
 E_{EO} , 53
 components, 53, 54, **56–60**, 66, 108, 110, 117
 for degradation, 77–79, **79**, 81, 102, **108–112**, 116, 117, 119
 for disinfection, 94
- Faraday’s Law, 63
- Henry’s Law, 35
- inorganic BPs (BrO_3^-), 29, **36–37**, 83–84, 99, 121
- mass spectrometry, 42, 44, 49, **49**, 104, 105, 113, 114, 122
- matrix effect, 71–81, 116, **120**
 on BP formation, 83–89
 on disinfection, 97–98
 on electricity consumption, 79
 on ozone production, 72, 75, 77, 80
 on the degradation of a target compound, 78, 97–98
- Ohm’s Law, 79
- photo-Fenton reaction, 30, 31, 45, 46, 48, 53–60, 101, 102, 104, 117, 138
- ROS, 29–31, 36, 46, 56, **61–63**, 67, 83, 91, 98, 115
- sulfamethoxazole, 41, 49, 101–113, 118, 121, 138
- THMs, 37, 47, **86**, 87, 89, 117
- transformation product, 38, 56, 101–112, 143
- UV/ H_2O_2 , 30, 31, 45, 46, 48, 50, 53, 55–60, 101–114, 117